CHAPTER FOUR

MINERALOGIC AND PETROGRAPHIC STUDIES

Chapter Four

Mineralogic And Petrographic Studies

This chapter aims to construct the mineral composition and highlight the petrographic characteristics of the studied sandstones. Data used in this study were obtained primarily by point counting surface and subsurface thin sections of epoxy-impregnated samples (four hundred counts were made per slide for a total of hundred and three slides). An additional forty-seven thin sections were examined. Prior to counting, thin sections were stained for calcite and feldspars. Techniques used in this study include petrographic and mineral examinations using the conventional polarizing microscope, X-ray diffractometry (XRD), heavy mineral analysis and scanning electron microscope (SEM).

The studied sandstones are mainly composed of three architectural components; framework grains (F), cement (C) and porosity (P). They are described in that order in the following sections. Detrital matrix (M) is very rare and constitutes a negligible amount of the sandstone composition. Although infiltrated clay is present in some samples, it is mostly of diagenetic origin. The rarity of detrital matrix is a conspicuous feature of the studied sandstones. In this concern, Naqus Sandstone ranges in composition of the three components from $F_{57.50}C_{2.50}P_{0.0}$ to $F_{79.25}C_{42.50}P_{27.75}$ with an average of $F_{69.49}C_{12.94}P_{17.57}$. Sandstone of Araba Formation ranges in composition of the three components from $F_{51.25}C_{19.25}P_{0.0}$ to $F_{75.75}C_{48.75}P_{11.50}$ with an average of $F_{62.29}C_{34.27}P_{3.45}$. On the other hand, the three components in the subsurface sandstone range from $F_{75.25}C_{2.00}P_{0.0}$ to $F_{88.25}C_{24.75}P_{14.75}$ with an average of $F_{82.03}C_{13.12}P_{4.86}$

(Table 4.1). Differences observed among the studied units, and in samples from the same unit, are primarily due to variations in diagenetic history.

Because clay matrix is absent, and quartz comprises the only framework mineral, the studied sandstones are classified as quartz arenites. Concerning mineral composition, they are mature to supermature. Texturally speaking, they are submature to mature as evidenced by the abundance of subrounded and rounded grains and the moderate-to-high degree sorting. The scarcity of detrital clay minerals and the nearly absence of rock fragments and feldspars may, however, be a compositional maturity obtained during diagenesis by the dissolution loss of unstable grains (diagenetic maturation); thus, these sandstones may be described as diagenetic quartz arenites.

The studied surface and subsurface sandstones are remarkably similar in their mineral composition and diagenetic characters. Thus, their petrographic and diagenetic features are considered together. Differences, if any, in these characters are emphasized in the discussion.

4.1 Framework composition

Microscopic investigation of the studied sandstone samples showed that they are composed of detrital quartz grains and varying minor proportions of highly altered feldspars, rock fragments, detrital clays and heavy minerals.

4.1.1 Quartz

Quartz is the most abundant detrital component in the studied sandstones. The average values for quartz in the Naqus and Araba rocks are 99.58 and 99.42 % of the framework composition, respectively. On the other hand, quartz in the subsurface sandstone has an average of 99.60 % of the framework composition (Table 4.2). Quartz grains are mostly moderately well-sorted, fine- to medium-grained, occasionally coarse-

grained, subangular to subrounded, sometimes well-rounded. Some of the studied samples have polymodal grain size distributions. Coarse sand grains are mixed together with very fine sand grains with some fragments in the intermediate size ranges. Such a texture may result from mixing of sediments from different sources, storm mixing of material in a high-energy depositional environment, or, in some cases, may be produced by burrowing or other *in situ* mixing processes. Banding on the scale of a thin section is locally observed (PLs. 4.1; 4.2 A, B).

Quartz grains are either monocrystalline or polycrystalline; the former are the most abundant making up to 98.95 % of the total quartz of Naqus Sandstone and up to 99.58 % of those of Araba Sandstone. The average values for monocrystalline quartz in the two formations are 88.13 and 97.02 %, respectively. On the other hand, monocrystalline quartz in the subsurface sandstone ranges from 87.62 % to 100.00 % with an average of 96.34 % (Table 4.3).

Monocrystalline quartz grains are either undulose or nonundulose. Monocrystalline quartz with straight extinction (nonundulose) is the most common. It makes up 96.58 % of the total monocrystalline quartz in Naqus Sandstone and up to 99.16 % of those in Araba Sandstone. The average values of nonundulose quartz in the two formations are 91.23 and 96.58 %, respectively. On the other hand, nonundulose monocrystalline quartz in the subsurface sandstone averages 95.31 % of the total monocrystalline quartz (Table 4.3). Undulose monocrystalline quartz forms a minor constituent. It makes up to 22.77 % of the total monocrystalline quartz of Naqus Sandstone and up to 5.68 % of those of Araba Sandstone. The average values of undulose quartz in the two formations are 8.77 and 3.42 %, respectively. On the other hand, the subsurface sandstone may lack undulose monocrystalline quartz, but may

Table 4-1: Point-count data for the studied sandstones. All values in volume percent

	Framework Composition of the Sandstones								Authigenic Mineral Cements and Replacement Minerals										Types of Porosity					Total
S No	MCQU	MCQN	PCQ	Feld	R F	H M	Det Clay	Total	Qtz Over	Kao P F	Kao Rep	Kao Total	Clay Coat	FeOx	Gyp	Halite	Calcite	Total	Inter	Intra	OVSP	Frac	Total	
1- Araba Formation																								
1	1 75	62.50	1 25	0 00	0 25	0 00	1.00	66.75	0.75	19 50	1.50	21.00	0.75	5 25	0 00	3.00	0.00	30 75	2 50	0 00	0.00	0.00	2.50	100
2	3 33	55 33	3 67	0 00	0.33	0.00	0.00	62 67	0 33	4 33	0 33	4 67	0.00	30.67	0.00	0 00	0 00	35.67	0 33	0 00	1 33	0 00	1 67	100
3	2 50	58 00	4.00	0.00	0.25	0 00	0 00	64 75	0 25	3 50	0 50	4.00	0 00	29 50	0 00	0 00	0.00	33 75	0 50	0 00	1 00	0 00	1 50	100
4	1 75	63.75	3 25	0 00	0 50	0 00	0 00	69 25	0 00	2 75	2 25	5.00	0.00	14 25	0.00	0.00	0 00	19 25	7 00	0 00	4 50	0 00	11.50	100
5	1 50	56 75	1 50	0.00	0 00	0 00	0.00	59 75	1.00	16 00	0 50	16.50	0 00	19 50	0 00	0 00	0 00	37 00	2 75	0 00	0.50	0.00	3 25	100
6	3 25	55 00	0 75	0 00	0 00	0.00	0 00	59 00	0 00	16 75	0 25	17.00	11.75	11 00	0 00	0 00	0.00	39 75	0 00	0 25	1 00	0 00	1 25	100
7	0.50	58 75	0 25	0.00	0 00	0 00	1 75	61 25	0 00	8 00	4 50	12 50	7.25	7 75	0 00	2 75	0.00	30 25	6 50	0 25	1 75	0 00	8 50	100
8	1 50	55 50	0 75	0 00	0 00	0 00	0 00	57 75	0 50	23 75	0 25	24 00	0 00	13 25	0 00	0 00	0 00	37 75	3 25	0 00	0 25	1 00	4 50	100
9	1 50	49 00	0 75	0 00	0 00	0 00	0 00	51 25	0 25	8 75	7 50	16 25	0 00	32 25	0 00	0 00	0 00	48 75	0 00	0 00	0 00	0 00	0.00	100
10	2 25	52 75	2 00	0 00	0 00	0 00	0 00	57 00	2 50	19 00	1 00	20 00	0 00	20 25	0 00	0 00	0 00	42 75	0 00	0 00	0 25	0 00	0 25	100
11	2 75	70 25	2 75	0.00	0 00	0 00	0 00	75 75	0 25	13 50	1 75	15 25	0.00	5.75	0 00	0 00	0.00	21.25	3.00	0.00	0 00	0 00	3 00	100
Max	3.33	70.25	4.00	0.00	0.50	0.00	1.75	75.75	2.50	23.75	7.50	24.00	11.75	32.25	0.00	3.00	0.00	48.75	7.00	0.25	4.50	1.00	11.50	
Min	0.50	49.00	0.25	0.00	0.00	0.00	0.00	51.25	0.00	2.75	0.25	4.00	0.00	5.25	0.00	0.00	0.00	19.25	0.00	0.00	0.00	0.00	0.00	
Avg	2.05	57.90	1.90	0.00	0.12	0.00	0.25	62.20	0.83	12.36	1.25	14.20	1.80	17.22	0.00	0.52	0.00	34.21	2.35	0.05	0.90	0.09	3.40	
2- Naqus Formation																								
12	4.67	64.67	2 33	0.00	0 00	0.00	0 00	71 67	0 33	1.00	2 67	3 67	0.00	0.33	0 00	0 00	0.00	4.33	20.67	0 00	3 33	0 00	24 00	100
13	5 00	51 00	6 25	0 00	0 00	0.25	0.00	62 50	2 25	17 25	0.00	17 25	1 00	2.50	0 00	0.50	1 75	25 25	4 75	0.00	7 50	0 00	12 25	100
15	2 00	55 25	7 50	0 00	0.00	0 00	0 00	64.75	3 25	12 50	0 00	12 50	0 00	2 00	0 00	0 25	0 00	18 00	4 50	0.00	12 75	0 00	17 25	100
18	3 00	55 00	11 33	0 00	0 00	0 33	0 00	69 67	1 00	2 00	15 00	17 00	0 00	0 00	0 00	0 00	0 00	18 00	9 33	0 00	3 00	0 00	12 33	100
22	3 25	52 50	11 00	0 00	0 75	0 00	0 00	67.50	0.50	7.00	0 25	7 25	0 00	0 75	0 00	1 00	0 00	9 50	14 00	0 00	9 00	0 00	23 00	100
25	4 50	55.00	9 75	0.00	1.25	0.00	0.00	70.50	1.75	10 00	0 00	10.00	0.25	3.75	0.00	1.50	0 00	17 25	3.25	0.00	9 00	0 00	12 25	100
28	6.50	43 25	20.00	0.00	0.00	0 00	0.75	70 50	2 50	9.50	0.00	9.50	0.00	1 50	0 00	0.50	0.00	14 00	2 00	0.00	13 50	0.00	15 50	100
31	7.00	45.50	20.00	0.00	0 00	0.00	0 00	72.50	0.00	1.75	0.50	2.25	0 00	0 25	0.00	0 00	0.00	2.50	21.00	2.75	1 25	0 00	25.00	100
33	6.00	57 25	9 75	0.00	0 50	0.00	0.00	73 50	1 00	5.00	0.75	5.75	0 00	1.50	0.00	0 00	0.00	8.25	1.75	0 75	15 00	0 75	18 25	100
35	4 50	58.00	9 50	0.00	0 00	0.25	0.75	73.00	1.25	14 25	1 25	15.50	0.00	1.75	0 00	3 50	0.00	22 00	1.75	0.00	3.25	0.00	5 00	100
39	2 50	66 25	4.50	0 00	0.00	0.00	0.00	73 25	0 50	19 50	2.25	21.75	0.00	1.00	0 00	0.00	0.00	23.25	1.50	0.00	2.00	0 00	3 50	100
40	4.00	52 50	9.50	0.00	0 50	0.00	0 00	66.50	0.00	15 00	0 00	15 00	0.00	6 50	0 00	0.50	0 00	22 00	9 75	1 50	0 25	0.00	11.50	100
43	4.50	50 50	2 50	0.00	0 00	0.00	0 00	57 50	0.00	37.00	0 00	37 00	2 50	1 25	0 00	1.75	0.00	42 50	0 00	0 00	0 00	0 00	0 00	100
45	6 25	57 75	10 00	0 00	0 00	0 00	0 00	74 00	2 00	13 00	0 00	13 00	0 00	1 75	0 00	0 00	0 00	16 75	4 00	0 25	5 00	0 00	9 25	100
47	11 50	39 00	20 00	0 00	0 00	0 00	0 00	70 50	1 50	2 25	0 00	2 25	0 00	0 25	0 00	0 00	0 50	4 50	12 75	0 75	11 50	0 00	25.00	100
51	5 00	54 75	7 00	0 00	0 50	0 00	0 00	67 25	1 00	22 00	1 00	23 00	0 75	3 00	0 00	0 00	0 00	27 75	3 00	0 75	1 25	0 00	5 00	100
52	6 00	44 75	13 75	0 00	0 00	0 00	0 00	64 50	1 25	8 00	0 50	8 50	0 50	1 00	0 00	0 00	0.00	11 25	22 50	0 00	1 75	0 00	24 25	100
55	4.25	55 75	5 00	0 00	0 00	0 00	0 00	65 00	2 75	2 25	0 50	2 75	0 00	1 75	0 00	0 00	0 00	7 25	23 75	0 00	4 00	0 00	27 75	100
58	3 25	55 50	3 25	0 00	0 25	0 00	0 00	62 25	0 75	3 25	0 00	3 25	0 00	3 00	0 00	3 00	0 00	10 00	26 00	0 00	1 75	0 00	27 75	100
61	2 75	62.50	4 25	0.00	0 00	0 00	0.00	69 50	0 25	12 00	1 75	13.75	0 00	1 00	0 00	7 00	0 00	22 00	7 00	0 75	0 75	0 00	8 50	100
62	4 25	58.75	7.25	0.00	0.00	0 00	0 00	70 25	1 25	5 75	0 00	5.75	0 00	1 00	0 00	3 25	0 00	11 25	15 25	1 25	2 00	0.00	18 50	100
65	4 00	55.25	5 25	0 00	0.00	0 00	0 00	64 50	2 25	9 25	0 00	9 25	0.00	0 75	0 00	0 75	0 00	13.00	17 75	0 75	4.00	0 00	22 50	100
67	4.75	57.75	3 75	0 00	0 00	0 00	0 00	66 25	1 75	10 25	0 00	10 25	0 75	0 25	0.00	1 25	0 00	14 25	14 25	0.00	5 25	0 00	19 50	100
70	8 50	57 50	8 75	0 00	2 00	0 00	0 00	76 75	1 25	11 75	0 00	11 75	0.00	6 00	0 00	0 50	0 00	19 50	2 75	0 00	1.00	0 00	3.75	100
73	9 00	57 25	8 25	0.00	1 25	0 00	0 00	75 75	1 75	11 25	0 00	11 25	0 50	5 25	0.00	1.00	0 00	19 75	3 50	0 00	1.00	0 00	4.50	100
76	7 50	55 00	5 50	0 00	0 00	1 00	0 00	69 00	1 50	10 50	0 00	10 50	0 00	1 50	0 00	0.00	2 00	15.50	12 50	0 00	3.00	0 00	15 50	100
79	8 25	48 75	22 25	0 00	0 00	0 00	0 00	79 25	0 25	0 00	0.00	0 00	4 25	0.00	0 00	0.00	0 00	4 50	14 25	0 25	1.75	0 00	16 25	100
80	5 50	55 50	6 25	0 00	0 00	0.75	0 00	68 00	1 00	8 00	0 00	8 00	0 00	1 50	0 00	0.00	0 00	10 50	19 25	0 00	2.25	0 00	21 50	100
83	7.75	57 25	8 25	0.00	0 00	0 50	0 00	73 75	1 25	5.50	0 00	5 50	0 00	1.00	0 00	0.25	0 75	8 75	15.50	0 00	2 00	0 00	17 50	100
85	2 00	56 50	14 75	0.00	0 00	0.00	0 00	73 25	0 25	0.75	0 00	0 75	0.25	0 00	0.00	1.75	0 00	3 00	20 25	0 50	3 00	0 00	23 75	100
88	3.50	64.25	5 50	0.00	0 00	0.00	0.00	73 25	1 25	1 50	0.00	1.50	0.00	1 50	0.00	0 00	0.00	4 25	20.25	0 00	2 25	0 00	22 50	100
91	3 00	58 75	3 50	0.00	0 00	0.00	0 00	65 25	2 50	5 75	0.00	5 75	0.25	1 25	0.00	5 75	0.00	15 50	17.50	0.00	1 75	0.00	19.25	100
93	6 25	49 25	7 25	0.00	0.00	0.00	0 00	62.75	1 75	0 25	0.00	0 25	9.00	2 25	0.00	1 50	0.00	14 75	20 50	0.00	2 00	0.00	22 50	100
96	3 25	58.75	9 25	0 00	0 00	0 00	0 00	71 25	1 75	1 75	0 00	1.75	1 00	1.00	0 00	1 00	0 25	6.75	20 75	1 25	0 00	0.00	22 00	100
99	5 75	55.75	9 00	0 00	0.00	1 00	0 00	71 50	1.00	2 00	0 00	2.00	0 25	1 25	0 00	0.00	0 25	4.75	21 00	0.00	2 75	0.00	23 75	100
98	7 50	52 25	10 75	0 00	0 00	0 75	0 00	71 25	2 50	1 75	0.00	1 75	1.50	1 25	0.00	1 25	0 00	8 25	19 25	0 00	1 25	0 00	20.50	100
99	6 75	52 75	2 75	0 00	0 00	0 00	0 00	62 25	2 00	9 25	0 00	9 25	1 25	1 50	0 00	0 25	0.00	14 25	20.25	0.00	3.25	0.00	23 50	100
99	5 75	52 75	12 50	0 00	0 00	0 00	0.00	71 00	1 50	0 25	0 00	0 25	6 75	1 00	0 00	0.00	0 00	9 50	18 50	0 00	1 00	0 00	19.50	100
100	5 25	53 00	5 75	0 00	0 00	0 00	0 00	64 00	1.25	3 50	0 00	3 50	5 25	0 75	0 00	3 50	0 00	14 25	19.75	0 00	2 00	0 00	21.75	100
102	7 00	55 25	7 50	0 00	0 00	0 00	0 00	69 75	3 00	0 75	0 00	0 75	5 50	1 25	0 00	0 00	0 00	10 50	17.00	0 00	2 75	0 00	19 75	100
104	5 00	66 25	3.50	0 00	0 00	0 00	0 00	74 75	1.25	0 50	0 00	0 50	0 75	0 75	0 00	0 75	0 00	4 00	20 75	0 00	0 50	0 00	21 25	100
106	3 75	59 25	3 75	0 00	0 00	0 00	0 00	66 75	0 75	6 50	0 00	6 50	3 00	1.75	0 00	1 75	0 00	13 75	19 50	0.00	0 00	0 00	19 50	100
107	8 50	56 75	9 50	0 00	0 00	0 00	0 00	74.75	1 00	0 00	0 00	0 00	1 00	0 75	0 00	1 25	0 00	4.00	21 00	0 00	0 25	0 00	21 25	100
110	4 25	66 25	0 75	0 00	0 00	0 00	0 00	71 25	1 00	0 00	0 00	0 00	1 00	0 50	0 00	0 00	0 00	2 50	25 75	0 00	0 50	0 00	26 25	100
111	3 50	65 25	5 25	0 00	0.00	0 00	0 00	74 00	1.00	0 00	0 00	0 00	7 00	1 00	0.00	0 00	0.00	9 00	15 75	0 00	1 25	0 00	17.00	100
Max	11.50	66.25	22.25	0.00	2.00	1.00	0.75	79.25	3.25	37.00	15.00	37.00	9.00	6.50	0.00	7.00	2.00	42.50	26.00	2.75	15.00	0.75	27.75	
Min	2.00	39.00	0.75	0.00	0.00	0.00	0.00	57.50	0.00	0.00	0.00	0.00	0.00	0.00	0.00	0.00	0.00	2.50	0.00	0.00	0.00	0.00	0.00	
Avg	5.26	55.61	6.31	0.00	0.15	0.11	0.05	69.49	1.33	7.14	0.69	7.73	1.21	1.55	0.00	1.01	0.12	12.94	13.91	0.26	3.39	0.02	17.67	

Table 4.1 *(Continued)*: Point–count data for the studied sandstones. All values in volume percent.

Well Name	Depth ft	Framework Composition of the Sandstones								Authigenic Mineral Cements and Replacement Minerals												Types of Porosity					Total
		MCQU	MCQN	PCQ	Feld.	R.F.	H.M.	Det. Clay	Total	Qtz. Over.	Mic. Qtz.	Opal	Kao. P.F.	Kao. Rep.	Kao Total	Clay Coat	FeOx	Gyp.	Halite	Calcite	Total	Inter	Intra	OVSP	Frac.	Total	
RB-A1	12340	11.25	61.50	2.00	0.00	0 25	0.25	0.00	75.25	1.00	0.00	0.50	10.00	0.00	10.00	1.75	11.50	0.00	0.00	0.00	24.75	0.00	0.00	0.00	0.00	0.00	100
RB-A1	12341	1.75	76.25	4.00	0.00	0.75	0.00	1.25	84.00	2.00	0.00	0.00	4.25	0.75	5.00	0.50	4.00	0.00	0.75	0.00	12.25	3 75	0.00	0.00	0.00	3.75	100
RB-A1	12460	10.00	69.00	7.75	0.00	0.00	0.00	0.00	86.75	0.75	0.00	0.00	0.00	0.00	0.00	0.00	1.25	0.00	0.00	0.00	2.00	11.25	0.00	0.00	0.00	11.25	100
RB-A5	12208	3.50	66.50	7.50	0.00	0.00	0.00	0.00	77.50	2.25	0.50	0.50	1.25	0.00	1.25	1.75	2.75	0.00	3.25	0.00	12.25	10.25	0.00	0.00	0.00	10.25	100
RB-A5	12262	4.00	66.75	10.00	0.00	0.00	0.25	2.25	83.25	3.25	0.00	0.00	1.25	0.00	1.25	3.50	5.75	0.00	0.00	0.00	13.75	3.00	0.00	0.00	0.00	3.00	100
RB-A5	12268	2.75	80.75	2.25	0.00	0.00	0.00	1.25	87.00	1.25	0.00	0.00	1.00	0.00	1.00	2.50	2.50	0.00	1.50	0.00	8.75	4.25	0 00	0.00	0.00	4.25	100
RB-A5	12287	3.25	71.25	4.25	0.00	0.00	0.00	0.00	78.75	0.25	0.00	0.00	0.00	0.00	0.00	17 00	4.00	0.00	0.00	0.00	21.25	0.00	0.00	0.00	0.00	0.00	100
RB-A5	12305	5.75	69.50	4 25	0.00	0.00	0.00	0.00	79.50	1.75	0.00	0.00	0.00	0.00	0.00	18.00	0.00	0 00	0.00	0.00	19.75	0.75	0.00	0.00	0.00	0.75	100
RB-A5	12308	2.25	78.50	1.00	0.00	0.00	0.00	0.75	82.50	0.75	0.00	0.00	0.00	0.00	0.00	8.50	1.25	0.00	5.25	0.00	15.75	1.75	0 00	0.00	0.00	1.75	100
RB-A5	12325	5.25	77.00	2.50	0.00	0.00	0.00	0.00	84.75	0.50	0 00	0.00	0.00	0.00	0.00	1.75	5.25	0.00	3.50	0.00	11.00	4.00	0 00	0.25	0.00	4.25	100
RB-A5	12332	6.50	75.50	5.00	0.00	0.00	0.00	0.00	87.00	0.25	0.00	0.00	0.00	0.00	0.00	0.25	9.50	0.00	0.25	0.00	10.25	2.50	0.00	0.25	0.00	2.75	100
RB-B3	12337	4.50	77.50	0.75	0.00	0.50	0.00	0.75	84.00	1.25	0 00	0.00	5 75	0.00	5.75	4.25	3.25	0.00	1.50	0 00	16.00	0.00	0.00	0.00	0.00	0.00	100
RB-B3	12366.7	2.50	74.00	5.50	0.00	0.25	0.00	0.75	83.00	1.25	0.00	0.00	1.25	0.00	1.25	2 25	10.00	0.00	1.75	0.00	16.50	0.50	0.00	0.00	0.00	0.50	100
RB-B3	12382.6	6.50	74.50	3.25	0.00	0.50	0.00	0.00	84.75	0.75	0.00	0.00	0.00	0.00	0.00	8.75	4.25	0.00	0.25	0.00	14.00	1 25	0.00	0.00	0 00	1 25	100
RB-B3	12401	5.00	69.75	5.25	0.00	0.50	0.00	0.00	80.50	2.00	0.00	0.00	0.00	0.00	0.00	2.25	2.75	0.00	1.50	2.25	10.75	8 75	0.00	0.00	0.00	8.75	100
RB-B4	12403	2.00	74.25	2.50	0.00	0.50	0.00	0.00	79.25	1.00	0.00	0 00	0.75	0.00	0.75	2.00	5.75	0.00	6.00	1.50	17.00	3 25	0 00	0.50	0.00	3.75	100
RB-B4	12404	2.00	69.75	7.25	0.00	0.00	0.00	0.00	79.00	1 25	0.00	0.00	0.50	0.00	0.50	1.75	0.50	0.00	1.50	0.75	6.25	14.00	0.00	0.75	0.00	14.75	100
RB-B4	12414	2.00	72.50	3.25	0.00	0.00	0.00	0.00	77.75	1 00	0.00	0.00	0.00	0.00	0.00	0.75	4.75	0.00	7 75	0.00	14.25	5.50	0 00	2.50	0.00	8.00	100
RB-B4	12420	6.25	67.75	5.00	0.00	0 50	0.00	0.00	79.50	1.25	2.50	0.00	0.25	0.00	0.25	0 75	3.50	0.00	1.00	0 00	9.25	9.50	0 00	1.75	0.00	11.25	100
RB-B4	12439	3.75	72.00	3.50	0.00	0.00	0.00	0.75	80.00	0.50	0.00	1.25	1.50	0.00	1 50	5.25	2.25	0.00	3 25	0 00	14.00	6.00	0 00	0.00	0.00	6.00	100
RB-B4	12454	2.50	77 50	1.75	0.00	0.00	0.25	0.00	82.00	0.25	0.00	0.00	3.00	0.00	3 00	4.50	5.75	0.00	1 25	0.00	14.75	3.25	0.00	0.00	0.00	3.25	100
RB-B4	12470	3.00	76.75	1.75	0.00	0.00	0.00	0.00	81.50	0.50	0.00	0.00	5.50	0.00	5.50	10.25	0.75	0.00	0.00	0.00	17.00	1.50	0.00	0.00	0.00	1.50	100
RB-B4	12492	1.00	74.50	4.75	0.00	0.00	0.00	0.00	80.25	1.00	0.00	0.00	0.75	0.00	0.75	1.75	1.25	0.00	2.00	1.50	8.25	10.50	0 00	1.00	0.00	11.50	100
RB-B4	12501	3.50	77.75	1.25	0.00	0.00	0.00	0.00	82.50	0.75	0.00	0.00	2.00	0.00	2.00	2 00	2.25	0.00	3.25	0.75	11.00	6.25	0.00	0.25	0.00	6.50	100
RB-B4	12509.6	2.50	78.50	0.75	0.00	0.00	0.00	0.00	81.75	0.50	0.00	0.00	0.50	0.00	0.50	1 50	10.75	0.00	1.00	0.00	14.25	3 75	0.00	0.25	0.00	4.00	100
RB-B4	12520	3.25	79.25	2.25	0.00	0.00	0.00	0.00	84.75	0.25	0.00	0.00	0 25	0.00	0.25	0.50	11.75	0.00	1.25	0.00	14.00	1.25	0 00	0.00	0.00	1 25	100
RB-B4	12526	2.75	78.00	0.75	0.00	0.00	0.00	0.00	81.50	0.25	0.00	0.00	3.75	0.00	3.75	2.75	5.25	0.00	0.25	0.00	12.25	5.25	0.00	1.00	0.00	6.25	100
RB-B4	12533	0.00	77.75	0.00	0.00	0.00	0.00	0.00	77.75	0.00	0.00	0.00	0.00	0.00	0.00	21.50	0.75	0.00	0.00	0.00	22.25	0.00	0 00	0 00	0.00	0 00	100
RB-B7	12194	2.00	76.25	0.00	0.00	0.00	0.25	0.00	78.50	0.25	0.00	0.00	0.25	0.00	0 25	2.00	2.00	0.00	5 75	0.25	10.50	10 50	0 25	0.25	0.00	11.00	100
RB-B7	12205	2.50	81.00	1.25	0.00	0.00	0 00	0.00	84.75	0.00	0.00	0.00	2.00	0.00	2.00	2.50	0.25	0.00	1.00	0.00	5.75	8.25	0 00	1.25	0 00	9.50	100
RB-B7	12213	4.50	80 75	0.50	0 00	0.00	0 00	0.00	85.75	0.00	0.00	0.00	0 25	0.00	0.25	3.00	3.00	0.00	4.75	0.00	11.00	3 25	0 00	0.00	0.00	3.25	100
RB-B7	12215	5.75	74.00	2.00	0.00	0.00	0 00	0.00	81.75	0.25	0.00	0.00	1 75	0.00	1.75	4 75	1.75	0.00	7.75	0.00	16.25	2.00	0 00	0.00	0.00	2.00	100
RB-B7	12236	2.75	82.75	1.25	0.00	0.00	0.00	0.00	86.75	0.00	0 00	0.00	1.00	0.00	1.00	1.25	5.50	0 00	0.00	0.25	8.00	5.25	0.00	0.00	0 00	5.25	100
RB-B7	12251	3.25	81.25	3.00	0.00	0.00	0.00	0.00	87.50	0.00	0.00	0.00	0 00	0.00	0.00	2.25	0.00	0.00	4 75	0.00	7.00	5.25	0.00	0.25	0.00	5 50	100
RB-B7	12253	6.25	70.50	4 25	0.00	0.00	0.00	0.00	81.00	0.00	0.00	0.00	0.75	0.00	0.75	2.75	0.50	0.00	2 00	0 00	6.00	9 50	0.00	3.50	0.00	13.00	100
RB-B7	12255	1.75	79 75	0.50	0.00	0.00	0.00	0.00	82.00	0.25	0.00	0.00	0.25	0.00	0 25	5.50	1.50	0.00	3 25	0.00	10 75	7.25	0 00	0 00	0.00	7.25	100
RB-B7	12273	2.00	84.00	2.25	0.00	0.00	0.00	0.00	88.25	0 25	0.00	0.00	0.50	0.00	0 50	3.50	2.50	0.00	1.00	0.00	7.75	4.00	0.00	0 00	0.00	4.00	100
RB-B7	12275	1.25	83.75	0.00	0.00	0.00	0.00	0.00	85.00	0 00	0.00	0.00	1.25	0 00	1.25	4 50	2 00	0.00	5.00	0.00	12.75	2.25	0.00	0 00	0.00	2.25	100
RB-B7	12291	4.25	72.75	0.75	0.00	0.25	0 00	0.00	78.00	0.25	0.00	0.00	0.00	0.00	0.00	8 50	10.75	0.00	0.00	0.00	19.50	2.50	0 00	0.00	0 00	2.50	100
RB-B7	12308	3.75	76.75	1.00	0.00	0.25	0.00	0.00	81.75	0.25	0.00	0.00	2.00	0.00	2.00	4.25	4.75	0.00	1.50	0.50	13.25	5 00	0.00	0.00	0.00	5.00	100
RB-B7	12311	2.50	80.50	0.25	0.00	0.00	0.00	0.00	83.25	0.25	0 00	0.00	0.25	0.00	0.25	5.50	6.50	0.00	2.25	0.00	14.75	2 00	0 00	0.00	0.00	2.00	100
RB-C2	12290	3.25	70.00	4.25	0.00	0.50	0.00	0.75	78.75	0.50	0.00	0.00	0.00	0.00	0.00	6.00	1.25	0 00	6.50	0.00	14.25	6 75	0.25	0.00	0.00	7.00	100
RB-C2	12341	1.25	74 25	3 25	0.00	0 50	0.00	0.00	79.25	2.50	0.00	0.00	3.50	0.00	3.50	1.25	13.50	0.00	0.00	0.00	20.75	0.00	0.00	0 00	0.00	0.00	100
RB-C2	12353	3.25	74.75	4.25	0.00	0.00	0.00	0.00	82.25	2.50	0.00	0.00	0.00	0.00	0.00	2.00	2.50	0.00	5 00	0.00	12.00	5.50	0 25	0 00	0.00	5.75	100
RB-C2	12368	5.50	70 25	5.00	0.00	0.00	0.00	0.00	80.75	0 00	0.00	0.00	0.00	0.00	0.00	11.25	0 25	0.00	5 00	0.00	16.50	2.75	0.00	0 00	0.00	2.75	100
Max		11.25	84.00	10.00	0.00	0.75	0.25	2.25	88.25	3.25	2.50	1.25	10.00	0.75	10.00	21.50	13.50	0.00	7.75	2.25	24.75	14.00	0.25	3.50	0.00	14.75	
Min		0.00	61.50	0.00	0.00	0.00	0.00	0.00	75.25	0.00	0.00	0.00	0.00	0.00	0.00	0.00	0.00	0.00	0.00	0.00	0.00	0.00	0.00	0.00	0.00	0.00	
Avg		3.67	75.06	2.97	0.00	0.12	0.02	0.19	82.03	0.76	0.07	0.05	1.27	0.02	1.29	4.42	4.04	0.00	2.30	0.17	13.12	4.63	0.02	0.31	0.00	4.66	

a e - : ompositionoie

S. No	% in the Framework Composition				
	Q %	Feld. %	R.F. %	H.M. %	Det. Clay %
1- Araba Formation					
1	98.13	0.00	0.37	0.00	1.50
2	99.47	0.00	0.53	0.00	0.00
3	99.61	0.00	0.39	0.00	0.00
4	99.28	0.00	0.72	0.00	0.00
5	100.00	0.00	0.00	0.00	0.00
6	100.00	0.00	0.00	0.00	0.00
7	97.14	0.00	0.00	0.00	2.86
8	100.00	0.00	0.00	0.00	0.00
9	100.00	0.00	0.00	0.00	0.00
10	100.00	0.00	0.00	0.00	0.00
11	100.00	0.00	0.00	0.00	0.00
Max	100.00	0.00	0.72	0.00	2.86
Min	97.14	0.00	0.00	0.00	0.00
Avg	99.42	0.00	0.18	0.00	0.40
2- Naqus Formation					
12	100.00	0.00	0.00	0.00	0.00
13	99.60	0.00	0.00	0.40	0.00
14	100.00	0.00	0.00	0.00	0.00
15	99.52	0.00	0.00	0.48	0.00
16	98.89	0.00	1.11	0.00	0.00
17	98.23	0.00	1.77	0.00	0.00
18	98.94	0.00	0.00	0.00	1.06
19	100.00	0.00	0.00	0.00	0.00
20	99.32	0.00	0.68	0.00	0.00
21	98.63	0.00	0.00	0.34	1.03
22	100.00	0.00	0.00	0.00	0.00
23	99.25	0.00	0.75	0.00	0.00
24	100.00	0.00	0.00	0.00	0.00
25	100.00	0.00	0.00	0.00	0.00
26	100.00	0.00	0.00	0.00	0.00
27	99.26	0.00	0.74	0.00	0.00
28	100.00	0.00	0.00	0.00	0.00
29	100.00	0.00	0.00	0.00	0.00
30	99.60	0.00	0.40	0.00	0.00
31	100.00	0.00	0.00	0.00	0.00
32	100.00	0.00	0.00	0.00	0.00
33	100.00	0.00	0.00	0.00	0.00
34	100.00	0.00	0.00	0.00	0.00
35	97.39	0.00	2.61	0.00	0.00
36	98.35	0.00	1.65	0.00	0.00
37	98.55	0.00	0.00	1.45	0.00
38	100.00	0.00	0.00	0.00	0.00
39	98.90	0.00	0.00	1.10	0.00
40	99.32	0.00	0.00	0.68	0.00
41	100.00	0.00	0.00	0.00	0.00
42	100.00	0.00	0.00	0.00	0.00
43	100.00	0.00	0.00	0.00	0.00
44	100.00	0.00	0.00	0.00	0.00
45	100.00	0.00	0.00	0.00	0.00
46	98.60	0.00	0.00	1.40	0.00
47	98.95	0.00	0.00	1.05	0.00
48	100.00	0.00	0.00	0.00	0.00
49	100.00	0.00	0.00	0.00	0.00
50	100.00	0.00	0.00	0.00	0.00
51	100.00	0.00	0.00	0.00	0.00
52	100.00	0.00	0.00	0.00	0.00
53	100.00	0.00	0.00	0.00	0.00
54	100.00	0.00	0.00	0.00	0.00
55	100.00	0.00	0.00	0.00	0.00
56	100.00	0.00	0.00	0.00	0.00
57	100.00	0.00	0.00	0.00	0.00
Max	100.00	0.00	2.61	1.45	1.06
Min	97.39	0.00	0.00	0.00	0.00
Avg	99.58	0.00	0.22	0.33	0.05

S. No	Sample No.	% in the Framework Composition				
		Q %	Feld. %	R.F. %	H.M. %	Det. Clay %
3- Subsurface						
RB-A1	12540	99.34	0.00	0.33	0.33	0.00
RB-A1	12544	97.62	0.00	0.89	0.00	1.49
RB-A1	12548	100.00	0.00	0.00	0.00	0.00
RB-A5	12268	100.00	0.00	0.00	0.00	0.00
RB-A5	12262	97.00	0.00	0.00	0.30	2.70
RB-A3	12266	98.56	0.00	0.00	0.00	1.44
RB-A5	12287	100.00	0.00	0.00	0.00	0.00
RB-A5	12285	100.00	0.00	0.00	0.00	0.00
RB-A5	12296	99.09	0.00	0.00	0.00	0.91
RB-A5	12635	100.00	0.00	0.00	0.00	0.00
RB-A5	12633	100.00	0.00	0.00	0.00	0.00
RB-B3	12457	98.51	0.00	0.60	0.00	0.89
RB-B3	12458	98.80	0.00	0.30	0.00	0.90
RB-B3	12462	99.41	0.00	0.59	0.00	0.00
RB-B3	12461	99.38	0.00	0.62	0.00	0.00
RB-B4	12463	99.37	0.00	0.63	0.00	0.00
RB-B4	12464	100.00	0.00	0.00	0.00	0.00
RB-B4	12414	100.00	0.00	0.00	0.00	0.00
RB-B4	12420	99.37	0.00	0.63	0.00	0.00
RB-B4	12409	99.06	0.00	0.00	0.00	0.94
RB-B4	12454	99.70	0.00	0.00	0.30	0.00
RB-B4	12470	100.00	0.00	0.00	0.00	0.00
RB-B4	12402	100.00	0.00	0.00	0.00	0.00
RB-B4	12504	100.00	0.00	0.00	0.00	0.00
RB-B4	12509	100.00	0.00	0.00	0.00	0.00
RB-B4	12520	100.00	0.00	0.00	0.00	0.00
RB-B4	12528	100.00	0.00	0.00	0.00	0.00
RB-B4	12533	100.00	0.00	0.00	0.00	0.00
RB-B7	12194	99.68	0.00	0.00	0.32	0.00
RB-B7	12205	100.00	0.00	0.00	0.00	0.00
RB-B7	12213	100.00	0.00	0.00	0.00	0.00
RB-B7	12215	100.00	0.00	0.00	0.00	0.00
RB-B7	12238	100.00	0.00	0.00	0.00	0.00
RB-B7	12251	100.00	0.00	0.00	0.00	0.00
RB-B7	12253	100.00	0.00	0.00	0.00	0.00
RB-B7	12255	100.00	0.00	0.00	0.00	0.00
RB-B7	12279	100.00	0.00	0.00	0.00	0.00
RB-B7	12279	100.00	0.00	0.00	0.00	0.00
RB-B7	12291	99.68	0.00	0.32	0.00	0.00
RB-B7	12309	99.69	0.00	0.31	0.00	0.00
RB-B7	12311	100.00	0.00	0.00	0.00	0.00
RB-B7	12290	98.41	0.00	0.63	0.00	0.95
RB-C2	12340	99.37	0.00	0.63	0.00	0.00
RB-C2	12359	100.00	0.00	0.00	0.00	0.00
RB-C2	12368	100.00	0.00	0.00	0.00	0.00
Max		100.00	0.00	0.89	0.33	2.70
Min		97.00	0.00	0.00	0.00	0.00
Avg		99.60	0.00	0.14	0.03	0.23

Table 4.3: Frequency distribution of different types of quartz.

S. No	MCQ			PCQ				Total	%MCQ	%PCQ	P/M	MCQU%	MCQN%	U/N	2-3%	3-5%	>5%
	MCQU	MCQN	Total	2-3	3-5	>5	Total	Quartz	In QT	In QT	Ratio	In MCQT	In MCQT	Ratio	In PCQ	In PCQ	In PCQ
1	1.75	62.50	64.25	0.00	0.75	0.50	1.25	65.50	98.09	1.91	0.02	2.72	97.28	0.03	0.00	60.00	40.00
2	3.33	55.33	58.67	1.00	1.33	1.33	3.67	62.33	94.12	5.88	0.06	5.68	94.32	0.06	27.27	36.36	36.36
3	2.50	58.00	60.50	0.50	0.50	3.00	4.00	64.50	93.80	6.20	0.07	4.13	95.87	0.04	12.50	12.50	75.00
4	1.75	63.75	65.50	2.50	0.25	0.50	3.25	68.75	95.27	4.73	0.05	2.67	97.33	0.03	76.92	7.69	15.38
5	1.50	56.75	58.25	0.50	0.25	0.75	1.50	59.75	97.49	2.51	0.03	2.58	97.42	0.03	33.33	16.67	50.00
6	3.25	55.00	58.25	0.50	0.25	0.00	0.75	59.00	98.73	1.27	0.01	5.58	94.42	0.06	66.67	33.33	0.00
7	0.50	58.75	59.25	0.00	0.00	0.25	0.25	59.50	99.58	0.42	0.00	0.84	99.16	0.01	0.00	0.00	100.00
8	1.50	55.50	57.00	0.25	0.25	0.25	0.75	57.75	98.70	1.30	0.01	2.63	97.37	0.03	33.33	33.33	33.33
9	1.50	49.00	50.50	0.25	0.25	0.25	0.75	51.25	98.54	1.46	0.01	2.97	97.03	0.03	33.33	33.33	33.33
10	2.25	52.75	55.00	0.50	0.50	1.00	2.00	57.00	96.49	3.51	0.04	4.09	95.91	0.04	25.00	25.00	50.00
11	2.75	70.25	73.00	1.50	0.75	0.50	2.75	75.75	96.37	3.63	0.04	3.77	96.23	0.04	54.55	27.27	18.18
Max	3.33	70.25	73.00	2.50	1.33	3.00	4.00	75.75	99.58	6.20	0.07	5.68	99.16	0.06	76.92	60.00	100.00
Min	0.50	49.00	50.50	0.00	0.00	0.00	0.25	51.25	93.80	0.42	0.00	0.84	94.32	0.01	0.00	0.00	0.00
Avg	2.05	57.96	60.02	0.68	0.46	0.76	1.90	61.92	97.02	2.98	0.03	3.42	96.58	0.04	32.99	25.95	41.05
12	4.67	64.67	69.33	0.00	0.67	1.67	2.33	71.67	96.74	3.26	0.03	6.73	93.27	0.07	0.00	28.57	71.43
13	5.00	51.00	56.00	0.75	1.00	4.50	6.25	62.25	89.96	10.04	0.11	8.93	91.07	0.10	12.00	16.00	72.00
15	2.00	55.25	57.25	1.25	1.00	5.25	7.50	64.75	88.42	11.58	0.13	3.49	96.51	0.04	16.67	13.33	70.00
18	3.00	55.00	58.00	2.00	3.67	5.67	11.33	69.33	83.65	16.35	0.20	5.17	94.83	0.05	17.65	32.35	50.00
22	3.25	52.50	55.75	4.00	2.00	5.00	11.00	66.75	83.52	16.48	0.20	5.83	94.17	0.06	36.36	18.18	45.45
25	4.50	55.00	59.50	2.75	3.25	3.75	9.75	69.25	85.92	14.08	0.16	7.56	92.44	0.08	28.21	33.33	38.46
28	6.50	43.25	49.75	4.25	5.50	10.25	20.00	69.75	71.33	28.67	0.40	13.07	86.93	0.15	21.25	27.50	51.25
31	7.00	45.50	52.50	2.50	1.25	16.25	20.00	72.50	72.41	27.59	0.38	13.33	86.67	0.15	12.50	6.25	81.25
32	6.00	57.25	63.25	3.50	2.50	3.75	9.75	73.00	86.64	13.36	0.15	9.49	90.51	0.10	35.90	25.64	38.46
35	4.50	58.00	62.50	2.75	2.50	4.25	9.50	72.00	86.81	13.19	0.15	7.20	92.80	0.08	28.95	26.32	44.74
39	2.50	66.25	68.75	1.25	1.25	2.00	4.50	73.25	93.86	6.14	0.07	3.64	96.36	0.04	27.78	27.78	44.44
40	4.00	52.50	56.50	1.00	0.75	7.75	9.50	66.00	85.61	14.39	0.17	7.08	92.92	0.08	10.53	7.89	81.58
43	4.50	50.50	55.00	0.00	1.00	1.50	2.50	57.50	95.65	4.35	0.05	8.18	91.82	0.09	0.00	40.00	60.00
45	6.25	57.75	64.00	1.75	0.50	7.75	10.00	74.00	86.49	13.51	0.16	9.77	90.23	0.11	17.50	5.00	77.50
47	11.50	39.00	50.50	5.75	3.00	11.25	20.00	70.50	71.63	28.37	0.40	22.77	77.23	0.29	28.75	15.00	56.25

Table 4.3 *(Ccontinued)*: Frequency distribution of different types of quartz.

S. No	MCQ			PCQ				Total Quartz	%MCQ in QT	%PCQ in QT	P/M Ratio	MCQU% in MCQT	MCQN% in MCQT	U/N Ratio	2-3% in PCQ	3-5% in PCQ	>5% in PCQ
	MCQU	MCQN	Total	2-3	3-5	>5	Total										
51	5.00	54.75	59.75	1.50	1.50	4.00	7.00	66.75	89.51	10.49	0.12	8.37	91.63	0.09	21.43	21.43	57.14
52	6.00	44.75	50.75	2.75	3.25	7.75	13.75	64.50	78.68	21.32	0.27	11.82	88.18	0.13	20.00	23.64	56.36
55	4.25	55.75	60.00	0.50	1.50	3.00	5.00	65.00	92.31	7.69	0.08	7.08	92.92	0.08	10.00	30.00	60.00
58	3.25	55.50	58.75	1.00	1.00	1.25	3.25	62.00	94.76	5.24	0.06	5.53	94.47	0.06	30.77	30.77	38.46
61	2.75	62.50	65.25	0.00	0.75	3.50	4.25	69.50	93.88	6.12	0.07	4.21	95.79	0.04	0.00	17.65	82.35
62	4.25	58.75	63.00	1.25	2.00	4.00	7.25	70.25	89.68	10.32	0.12	6.75	93.25	0.07	17.24	27.59	55.17
65	4.00	55.25	59.25	1.75	0.75	2.75	5.25	64.50	91.86	8.14	0.09	6.75	93.25	0.07	33.33	14.29	52.38
67	4.75	57.75	62.50	0.25	0.25	3.25	3.75	66.25	94.34	5.66	0.06	7.60	92.40	0.08	6.67	6.67	86.67
70	8.50	57.50	66.00	2.00	2.50	4.25	8.75	74.75	88.29	11.71	0.13	12.88	87.12	0.15	22.86	28.57	48.57
73	9.00	57.25	66.25	1.50	3.00	3.75	8.25	74.50	88.93	11.07	0.12	13.58	86.42	0.16	18.18	36.36	45.45
76	7.50	55.00	62.50	0.00	0.50	5.00	5.50	68.00	91.91	8.09	0.09	12.00	88.00	0.14	0.00	9.09	90.91
79	8.25	48.75	57.00	0.50	5.00	16.75	22.25	79.25	71.92	28.08	0.39	14.47	85.53	0.17	2.25	22.47	75.28
80	5.50	55.50	61.00	0.75	1.50	4.00	6.25	67.25	90.71	9.29	0.10	9.02	90.98	0.10	12.00	24.00	64.00
83	7.75	57.25	65.00	2.50	2.00	3.75	8.25	73.25	88.74	11.26	0.13	11.92	88.08	0.14	30.30	24.24	45.45
85	2.00	56.50	58.50	3.50	5.00	6.25	14.75	73.25	79.86	20.14	0.25	3.42	96.58	0.04	23.73	33.90	42.37
86	3.50	64.25	67.75	1.50	0.75	3.25	5.50	73.25	92.49	7.51	0.08	5.17	94.83	0.05	27.27	13.64	59.09
87	3.00	58.75	61.75	0.75	0.50	2.25	3.50	65.25	94.64	5.36	0.06	4.86	95.14	0.05	21.43	14.29	64.29
90	6.25	49.25	55.50	1.50	1.25	4.50	7.25	62.75	88.45	11.55	0.13	11.26	88.74	0.13	20.69	17.24	62.07
92	3.25	58.75	62.00	1.25	4.75	3.25	9.25	71.25	87.02	12.98	0.15	5.24	94.76	0.06	13.51	51.35	35.14
94	5.75	55.75	61.50	0.75	2.00	6.25	9.00	70.50	87.23	12.77	0.15	9.35	90.65	0.10	8.33	22.22	69.44
96	7.50	52.25	59.75	0.75	2.25	7.75	10.75	70.50	84.75	15.25	0.18	12.55	87.45	0.14	6.98	20.93	72.09
98	6.75	52.75	59.50	0.75	0.50	1.50	2.75	62.25	95.58	4.42	0.05	11.34	88.66	0.13	27.27	18.18	54.55
99	5.75	52.75	58.50	3.00	1.50	8.00	12.50	71.00	82.39	17.61	0.21	9.83	90.17	0.11	24.00	12.00	64.00
100	5.25	53.00	58.25	2.75	1.00	2.00	5.75	64.00	91.02	8.98	0.10	9.01	90.99	0.10	47.83	17.39	34.78
102	7.00	55.25	62.25	2.25	2.75	2.50	7.50	69.75	89.25	10.75	0.12	11.24	88.76	0.13	30.00	36.67	33.33
104	5.00	66.25	71.25	0.50	1.75	1.25	3.50	74.75	95.32	4.68	0.05	7.02	92.98	0.08	14.29	50.00	35.71
106	3.75	59.25	63.00	1.25	0.25	2.25	3.75	66.75	94.38	5.62	0.06	5.95	94.05	0.06	33.33	6.67	60.00
107	8.50	56.75	65.25	2.25	2.50	4.75	9.50	74.75	87.29	12.71	0.15	13.03	86.97	0.15	23.68	26.32	50.00
110	4.25	66.25	70.50	0.50	0.25	0.00	0.75	71.25	98.95	1.05	0.01	6.03	93.97	0.06	66.67	33.33	0.00
111	3.50	65.25	68.75	2.25	1.25	1.75	5.25	74.00	92.91	7.09	0.08	5.09	94.91	0.05	42.86	23.81	33.33
Max	11.50	66.25	71.25	5.75	5.50	16.75	22.25	79.25	98.95	28.67	0.40	22.77	96.58	0.29	66.67	51.35	90.91
Min	2.00	39.00	49.75	0.00	0.25	0.00	0.75	57.50	71.33	1.05	0.01	3.42	77.23	0.04	0.00	5.00	0.00
Avg	5.26	55.61	60.88	1.67	1.86	4.78	8.31	69.19	88.13	11.87	0.14	8.77	91.23	0.10	21.13	23.06	55.81

Table 4.3 *(Continued)*: Frequency distribution of different types of quartz.

Well Name	Depth Ft	MCQ			PCQ				Total Qtz	%MCQ in QT	%PCQ in QT	P/M Ratio	MCQU% in MCQT	MCQN% in MCQT	U/N Ratio	2-3% in PCQ	3-5% in PCQ	>5% in PCQ
		MCQU	MCQN	Total	2-3	3-5	>5	Total										
RB-A1	12340	11.25	61.50	72.75	0.25	1.25	0.50	2.00	74.75	97.32	2.68	0 03	15.46	84.54	0 18	12 50	62.50	25.00
RB-A1	12341	1.75	76.25	78.00	1.25	2.75	0.00	4.00	82.00	95.12	4.88	0.05	2 24	97.76	0 02	31.25	68.75	0.00
RB-A1	12460	10.00	69.00	79.00	2.50	1.50	3.75	7.75	86.75	91.07	8.93	0.10	12.66	87.34	0.14	32.26	19.35	48.39
RB-A5	12208	3.50	66.50	70.00	2 00	1.75	3.75	7.50	77.50	90.32	9.68	0 11	5 00	95.00	0 05	26.67	23.33	50.00
RB-A5	12262	4.00	66.75	70 75	4.50	3.00	2.50	10 00	80.75	87.62	12.38	0.14	5.65	94.35	0.06	45.00	30.00	25.00
RB-A5	12268	2.75	80.75	83 50	0.75	1.00	0.50	2 25	85.75	97.38	2.62	0.03	3.29	96.71	0.03	33.33	44.44	22.22
RB-A5	12287	3.25	71.25	74.50	2.75	0.50	1.00	4.25	78.75	94.60	5 40	0.06	4.36	95.64	0.05	64.71	11.76	23.53
RB-A5	12305	5 75	69.50	75.25	2.25	2 00	0.00	4.25	79.50	94.65	5.35	0.06	7.64	92.36	0.08	52.94	47.06	0 00
RB-A5	12808	2.25	78.50	80 75	0.50	0.50	0.00	1.00	81.75	98.78	1.22	0 01	2 79	97.21	0 03	50 00	50.00	0 00
RB-A5	12825	5.25	77.00	82.25	0.50	0 50	1.50	2.50	84.75	97.05	2 95	0.03	6.38	93.62	0.07	20.00	20.00	60.00
RB-A5	12832	6.50	75.50	82.00	2.00	2.50	0.50	5.00	87.00	94 25	5.75	0 06	7.93	92 07	0.09	40.00	50 00	10.00
RB-B3	12357	4.50	77.50	82.00	0.25	0.25	0.25	0.75	82.75	99 09	0.91	0.01	5.49	94.51	0.06	33.33	33.33	33.33
RB-B3	12368.7	2.50	74.00	76.50	2.00	2.50	1.00	5.50	82.00	93.29	6.71	0.07	3.27	96.73	0.03	36.36	45.45	18.18
RB-B3	12382.6	6.50	74.50	81.00	1.75	0.25	1.25	3.25	84.25	96.14	3.86	0.04	8.02	91.98	0.09	53.85	7.69	38.46
RB-B3	12401	5.00	69.75	74.75	1.25	2.75	1.25	5.25	80.00	93.44	6 56	0.07	6 69	93.31	0.07	23 81	52.38	23.81
RB-B4	12403	2.00	74.25	76.25	1.50	0 50	0.50	2.50	78.75	96.83	3.17	0.03	2.62	97.38	0 03	60.00	20.00	20.00
RB-B4	12404	2.00	69.75	71.75	1.75	4.00	1.50	7.25	79.00	90.82	9.18	0.10	2.79	97 21	0.03	24.14	55.17	20 69
RB-B4	12414	2.00	72.50	74.50	0.00	2.00	1.25	3.25	77.75	95.82	4.18	0.04	2.68	97.32	0.03	0.00	61.54	38.46
RB-B4	12420	6.25	67.75	74.00	2.25	1.00	1.75	5.00	79.00	93.67	6.33	0.07	8 45	91.55	0 09	45.00	20.00	35.00
RB-B4	12439	3.75	72.00	75.75	0.25	1.50	1.75	3.50	79.25	95.58	4.42	0.05	4.95	95.05	0.05	7.14	42.86	50.00
RB-B4	12454	2.50	77.50	80.00	0.75	0.50	0.50	1.75	81.75	97.86	2.14	0.02	3.13	96.88	0.03	42.86	28.57	28.57
RB-B4	12470	3.00	76.75	79.75	0.25	1.25	0.25	1.75	81.50	97.85	2.15	0.02	3.76	96.24	0.04	14.29	71.43	14.29
RB-B4	12492	1.00	74.50	75.50	2.00	1.25	1.50	4.75	80.25	94.08	5.92	0.06	1.32	98.68	0.01	42.11	26.32	31.58
RB-B4	12501	3.50	77.75	81.25	0.50	0.75	0.00	1.25	82.50	98.48	1.52	0.02	4.31	95.69	0.05	40.00	60.00	0.00
RB-B4	12509.6	2.50	78.50	81.00	0.50	0.25	0.00	0.75	81.75	99.08	0.92	0.01	3.09	96.91	0.03	66.67	33.33	0.00
RB-B4	12520	3.25	79.25	82.50	1.25	1.00	0.00	2.25	84.75	97.35	2.65	0.03	3.94	96.06	0.04	55.56	44.44	0.00
RB-B4	12526	2.75	78.00	80.75	0.25	0.50	0.00	0.75	81.50	99.08	0.92	0.01	3.41	96.59	0.04	33.33	66.67	0.00
RB-B4	12533	0.00	77.75	77.75	0.00	0.00	0.00	0.00	77.75	100.00	0.00	0 00	0.00	100.00	0.00	0.00	0.00	0.00
RB-B7	12194	2.00	76.25	78.25	0.00	0 00	0.00	0.00	78.25	100.00	0.00	0.00	2.56	97.44	0.03	0 00	0.00	0.00
RB-B7	12205	2.50	81.00	83.50	0.00	0.00	1.25	1.25	84.75	98.53	1.47	0 01	2.99	97 01	0.03	0.00	0.00	100.00
RB-B7	12213	4.50	80.75	85.25	0.00	0.50	0.00	0.50	85.75	99.42	0.58	0.01	5.28	94.72	0.06	0.00	100.00	0.00
RB-B7	12215	5.75	74.00	79.75	0.75	0.25	1.00	2.00	81.75	97.55	2.45	0.03	7 21	92.79	0.08	37.50	12.50	50.00
RB-B7	12236	2.75	82.75	85.50	0.50	0.00	0.75	1.25	86.75	98.56	1.44	0.01	3 22	96.78	0.03	40.00	0.00	60.00
RB-B7	12251	3.25	81.25	84.50	0.25	1.50	1 25	3.00	87.50	96.57	3.43	0.04	3.85	96.15	0.04	8.33	50.00	41.67
RB-B7	12253	6.25	70.50	76.75	1.25	0.00	3.00	4.25	81.00	94.75	5.25	0.06	8.14	91.86	0.09	29.41	0.00	70.59
RB-B7	12266	1.75	79.75	81.50	0.00	0.50	0.00	0.50	82.00	99.39	0.61	0.01	2.15	97.85	0.02	0.00	100.00	0.00
RB-B7	12273	2.00	84.00	86.00	1.50	0.75	0.00	2.25	88.25	97.45	2.55	0.03	2.33	97.67	0.02	66.67	33.33	0.00
RB-B7	12275	1.25	83.75	85.00	0.00	0.00	0.00	0.00	85.00	100.00	0.00	0.00	1.47	98.53	0.01	0.00	0.00	0.00
RB-B7	12291	4.25	72.75	77.00	0.50	0.25	0.00	0.75	77.75	99.04	0.96	0.01	5.52	94.48	0.06	66 67	33.33	0.00
RB-B7	12308	3.75	76.75	80.50	0.75	0.25	0.00	1.00	81.50	98.77	1.23	0.01	4.66	95.34	0.05	75 00	25.00	0.00
RB-B7	12311	2.50	80.50	83.00	0.25	0.00	0.00	0.25	83.25	99.70	0.30	0.00	3.01	96.99	0.03	100.00	0.00	0.00
RB-C2	12290	3.25	70.00	73.25	2.25	1.25	0.75	4.25	77.50	94.52	5.48	0.06	4.44	95.56	0.05	52.94	29.41	17.65
RB-C2	12341	1.25	74.25	75.50	1.25	1.00	1.00	3.25	78.75	95.87	4.13	0.04	1.66	98.34	0.02	38.46	30.77	30.77
RB-C2	12353	3.25	74.75	78.00	1.75	1.75	0.75	4.25	82.25	94.83	5.17	0.05	4.17	95.83	0.04	41.18	41.18	17.65
RB-C2	12368	5.50	70.25	75.75	0.50	1.25	3.25	5.00	80.75	93.81	6.19	0.07	7.26	92.74	0.08	10.00	25.00	65.00
Max		11.25	84.00	86.00	4.50	4.00	3.75	10.00	88.25	100.00	12.38	0.14	15.46	100.00	0.18	100.00	100.00	100.00
Min		0.00	61.50	70.00	0.00	0.00	0.00	0.00	74.75	87.62	0.00	0.00	0.00	84.54	0.00	0.00	0.00	0.00
Avg		3.67	75.06	78.73	1.05	1.04	0.88	2.97	81.70	96.34	3.66	0.04	4.69	95.31	0.05	34.52	35.04	29.77

Table 4.4: Point-counted porosity data for the studied sandstones.

S. No.	% porosity in total volume					% of different types in total porosity					1st Por.	2nd Por.	Oversize Pores							
	Inter.	Intra	OSP	Frac.	Total	Inter.	Intra	OSP	Frac.	Total	%	%	Empty	Filled by Cement	Total	Cement	PCP	PLoss Comp	PLoss Cement	Comp Index
1- Araba Formation																				
1	2.5	0.0	0.0	0.0	2.5	100.0	0.0	0.0	0.0	100.0	100.0	0.0	0.0	7.0	7.0	23.8	26.3	25.4	17.7	0.6
2	0.3	0.0	1.3	0.0	1.7	20.0	0.0	80.0	0.0	100.0	20.0	80.0	1.3	3.7	5.0	32.0	32.3	18.7	26.0	0.4
3	0.5	0.0	1.0	0.0	1.5	33.3	0.0	66.7	0.0	100.0	33.3	66.7	1.0	3.3	4.3	30.5	31.0	20.3	24.3	0.5
4	7.0	0.0	4.5	0.0	11.5	60.9	0.0	39.1	0.0	100.0	60.9	39.1	4.5	4.0	8.5	15.3	22.3	29.3	10.8	0.7
5	2.8	0.0	0.5	0.0	3.3	84.6	0.0	15.4	0.0	100.0	84.6	15.4	0.5	5.3	5.8	31.6	34.5	16.0	26.7	0.4
6	0.0	0.3	1.0	0.0	1.3	0.0	20.0	80.0	0.0	100.0	0.0	100.0	1.0	3.3	4.3	36.5	36.5	13.4	31.6	0.3
7	6.5	0.3	1.8	0.0	8.5	76.5	2.9	20.6	0.0	100.0	76.5	23.5	0.0	6.3	6.3	24.0	30.5	20.9	19.0	0.5
8	3.3	0.0	0.3	1.0	4.5	72.2	0.0	5.6	22.2	100.0	72.2	27.8	0.3	3.8	4.0	34.0	37.3	12.4	29.8	0.3
9	0.0	0.0	0.0	0.0	0.0	0.0	0.0	0.0	0.0	0.0	0.0	0.0	0.0	11.3	11.3	37.5	37.5	12.0	33.0	0.3
10	0.0	0.0	0.3	0.0	0.3	0.0	0.0	100.0	0.0	100.0	0.0	100.0	0.3	4.8	5.0	38.0	38.0	11.3	33.7	0.3
11	3.0	0.0	0.0	0.0	3.0	100.0	0.0	0.0	0.0	100.0	100.0	0.0	0.0	2.5	2.5	18.8	21.8	29.7	13.2	0.7
Max	7.0	0.3	4.5	1.0	11.5	100.0	20.0	100.0	22.2	100.0	100.0	100.0	4.5	11.3	11.3	38.0	38.0	29.7	33.7	0.7
Min	0.0	0.0	0.0	0.0	0.0	0.0	0.0	0.0	0.0	0.0	0.0	0.0	0.0	2.5	2.5	15.3	21.8	11.3	10.8	0.3
Avg	2.3	0.0	1.0	0.1	3.4	49.8	2.1	37.0	2.0	90.9	64.8	45.3	0.8	5.9	6.8	29.3	31.6	19.0	24.2	0.4
2- Naqus Formation																				
12	20.7	0.0	3.3	0.0	24.0	86.1	0.0	13.9	0.0	100.0	86.1	13.9	3.3	2.7	6.0	1.7	22.3	29.2	1.2	1.0
13	4.8	0.0	7.5	0.0	12.3	38.8	0.0	61.2	0.0	100.0	38.8	61.2	7.5	5.8	13.3	19.5	24.3	27.4	14.2	0.7
14	4.5	0.0	12.8	0.0	17.3	26.1	0.0	73.9	0.0	100.0	26.1	73.9	12.8	7.8	20.5	10.3	14.8	35.5	6.6	0.8
15	9.3	0.0	3.0	0.0	12.3	75.7	0.0	24.3	0.0	100.0	75.7	24.3	3.0	15.0	18.0	3.0	12.3	37.3	1.9	1.0
16	14.0	0.0	9.0	0.0	23.0	60.9	0.0	39.1	0.0	100.0	60.9	39.1	9.0	2.5	11.5	7.0	21.0	30.4	4.9	0.9
17	3.3	0.0	9.0	0.0	12.3	26.5	0.0	73.5	0.0	100.0	26.5	73.5	9.0	5.3	14.3	12.0	15.3	35.1	7.8	0.8
18	2.0	0.0	13.5	0.0	15.5	12.9	0.0	87.1	0.0	100.0	12.9	87.1	13.5	6.0	19.5	8.0	10.0	38.9	4.9	0.9
19	21.0	2.8	1.3	0.0	25.0	84.0	11.0	5.0	0.0	100.0	84.0	16.0	1.3	1.0	2.3	1.5	22.5	29.0	1.1	1.0
20	1.8	0.8	15.0	0.8	18.3	9.6	4.1	82.2	4.1	100.0	9.6	90.4	15.0	3.3	18.3	5.0	6.8	41.0	2.9	0.9
21	1.8	0.0	3.3	0.0	5.0	35.0	0.0	65.0	0.0	100.0	35.0	65.0	3.3	15.0	18.3	7.0	8.8	39.7	4.2	0.9
22	1.5	0.0	2.0	0.0	3.5	42.9	0.0	57.1	0.0	100.0	42.9	57.1	2.0	17.0	19.0	6.3	7.8	40.4	3.7	0.9
23	9.8	1.5	0.3	0.0	11.5	84.8	13.0	2.2	0.0	100.0	84.8	15.2	0.3	12.0	12.3	10.0	19.8	31.5	6.9	0.8
24	0.0	0.0	0.0	0.0	0.0	0.0	0.0	0.0	0.0	0.0	0.0	0.0	0.0	28.0	28.0	14.5	14.5	35.7	9.3	0.8
25	4.0	0.3	5.0	0.0	9.3	43.2	2.7	54.1	0.0	100.0	43.2	56.8	5.0	9.5	14.5	7.3	11.3	38.0	4.5	0.9
26	12.8	0.8	11.5	0.0	25.0	51.0	3.0	46.0	0.0	100.0	51.0	49.0	11.5	0.8	12.3	3.8	16.5	34.1	2.5	0.9
27	3.0	0.8	1.3	0.0	5.0	60.0	15.0	25.0	0.0	100.0	60.0	40.0	1.3	8.3	9.5	19.5	22.5	29.0	13.8	0.7
28	22.5	0.0	1.8	0.0	24.3	92.8	0.0	7.2	0.0	100.0	92.8	7.2	1.8	3.8	5.5	7.5	30.0	21.4	5.9	0.8
29	23.8	0.0	4.0	0.0	27.8	85.6	0.0	14.4	0.0	100.0	85.6	14.4	4.0	0.8	4.8	6.5	30.3	21.1	5.1	0.8
30	26.0	0.0	1.8	0.0	27.8	93.7	0.0	6.3	0.0	100.0	93.7	6.3	1.8	4.8	6.5	5.3	31.3	20.0	4.2	0.8
31	7.0	0.8	0.8	0.0	8.5	82.4	8.8	8.8	0.0	100.0	82.4	17.6	0.8	11.3	12.0	10.8	17.8	33.1	7.2	0.8
32	15.3	1.3	2.0	0.0	18.5	82.4	6.8	10.8	0.0	100.0	82.4	17.6	2.0	3.5	5.5	7.8	23.0	28.6	5.5	0.8
33	17.8	0.8	4.0	0.0	22.5	78.9	3.3	17.8	0.0	100.0	78.9	21.1	4.0	3.5	7.5	9.5	21.3	30.2	6.6	0.8
34	14.3	0.0	5.3	0.0	19.5	73.1	0.0	26.9	0.0	100.0	73.1	26.9	5.3	3.0	8.3	11.3	17.3	33.5	7.5	0.8
35	2.8	0.0	1.0	0.0	3.8	73.3	0.0	26.7	0.0	100.0	73.3	26.7	1.0	10.0	11.0	9.5	12.8	37.0	6.0	0.9
36	3.5	0.0	1.0	0.0	4.5	77.8	0.0	22.2	0.0	100.0	77.8	22.2	1.0	9.5	10.5	10.3	13.0	36.8	6.5	0.9
37	12.5	0.0	3.0	0.0	15.5	80.6	0.0	19.4	0.0	100.0	80.6	19.4	3.0	8.8	11.8	6.8	21.3	30.2	4.7	0.9
38	14.3	0.3	1.8	0.0	16.3	87.7	1.5	10.8	0.0	100.0	87.7	12.3	1.8	0.0	1.8	4.5	14.3	35.9	2.9	0.9
39	19.3	0.0	2.3	0.0	21.5	89.5	0.0	10.5	0.0	100.0	89.5	10.5	2.3	2.5	4.8	8.0	21.8	29.7	5.6	0.8
40	15.5	0.0	2.0	0.0	17.5	88.6	0.0	11.4	0.0	100.0	88.6	11.4	2.0	4.5	6.5	4.3	20.0	31.3	2.9	0.9
41	20.3	0.5	3.0	0.0	23.8	85.3	2.1	12.6	0.0	100.0	85.3	14.7	3.0	0.8	3.8	2.3	21.0	30.4	1.6	1.0
42	20.3	0.0	2.3	0.0	22.5	90.0	0.0	10.0	0.0	100.0	90.0	10.0	2.3	0.0	2.3	4.3	20.3	31.0	2.9	0.9
43	17.5	0.0	1.8	0.0	19.3	90.9	0.0	9.1	0.0	100.0	90.9	9.1	1.8	2.5	4.3	13.0	20.0	31.3	8.9	0.8
44	20.5	0.0	2.0	0.0	22.5	91.1	0.0	8.9	0.0	100.0	91.1	8.9	2.0	2.8	4.8	12.0	23.3	28.3	8.6	0.8
45	20.8	1.3	0.0	0.0	22.0	94.3	5.7	0.0	0.0	100.0	94.3	5.7	0.0	1.0	1.0	5.8	21.8	29.7	4.0	0.9
46	21.0	0.0	2.8	0.0	23.8	88.4	0.0	11.6	0.0	100.0	88.4	11.6	2.8	0.8	3.5	4.0	21.8	29.7	2.8	0.9
47	19.3	0.0	1.3	0.0	20.5	93.9	0.0	6.1	0.0	100.0	93.9	6.1	1.3	0.5	1.8	7.8	19.8	31.5	5.3	0.9
48	20.3	0.0	3.3	0.0	23.5	86.2	0.0	13.8	0.0	100.0	86.2	13.8	3.3	3.8	7.0	10.5	24.0	27.6	7.6	0.8
49	18.5	0.0	1.0	0.0	19.5	94.9	0.0	5.1	0.0	100.0	94.9	5.1	1.0	0.8	1.8	8.8	19.3	31.9	6.0	0.8
50	19.8	0.0	2.0	0.0	21.8	90.8	0.0	9.2	0.0	100.0	90.8	9.2	2.0	1.8	3.8	12.5	21.5	29.9	8.8	0.8
51	17.0	0.0	2.8	0.0	19.8	86.1	0.0	13.9	0.0	100.0	86.1	13.9	2.8	1.0	3.8	9.5	18.0	32.9	6.4	0.8
52	20.8	0.0	0.5	0.0	21.3	97.6	0.0	2.4	0.0	100.0	97.6	2.4	0.5	0.5	1.0	3.5	21.3	30.2	2.4	0.9
53	19.5	0.0	0.0	0.0	19.5	100.0	0.0	0.0	0.0	100.0	100.0	0.0	0.0	2.0	2.0	11.8	21.5	29.9	8.2	0.8
54	21.0	0.0	0.3	0.0	21.3	98.8	0.0	1.2	0.0	100.0	98.8	1.2	0.3	0.0	0.3	4.0	21.0	30.4	2.8	0.9
55	25.8	0.0	0.5	0.0	26.3	98.1	0.0	1.9	0.0	100.0	98.1	1.9	0.5	0.0	0.5	2.5	25.8	25.9	1.9	0.9
56	15.8	0.0	1.3	0.0	17.0	92.6	0.0	7.4	0.0	100.0	92.6	7.4	1.3	0.0	1.3	9.0	15.8	34.7	5.9	0.9
Max	26.0	2.8	15.0	0.8	27.8	100.0	15.0	87.1	4.1	100.0	100.0	90.4	15.0	28.0	28.0	19.5	31.3	41.0	14.2	1.0
Min	0.0	0.0	0.0	0.0	0.0	0.0	0.0	0.0	0.0	0.0	0.0	0.0	0.0	0.0	0.3	1.5	6.8	20.0	1.1	0.7
Avg	13.0	0.3	3.4	0.0	17.6	73.4	1.7	22.6	0.1	97.8	75.1	24.9	3.4	5.0	8.4	8.0	19.1	31.7	5.4	0.9

Table 4.4 *(Continued)*: Point-counted porosity data for the studied sandstones.

Well name	Depth, m	% porosity in total volume					% of different types in total porosity					1st Por. %	2nd Por. %	Oversize Pores			Cement	PCP	PLoss		Comp. index
		Inter	Intra	OSP	Frac	Total	Inter	Intra	OSP	Fra	Total			Empty	Filled by Cement	Total			Comp.	Cement	
RB-A1	12340.0	0.0	0.0	0.0	0 0	0.0	0.0	0.0	0 0	0.0	0.0	0.0	0 0	0.0	2 0	2 0	22.8	22.8	28 8	16.2	0.6
RB-A1	12341.0	3.8	0.0	0.0	0.0	3.8	100.0	0.0	0 0	0 0	100.0	100.0	0.0	0 0	1.5	1 5	10.8	14.5	35 7	6 9	0.8
RB-A1	12460.0	11.3	0.0	0.0	0.0	11.3	100.0	0.0	0 0	0.0	100.0	100.0	0 0	0 0	0.0	0 0	2 0	13.3	36.6	1.3	1.0
RB-A5	12298.0	10.3	0.0	0.0	0.0	10.3	100.0	0.0	0.0	0.0	100.0	100.0	0.0	0 0	1.0	1.0	11.3	21.5	29 9	7.9	0.8
RB-A5	12262.0	3.0	0.0	0 0	0.0	3.0	100.0	0.0	0.0	0.0	100.0	100.0	0.0	0.0	1.3	1.3	12.5	15.5	34.9	8.1	0.8
RB-A5	12268.0	4.3	0 0	0.0	0.0	4.3	100.0	0.0	0.0	0.0	100.0	100.0	0.0	0.0	0.5	0.5	8.3	12.5	37.1	5.2	0.9
RB-A5	12287.0	0.0	0.0	0.0	0.0	0.0	0.0	0.0	0.0	0.0	0.0	0.0	0.0	0 0	1.0	1.0	20.3	20.3	31.0	14.0	0 7
RB-A5	12305.0	0 8	0.0	0.0	0.0	0.8	100.0	0.0	0 0	0.0	100.0	100 0	0 0	0.0	0.0	0.0	19.8	20.5	30.8	13.7	0.7
RB-A5	12808.0	1.8	0.0	0.0	0.0	1.8	100.0	0.0	0.0	0.0	100.0	100.0	0.0	0.0	0.0	0 0	15.8	17.5	33 3	10.5	0.8
RB-A5	12825.0	4.0	0.0	0.3	0.0	4.3	94.1	0.0	5.9	0.0	100 0	94.1	5.9	0.3	0.0	0.3	11 0	15.0	35.3	7.1	0.8
RB-A5	12832.0	2.5	0.0	0.3	0.0	2.8	90.9	0.0	9.1	0.0	100.0	90.9	9.1	0.3	0.0	0 3	10.3	12.8	37.0	6.5	0 9
RB-B3	12357.0	0.0	0.0	0.0	0.0	0.0	0 0	0.0	0.0	0.0	0.0	0.0	0.0	0 0	1.5	1.5	14.5	14.5	35 7	9 3	0.8
RB-B3	12368.7	0.5	0.0	0.0	0.0	0.5	100.0	0.0	0.0	0.0	100.0	100.0	0.0	0 0	0.8	0.8	15.8	16.3	34.3	10.3	0.8
RB-B3	12382.6	1.3	0 0	0.0	0.0	1.3	100.0	0.0	0.0	0.0	100.0	100.0	0.0	0.0	0 0	0.0	14.0	15.3	35.1	9.1	0.8
RB-B3	12401.0	8.8	0.0	0.0	0.0	8.8	100.0	0.0	0.0	0.0	100.0	100.0	0.0	0.0	0.0	0.0	10.8	19.5	31.7	7.3	0.8
RB-B4	12403.0	3.3	0.0	0.5	0.0	3.8	86.7	0.0	13.3	0.0	100.0	86.7	13.3	0.5	2.0	2.5	15.0	18.3	32.7	10.1	0.8
RB-B4	12404.0	14.0	0.0	0.8	0.0	14.8	94.9	0.0	5.1	0.0	100.0	94.9	5.1	0.8	0.0	0 8	6.3	20.3	31.0	4.3	0.9
RB-B4	12414.0	5.5	0.0	2.5	0.0	8.0	68.8	0.0	31.3	0.0	100.0	68.8	31 3	2.5	0 0	2.5	14.3	19.8	31 5	9.8	0.8
RB-B4	12420.0	9.5	0.0	1.8	0.0	11.3	84.4	0.0	15.6	0.0	100.0	84.4	15.6	1.8	0.0	1.8	9.3	18.8	32.3	6.3	0.8
RB-B4	12439.0	6.0	0.0	0.0	0.0	6.0	100.0	0.0	0.0	0.0	100.0	100.0	0.0	0.0	0.8	0.8	13.3	19.3	31.9	9.0	0.8
RB-B4	12454.0	3.3	0.0	0.0	0.0	3.3	100 0	0.0	0.0	0.0	100.0	100 0	0.0	0.0	1.3	1.3	13 5	16.8	33.9	8.9	0.8
RB-B4	12470.0	1.5	0.0	0.0	0 0	1.5	100.0	0.0	0 0	0.0	100.0	100.0	0.0	0 0	1.5	1.5	15.5	17.0	33.7	10.3	0.8
RB-B4	12492.0	10.5	0.0	1.0	0.0	11.5	91.3	0.0	8.7	0.0	100 0	91.3	8.7	1.0	0.8	1.8	7.5	18.0	32.9	5.0	0.9
RB-B4	12501.0	6.3	0.0	0.3	0.0	6.5	96.2	0.0	3.8	0.0	100.0	96.2	3.8	0.3	1 0	1.3	10 0	16.3	34.3	6.6	0.8
RB-B4	12509.6	3.8	0.0	0.3	0.0	4.0	93.8	0.0	6.3	0.0	100.0	93.8	6.3	0.3	0.0	0.3	14.3	18 0	32.9	9.6	0.8
RB-B4	12520.0	1.3	0.0	0.0	0 0	1.3	100.0	0.0	0.0	0.0	100.0	100.0	0.0	0.0	0.0	0.0	14.0	15.3	35.1	9.1	0.8
RB-B4	12526.0	5.3	0.0	1.0	0.0	6.3	84.0	0.0	16.0	0.0	100.0	84.0	16.0	1.0	1.0	2.0	11.3	16.5	34.1	7.4	0.8
RB-B4	12533.0	0.0	0.0	0.0	0.0	0.0	0.0	0.0	0.0	0.0	0.0	0.0	0.0	0.0	2.5	2.5	19.8	19.8	31.5	13.5	0.7
RB-B7	12194.0	10.5	0.3	0.3	0.0	11.0	95.5	2.3	2.3	0.0	100.0	95.5	4.5	0.3	0.0	0.3	10.5	21.0	30.4	7.3	0.8
RB-B7	12205.0	8.3	0.0	1.3	0.0	9.5	86.8	0.0	13.2	0.0	100.0	86.8	13.2	1.3	0.0	1.3	5.8	14.0	36.0	3.7	0.9
RB-B7	12213.0	3.3	0.0	0.0	0.0	3.3	100.0	0 0	0.0	0.0	100.0	100.0	0.0	0.0	0.0	0.0	11.0	14.3	35.9	7.1	0.8
RB-B7	12215.0	2.0	0.0	0.0	0.0	2.0	100.0	0.0	0.0	0.0	100.0	100.0	0.0	0.0	0.5	0.5	15.8	17.8	33.1	10.5	0.8
RB-B7	12236.0	5.3	0.0	0.0	0.0	5.3	100.0	0.0	0.0	0.0	100.0	100.0	0.0	0.0	0.0	0.0	8.0	13 3	36.6	5.1	0.9
RB-B7	12251.0	5.3	0 0	0.3	0.0	5.5	95.5	0.0	4.5	0.0	100.0	95.5	4.5	0.3	0.8	1.0	6.3	11.5	37.9	3.9	0.9
RB-B7	12253.0	9.5	0.0	3.5	0.0	13.0	73.1	0.0	26.9	0.0	100.0	73.1	26.9	3 5	0.8	4.3	5.3	14.8	35.5	3.4	0.9
RB-B7	12255.0	7.3	0.0	0.0	0.0	7.3	100.0	0.0	0.0	0.0	100.0	100.0	0.0	0.0	0.5	0.5	10.3	17.5	33.3	6.8	0.8
RB-B7	12273.0	4.0	0.0	0.0	0.0	4.0	100.0	0 0	0.0	0.0	100.0	100.0	0.0	0.0	0.0	0.0	7.8	11.8	37.7	4.8	0.9
RB-B7	12275.0	2.3	0.0	0.0	0.0	2.3	100.0	0.0	0.0	0.0	100.0	100.0	0.0	0.0	1.0	1.0	11.8	14.0	36.0	7 5	0.8
RB-B7	12291.0	2.5	0.0	0.0	0.0	2.5	100.0	0.0	0.0	0.0	100.0	100.0	0.0	0.0	0.8	0.8	18.8	21.3	30 2	13.1	0.7
RB-B7	12308.0	5.0	0.0	0.0	0.0	5.0	100.0	0.0	0.0	0.0	100.0	100.0	0.0	0.0	0.0	0 0	13.3	18.3	32.7	8.9	0.8
RB-B7	12311.0	2.0	0.0	0.0	0.0	2.0	100.0	0.0	0.0	0.0	100.0	100.0	0.0	0.0	1.3	1.3	13.5	15.5	34.9	8.8	0.8
RB-C2	12290.0	6.8	0.3	0.0	0.0	7.0	96.4	3.6	0.0	0.0	100.0	96.4	3.6	0.0	0.0	0.0	14.3	21.0	30.4	9.9	0.8
RB-C2	12341.0	0.0	0.0	0.0	0.0	0.0	0.0	0.0	0.0	0.0	0.0	0.0	0.0	0.0	2.3	2.3	18.5	18.5	32.5	12.5	0.7
RB-C2	12353.0	5.5	0.3	0.0	0.0	5.8	95.7	4.3	0.0	0.0	100.0	95.7	4.3	0.0	0.0	0.0	12.0	17.5	33.3	8.0	0.8
RB-C2	12368.0	2.8	0.0	0.0	0.0	2.8	100.0	0.0	0.0	0.0	100.0	100.0	0.0	0.0	1.3	1.3	15.3	18.0	32.9	10.2	0.8
Max		14.0	0.3	3.5	0.0	14.8	100.0	4.3	31.3	0.0	100.0	100.0	31.3	3.5	2.5	4.3	22.8	22.8	37.9	16.2	1.0
Min		0.0	0.0	0.0	0.0	0.0	0.0	0.0	0.0	0.0	0.0	0.0	0.0	0.0	0.0	0.0	2.0	11.5	28.8	1.3	0.6
AVG		4.6	0.0	0.3	0.0	4.9	88.1	0.2	3.8	0.0	88.9	95.7	4.3	0.3	0.7	1.0	12.5	17.0	33.7	8.3	0.8

have a content up to 15.46 % with an average of 4.69 %. The average ratios of the undulose to nonundulose types are 0.10, 0.04 and 0.05 in the Naqus, Araba and subsurface sandstones, respectively (Table 4.3).

Polycrystalline quartz is the second in abundance. It makes up to 28.67 % of the total quartz of Naqus Sandstone and up to 6.20 % of those of Araba Sandstone. The average values of polycrystalline quartz in the two formations are 11.87 and 2.98 %, respectively. On the other hand, polycrystalline quartz in the subsurface sandstone may reach 12.38 % of the total quartz with an average of 3.66 %. The average ratios of polycrystalline to monocrystalline types are 0.14, 0.03 and 0.04 in the Naqus, Araba and subsurface sandstones, respectively (Table 4.3).

Polycrystalline quartz grains which are composed of two to three individual grains may reach 66.67 % of the total polycrystalline quartz in Naqus Sandstone and 76.92 % of those in Araba Sandstone. The average values of these grains in the two formations are 21.13 and 32.99 %, respectively. On the other hand, they have an average of 34.52 % of the total polycrystalline quartz in the subsurface sandstone (Table 4.3). Those consisting of four to five individual grains make up to 51.35 % of the total polycrystalline quartz in Naqus Sandstone and up to 60.00 % of those in Araba Sandstone. The average values of these garins in the two formations are 23.06 and 25.95 %, respectively. On the other hand, they may reach 100.00 % with an average of 35.04 % of the total polycrystalline quartz in the subsurface sandstone (Table 4.3). Grains made up of more than five individuals may reach 90.91 % of the total polycrystalline quartz in Naqus Sandstone and 100.00 % of those in Araba Sandstone. The average values of these grains in the two formations are 51.35 and 41.05 %, respectively. On the other hand, they

make up to 100.00 % with an average of 41.05 % of the total polycrystalline quartz in the subsurface sandstone (Table 4.3).

The complete spectrum of quartz types present in the studied sandstones is: common, volcanic, recrystallized metamorphic, stretched metamorphic and quartz vein (c.f Folk, 1980). Petrographic observations indicate that the common quartz, typical of plutonic and some metamorphic rocks, is by far the most abundant, whereas other quartz types are subequal in abundance. Monocrystalline quartz having straight extinction with no inclusions is very common (PLs. 4.1; 4.2). This type of quartz is believed to be plutonic in origin (Folk, 1980), but it can be derived from other sources as well (Basu, 1985). Fractured monocrystalline quartz grains having straight extinction with iron oxides infilling the fracture planes have frequently been recognized (PL. 4.2C, D). These fractures probably originated in the precursor source rocks or developed through burial compaction. Intrastratal solution infiltrated iron bearing materials which inhealed the rock grains and then moved to the basin. This type of quartz is most probably of plutonic origin (Abdel-Wahab, 1985). Quartz grains with open fracture planes are also observed (PL. 4.3A). These open fractures enhance the porosity and permeability and, hence, the reservoir quality.

Monocrystalline quartz grains with elongate shape were recorded (PL.4.3B, C). They may have been derived from either schistose quartz (Pettijohn, 1975; Folk, 1980) or hydrothermal quartz veins. Elongate monocrystalline quartz grains with concave boundaries indicate pressure solution, a deformation mechanism typically found in greenschist-facies rocks (Willner, et al., 2001).

Monocrystalline quartz with straight extinction, a euhedral outline, and a large "negative crystal" or vacuole has been occasionally recorded (PL.

4.3D). The vacuole has the same crystallographic orientation as the complete quartz grain, hence the term "negative crystal". This feature is common but not ubiquitous in quartz of volcanic origin (Scholle, 1979).

Monocrystalline quartz grains having idiomorphic hexagonal shape with perfectly straight boundaries, rounded corners and nonundulose extinction are present locally (PL. 4.4A). This type is referred to as volcanic quartz and is derived from erosion of volcanic and shallow intrusive rocks (Folk, 1980). Another type of volcanic quartz is represented by grains with euhedral, bipyramidal outline, and straight extinction (PL. 4.4B). Euhedral shape, embayments, straight extinction, and scarcity of inclusions are all indicative of an extrusive igneous source, but none, by itself, is conclusive evidence (Scholle, 1979).

Monocrystalline detrital quartz grains with rounded overgrowths suggestive of reworked origin (worn overgrowth) were occasionally recognized (PL. 4.4C). The reworked overgrowth was formed on older sandstone grains. Such grains may indicate a nearby source because they broken up rapidly during transportation (Folk, 1980).

Monocrystalline quartz with regular and irregular segmented undulosity was also recorded (PLs. 4.4D; 4.5). This texture is attributed to recovery of the strained grain (Bell and Etheridge, 1973). In some grains, extinction takes place as independent gradational bands across the crystal (PL. 4.6A), a feature known as deformation bands (Young, 1976). This type of quartz may be inherited from plutonic sources (Folk, 1980; Blatt et al., 1980), metamorphic sources (Young, 1976), and/or deformed sedimentary rocks (Blatt, 1992). However, it is not recommended to use the undulatory extinction as the only parameter to identify the source rock. Slightly undulose quartz can be derived from most types of source terrains, while quartz grains with strongly undulose extinction (PL. 4.6B)

may be more abundant in strained source rocks (especially metamorphics), but evidence is still incomplete (Scholle, 1979). Intense strain deformation of quartz grains may produce warped, subparallel lines of very small bubbles (PL. 4.6C), a feature known as Boehm lamellae (Folk, 1980). This type of quartz may be derived from a plutonic (Folk, 1980) or a metamorphic source (Young, 1976).

Quartz grains with different types of inclusions are common. Monocrystalline grains with abundant vacuoles of uneven shapes and sizes are locally observed (PL. 4.6D). Such vacuole-rich quartz does appear to be most commonly derived from a source of low temperature origin, such as hydrothermal veins (Folk, 1980; Blatt et al., 1980). Veins form from solutions that are analogous to aqueous subsurface brines, rather than to silicate magmas. As a result, vein quartz can contain unusually large volumes of water-filled vacuoles, which give the quartz a milky color (Blatt, 1992).

Quartz grains with bipyramidal and subhedral prismatic zircon inclusions were observed (PL. 4.7A-C). Also, those with Tourmaline (blue, green and brown) inclusions as microlites of prismatic and platy shapes exist (PLs. 4.7C, D; 4.8A). These may serve as a characteristic feature of late-stage acid igneous verities and metamorphic rocks (Blatt, et al., 1980; Mackenzie and Guilford, 1986). Rectangular anatase inclusions were also recorded in some quartz grains (PL. 4.8B). A relatively uncommon type of quartz is the monocrystalline grains with needle (fibrolite), prismatic and hair-like sillimanite and rutile inclusions (PLs. 4.8C, D; 4.9A-C). Sillimanite is a common mineral in metamorphic rocks (mainly high-grade schists and contact metamorphics) and quartz grains with sillimanite inclusions are considered to be an excellent evidence for a metamorphic source (Scholle, 1979), while rutile is an

excellent index and a regional marker, but its genetic significance is unknown other than the parent rock contains titanium (Folk, 1980). However, Blatt et al. (1980) emphasized that acicular inclusions of rutile may be diagnostic of granitic quartz.

Quartz grains with muscovite microlites (PL. 4.9D) are not uncommon. Because muscovite can occur in a wide range of source rocks, these particular inclusions have a relatively little provenance significance. However, they can still be useful as indicative markers in correlation (Scholle, 1979). Uncommon type of quartz is monocrystalline grains with kyanite inclusions (PL. 4.9D). Kyanite is found only in high-grade metamorphic source areas and thus is a valuable provenance indicator. Many varieties commonly make it useful for correlation (Scholle, 1979).

The recorded polycrystalline quartz grains of two to five grains with straight to slightly curved intercrystalline boundaries (PL. 4.10A, B) may be derived from granitic sources (Blatt et al., 1980). On the other hand, sutured quartz grains (PLs. 4.10C, D; 4.11A) are common in both igneous and metamorphic rocks (Blatt, 1992). Thus, intercrystalline suturing among quartz grains is, by itself, unreliable criterion to use for provenance.

The more quartz grains in a detrital polycrystalline grain of a given size, the more likely the grain is to be of metamorphic origin. A sand sized polycrystalline quartz grain composed of more than five separate grains is probably of metamorphic derivation (Blatt, 1992). This type of quartz is usually derived from schists and gneisses. Polycrystalline quartz with ten or more individual grains is an excellent indicator of metamorphic origin (Basu et al., 1975; Scholle, 1979). The individual grains are almost elongated, crenulated and welded together with strongly

sutured intercrystalline boundaries (PLs. 4.10C; 4.11B-D). Such stretched quartz grains have been deformed in a nonhydrostatic stress field and are commonly found in foliated metamorphic rocks, such as schists and gneisses (Blatt, 1992). Stretched quartz grains are also found along and adjacent to fault surfaces, where extreme stretching can be accompanied by granulation and recrystallization to produce the rocks mylonite and phyllonite (Blatt, 1992). Also present are stretched quartz grains of metamorphic origin, formed when quartz-bearing rocks such as sandstones, granites, schists, or vein quartz, are sheared or strained in the absence of recrystalization (Folk, 1980).

Polycrystalline grains with sutured grain boundaries, and generally abundant mylonites with incipient recrystallization to a small grain size indicate the presence of important low-grade shear zones. Some polycrystalline grains show a great variation in their individual grains sizes, commonly a bimodal distribution of crystal sizes (PL. 4.12A), illustrating a recrystallization "caught in the act". This type characterizes recrystallized rocks (metamorphic) and is derived from naturally disintegrated gneiss (Blatt, 1967a; Blatt et al., 1980; Blatt, 1992). Recrystallization begins at points of stress concentration within the rock rather than simultaneously at all locations. Thus, when recrystallization ends, some quartz grains are in a different state of process than others. The smaller grains are the newly developing ones that have not yet grown to equilibrium size (Blatt, 1992).

In some polycrystalline quartz grains, the intercrystalline boundaries among quartz grains are straight and intersect at an angle of 120° (triple-point texture), reflecting the most efficient use of space by grains that form simultaneously (PL. 4.12B). Such polygonized quartz suggests a metamorphic origin and indicates a thermally induced recrystallization

occurring as the last recrystallization event in the history of the rock (Blatt, 1992).

Polycrystalline quartz with individual, elongate, slightly undulose grains having straight intercrystalline boundaries (PL. 4.12C) is indicative of schistose origin (Folk, 1980). Polycrystalline quartz having silt-size individual grains (PL. 4.12D) may have originated from metamorphic source (Blatt et al., 1980). In some polycrystalline quartz grains the subgrains are well defined by dust lines that define undulose boundaries (PL. 4.13). This type of "common" quartz may suggest a plutonic origin (Folk, 1980). Semicomposite quartz grains with slightly undulose extinction are occasionally recorded in the investigated sandstones, these grains consist of a number of separate quartz grains with very closely aligned optic c-axes (PL. 4.14A). Such grains are common in hydrothermal veins but also occur in many other metamporphic and plutonic rock types (Scholle, 1979).

In order to have a better understanding of the nature of quartz in the studied sandstones, the relative abundance of the different varieties of macrocrystalline quartz (nonundulatory monocrystalline, undulatory monocrystalline and polycrystalline) were drawn versus each other and against the graphic mean size (Fig. 4.1).

A negative correlation exists between the abundance of nonundulatory and polycrystalline quartz in both Naqus and subsurface sandstones (Fig. 4.1A, B). This negative trend is supported by the mechanical stability argument. Generally, the most durable variety of quartz in sedimentary environments is nonundulatory monocrystalline quartz that does not contain inclusions. Polycrystalline grains are weaker because of their internal discontinuity surfaces (crystal boundaries). Grains with undulatory extinction are weaker because they have been plastically

deformed. Grains with inclusions are weak because they are composed of two distinct phases, either two solid phases or a solid and a liquid (or gaseous) phase, as with polycrystalline grains, discontinuity surfaces are present within these grains (Blatt, 1992). Because of these differences in durability, the concept of survival of the fittest can be applied to quartz in the sedimentary environment (Blatt, 1992). Assemblages of quartz grains that have spent more time in the sedimentary environment should be relatively enriched in nonundulatory monocrystalline grains and depleted in undulatory polycrystalline grains, that is, the more the maturity of the sandstones, the more nonundulatory quartz and the less polycrystalline grains they have. Examination of thin sections of the studied sandstones revealed that this is indeed the case. However, the relationship between nonundulatory and polycrystalline quartz in Araba Formation showed unexpected slight positive correlation (Fig. 4.1B).

The plot of undulatory quartz versus polycrystalline quartz shows a moderate positive correlation (Fig. 4.1C). Blatt and Christie (1963) concluded that when the percentage of undulatory quartz grains is high, there is no correlation between their abundance and the abundance of polycrystalline grains. However, when the proportion of undulatory grains is low, polycrystalline grains are extremely rare.

No particular correlation was found between undulose and nonundulose quartz in Araba Formation. However, a moderate negative relation exists between the two parameters in both Naqus and subsurface sandstones (Fig. 4.1D). This relation is expected between these two parameters as they are the main quartz types identified herein and the polycrystalline quartz constitutes a minor amount of the total quartz.

As one would anticipate, the amount of polycrystalline quartz, nonundulose monocrystalline quartz and undulose monocrystalline quartz

in the total quartz are size dependent. Plot of mean grain size versus polycrystalline quartz for both Naqus and Araba formations showed a moderate positive correlation indicating that increasing of mean grain size is associated with increasing in the amount of polycrystalline quartz in the total quartz (Fig. 4.1E, H). An inverse relation is suggested in the crossplot of nonundulose monocrystalline quartz against mean size. This is true for Naqus Formation, however, for Araba Formation the relationship between the two parameters is reversed indicating a slight positive correlation (Fig. 4.1F) i.e. the finer the grain size, the lower the percentage of nonundulatory quartz among monocrystalline quartz grains. Plot of mean size versus undulatory quartz for both Naqus and Araba formations shows a moderate positive correlation indicating that increasing of mean size is associated with increasing in the amount of undulatory quartz in the total quartz (Fig. 4.1G). These results are compatible with Blatt (1967a), who suggested that higher proportions of polycrystalline and undulose quartz grains occur in the coarser size fraction, whereas the percentage of nonundulatory quartz in the total quartz increases with decreasing grain size. This relation can be interpreted through the size reduction caused by sedimentary processes. Polycrystalline gains are probably reduced in size by fracturing along quartz crystal boundaries when large undulatory quartz grains are fragmented into smaller grains. Monocrystalline quartz may be reduced in size by breaking along planes of structural weakness such as hairline fractures and planes of bubble inclusions. An alternative possibility for achieving size reduction of relatively unstable monocrystalline undulatory quartz grains is through chemical activity during soil formation (Blatt, 1967a).

The unexpected relations in Araba Formation such as the absence of correlation between undulose and nonundulose quartz, the slight positive correlation between nonundulatory and polycrystalline quartz and the slight increase in the amount of nonundeulatory quartz with the increase of mean size may be attributed to the grain size distributions (fine and very fine) and the extensive diagenesis that modified the texture and mineral constituents of the formation. Blatt (1967a) suggested that monocrystalline quartz grains with undulatory extinction are coarser in size than nonundulatory grains, therefore differences in percentages of nonundulatory quartz among different lithic units or among thin sections from the same unit cannot be contrasted unless the mean size of the quartz grains is specified. Mean percents of polycrystalline quartz, nonundulose monocrystalline quartz and undulose monocrystalline quartz have been calculated for different size classes in the range -1 ϕ to 4 ϕ (very coarse, coarse, medium, fine and very fine). Strong relations were found between these mean values and grain size (Fig. 4.1H).

4.1.2 Feldspar minerals

Feldspar minerals are essentially absent in the studied sandstones, except for a few extensively altered to almost completely dissolved grains on the scale of a thin section (PLs. 4.14B-D; 4.15; 4.16). Such grains were not tabulated in the point counts. The scarcity of feldspars may have resulted from one or more of the following: 1) deposition in a high-energy regime which selectively destroyed feldspar grains; 2) poverty of source rock-bearing feldspars; 3) low topography of the source area associated with the predominance of a warm, humid climate that may destroy feldspars (Suttner et al., 1981); and 4) extensive diagenetic modification due to intrastratal solution (Folk, 1980; Abdel-Wahab et al., 1988; Abdel-Wahab and Abu El-Maati, 1989).

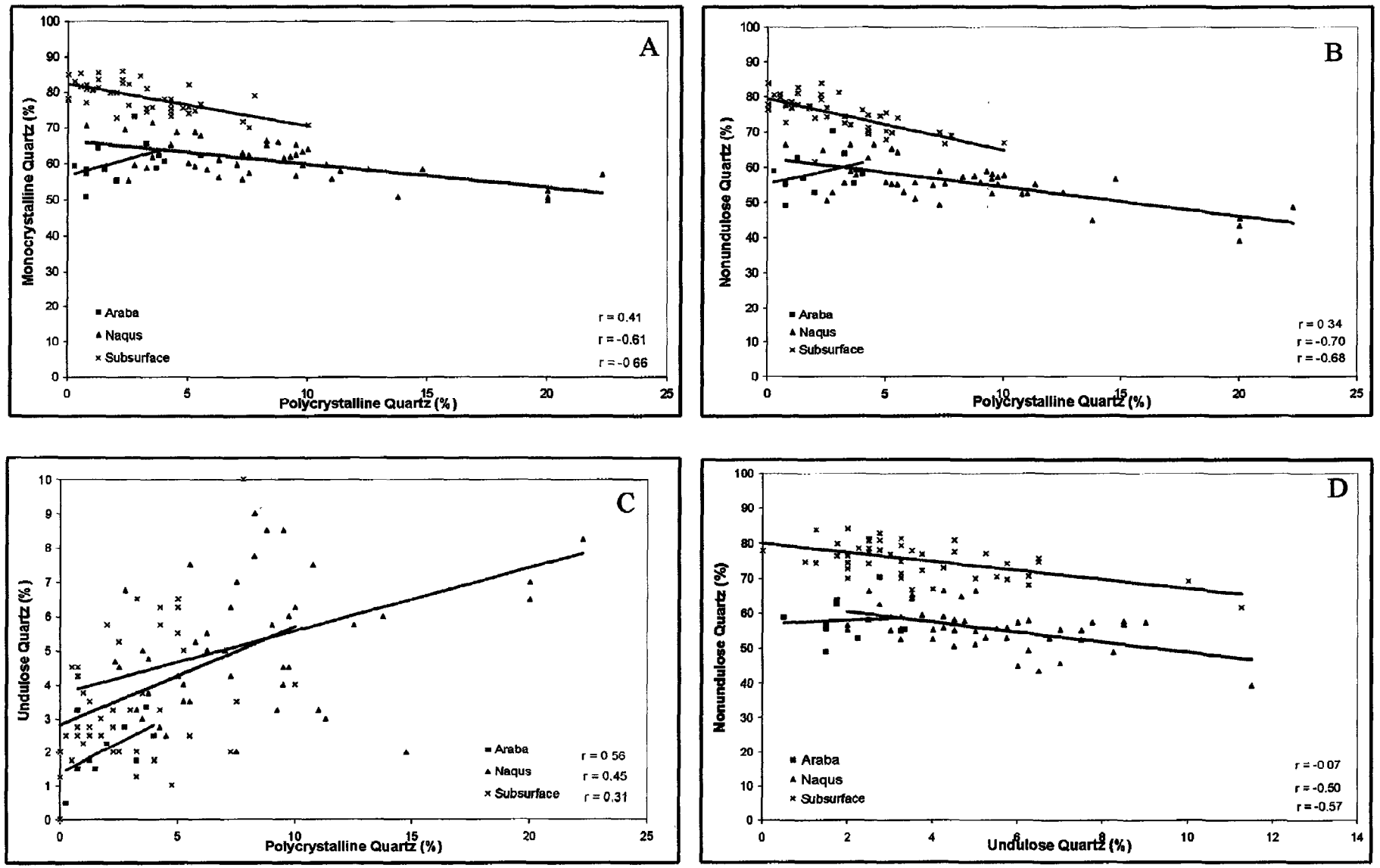

Fig. 4.1: Cross plots of polycrystalline versus monocrystalline quartz (A), polycrystalline versus nonundulose quartz (B) polycrystalline versus undulose quartz (C) and undulose versus nonundulose quartz (D).

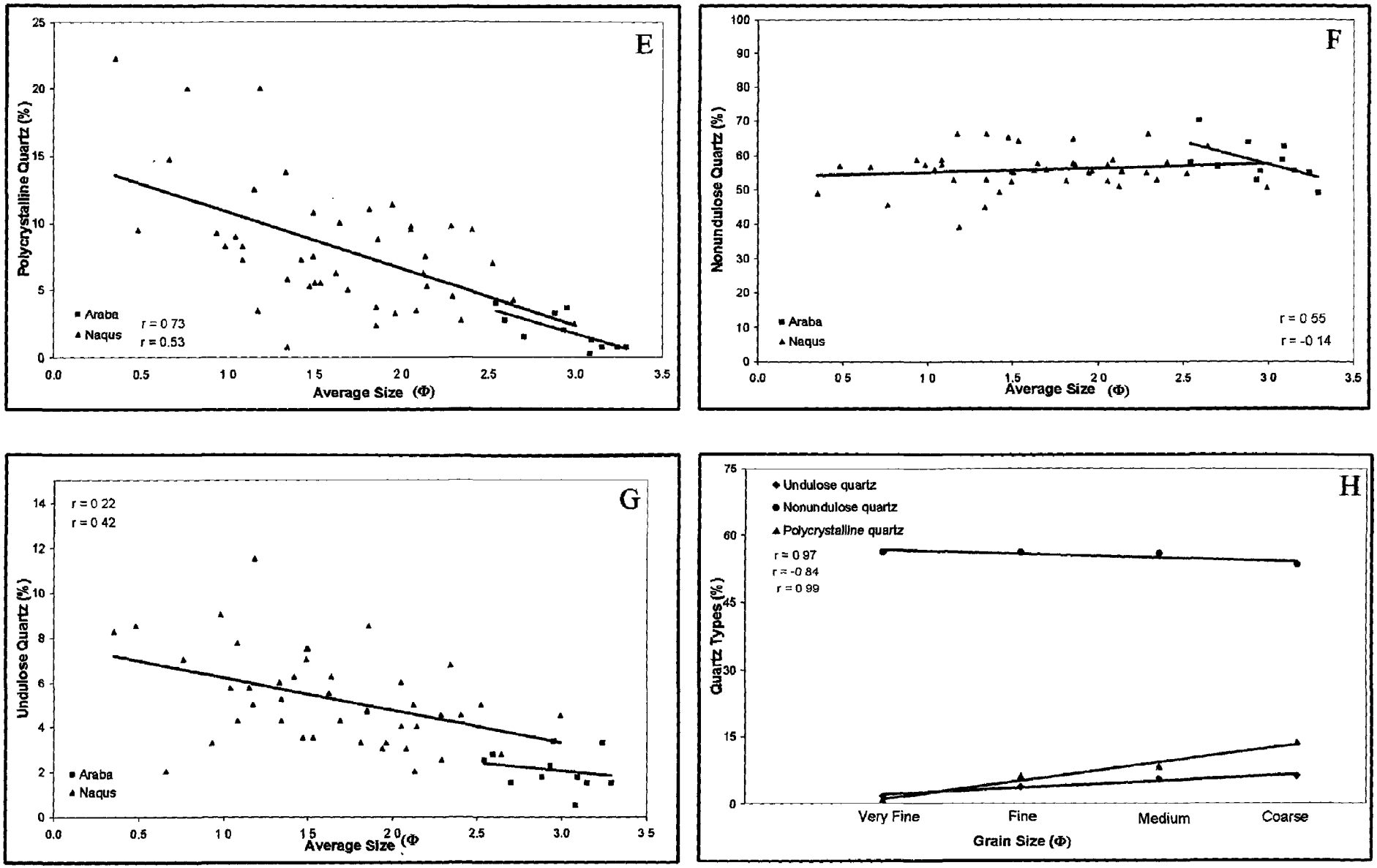

Fig. 4.1*(Continued)*: Cross plots of average size versus polycrystalline quartz (E), average size versus nonundulose quartz (F), average size versus undulose quartz (G) and average size versus quartz types (H).

In the studied sandstones, it is believed that the original feldspar minerals were lost due to grain dissolution by ground water in an active hydrologic regime and/or due to excessive alteration during burial diagenesis. Many feldspar grains were almost completely dissolved leaving behind skeletal remnants or showing no evidence of their former presence (PL. 4.16C, D). In the latter case, the dissolved grains left behind only oversized pores that indicate their original presence. The proportions of feldspars lost by the effect of these processes were determined assuming that 80 % of the oversized pores (pores originally inferred to have been occupied by feldspar grains) and of grains pseudomorphed by kaolinite and calcite were originally feldspars (cf. McBride 1985, 1987).

According to Blatt (1992), several types of alterations of feldspars are commonly recorded in thin sections of sandstones: vacuolization, illitization, smectitization and kaolinization. In the studied sandstones, kaolinitization (PLs. 4.14B-D; 4.15A, B) is the most observed. Kaolinization, the chemical transformation of either potassic, sodic, or calcic feldspar to kaolinite, reflects a more intense and/or prolonged process of alteration than either illitization or smectitization.

Correcting framework composition for feldspar dissolution is accomplished by assigning 80 % of the oversized pores and pseudomorphed grains to the feldspars category. The philosophy taken during point counting was that if an intergranular area is of the size or shape of typical detrital particle, then it is counted as an oversized pore. Some rock fragments and unstable ferromagnesian minerals could contribute to the population of oversized pores (McBride, 1987), but these grains are far less abundant than feldspars in the studied sandstones.

The most common indicators of missing feldspars in the studied sandstones are the presence of oversized pores and oversized pores filled with cement. The filling cements include: kaolinite, iron oxides, halite and gypsum. Oversized calcite cement patches (rare), interpreted as detrital grains replaced by calcite or dissolution pores filled by calcite, are also considered to have been feldspars. Based on the abundance of oversized pores, the volume of feldspars lost due to dissolution averages about 6.69, 4.64 and 0.77 volume % in the Naqus, Araba and subsurface sandstones, respectively.

Because the studied surface sandstone has not been deeply buried, compaction has no significant effect on the destruction of secondary pores and hence, on oversized pores. Based on the abundance of oversized pores, some samples originally had up to 28 % feldspars by volume. On the other hand, the subsurface sandstones were deeply buried and most of the oversized pores had been lost by compaction, resulting in underestimation of the original feldspar content.

4.1.3 Rock fragments and mica

Rock fragments are minor constituent in the studied sandstones. They make up to 2.61 % of the framework composition in Naqus Sandstone and up to 0.72 % of those in Araba Sandstone. The average values for rock fragments in the two formations are 0.22 and 0.18 %, respectively. On the other hand, rock fragments in the subsurface sandstone may reach 0.89 % with an average of 0.14 % of the framework composition (Table 4.1). The recorded rock fragments are sedimentary and, much less commonly metamorphic and volcanic.

Sedimentary rock fragments consist mainly of chert, fine-grained siliceous and ferruginous sandstones, siltstones and mudstones. Chert fragments are mostly made up of subrounded to well-rounded

microcrystalline quartz (PL. 4.17A-C) suggestive of a polycyclic origin. They were generally mechanically and chemically stable during diagenesis. However, some chert fragments have undergone partial dissolution which resulted in the development of microporosity (PL. 4.17D). The outlines of some chert fragments are embayed by quartz grains indicating a higher stability of quartz relative to chert. Silica-cemented siltstone and sandstone clasts are present locally (PL. 4.18A, B). Hematite-cemented sandstone fragments are occasionally observed (PL. 4.18C). Individual clasts (particularly muddy and silty ones) may be plastically deformed suggesting erosion and redeposition while still partly unconsolidated or compaction during burial (PL. 4.18D).

Metamorphic rock fragments are mainly represented by quartz mica schist and quartz gneiss (PLs. 4.9A; 4.19A). Different ductile grains represented mainly by mica flakes are also recorded (PLs. 4.6D; 4.19B). These grains are relatively stable chemically, but they are easily deformed during compaction. Muscovite flakes are by far more common than biotite flakes, probably due to their abundance in source rocks and greater resistance to chemical weathering and transportation. Gypsum flakes are also recorded (PL. 4.19C, D).

Although, like feldspars, some rock fragments were probably lost through dissolution during diagenesis (lithic fragments, particularly volcanic ones, are frequently dissolved and/or altered to clay minerals), they were probably never very abundant. Assuming that 80 % of the oversized pores are formed by dissolution of feldspars, and 20 % by dissolution of other grain types (McBride, 1985, 1987; Milliken et al. 1989) the volume of rock fragments lost because of dissolution averages about 1.67, 1.16 and 0.19 % in Naqus, Araba and subsurface sandstones, respectively. It is important to note that feldspars are able to survive a

greater number of sedimentary cycles, i.e., more reworking, than can rock fragments. This observation may be attributed to the polygranular character of rock fragments (Blatt and Christie, 1963).

4.1.4 Detrital clays

Detrital clays are essentially absent except as rare claystone rip-up clasts (PL. 4.18D). They make up to 1.06 % of the framework composition in Naqus Sandstone and up to 2.86 % of those in Araba Sandstone. The average values for detrital clays in the two formations are 0.05 and 0.4 %, respectively. On the other hand, the subsurface sandstone has detrital clays that may reach 2.70 % with an average of 0.23 % of the framework composition (Table 4.1). These clasts are recognized as structurless grains, homogeneous in composition and commonly deformed ductilely between more rigid framework components. They are composed of well oriented clays with little or no silt and are believed to be intrabasinal in origin.

4.1.5 Heavy minerals

Heavy minerals in the studied sandstones are among the nonessential constituents that were not used for classification. They may reach up to 1.45 % (average of 0.15 %) of the framework composition in the Naqus Formation while constitute a minor proportion of those in the Araba Formation. On the other hand, heavy minerals in the subsurface sandstone may reach 0.33 % with an average of 0.03 % of the framework composition (Table 4.1).

4.1.5.1 Opaque minerals

Opaque minerals make up to 65.55 % of the total heavies in Naqus Sandstone and up to 78.06 % of those in Araba Sandstone. The average values of opaques in the two formations are 54.18 and 52.49 %, respectively (Fig. 4.2; Table 4.5). Opaques seem to be size-dependent,

constituting the major part of the total heavy minerals (averaging 63.24 %) of the very fine sand fraction (Table 4.6). This may be attributed to selective sorting during transport and deposition. In the studied sandstones, opaques are mainly represented by hematite, goethite, hydrogoethite and Fe-Ti oxides.

4.1.5.2 Non-opaque minerals

Non-opaque minerals make up to 70.92 % of the total heavies in Naqus Sandstone and up to 71.03 % of those in Araba Sandstone. The average values of non-opaques in the two formations are 45.82 and 47.51 %, respectively (Table 4.5). Non-opaques also seem to be size-dependent showing minimum percentages (average 36.76 %) in the very fine sand fraction and maximum values (average 49.01 %) in both the fine and medium sand fraction (Table 4.6). Ten non-opaque, ultrastable (zircon, tourmaline and rutile) and metastable (garnet, sphene, epidote, staurolite, sillimanite, monazite and hornblende) heavy minerals were identified. Micas were excluded from the heavy mineral assemblage because of their extremely platy shape which results in anomalous behavior during transport (Blatt 1992). The ultrastable minerals are the most abundant nonopaques in the studied sandstones. They were recorded in all the examined samples with relatively high frequencies. These minerals can survive prolonged transport and were mostly recycled from older sedimentary rocks. The lack of other heavies may be attributed to their rarity in the source rocks and/or their relatively low stability during chemical weathering, transport and burial.

4.1.5.2.1 Zircon

Zircon is the most common nonopaque mineral recognized in the studied sandstones. It constitutes an average of 47.22 and 62.91 % of all nonopaques in Naqus and Araba formations, respectively (Table 4.7). Extreme relief, characteristic morphology and strong birefringence are

Table 4.5: Frequency distribution of heavy minerals in the studied sandstones.

S. No	Opaques	Non Opaques											Total
		Zircon	Tourmaline	Rutile	Garnet	Epidote	Staurolite	Hornblende	Sphene	Monazite	Sillimanite	Total	
1- Araba Formation													
1	55.45	26.07	6.16	7.58	0.95	0.47	1.90	0.47	0.95	0.00	0.00	44.5	100
2	41.28	41.28	5.03	9.40	1.34	0.00	1.68	0.00	0.00	0.00	0.00	58.7	100
3	28.97	40.69	8.97	11.72	3.45	2.07	1.38	0.69	0.00	2.07	0.00	71.0	100
4	45.63	45.63	3.04	5.70	0.00	0.00	0.00	0.00	0.00	0.00	0.00	54.4	100
5	53.41	38.28	1.78	6.23	0.00	0.00	0.30	0.00	0.00	0.00	0.00	46.6	100
6	78.06	10.71	5.10	3.57	1.53	0.00	0.00	0.51	0.51	0.00	0.00	21.9	100
7	53.54	28.76	5.31	8.85	2.65	0.00	0.00	0.00	0.88	0.00	0.00	46.5	100
8	70.15	16.12	4.78	6.87	2.09	0.00	0.00	0.00	0.00	0.00	0.00	29.9	100
9	59.02	27.46	2.05	8.20	2.87	0.41	0.00	0.00	0.00	0.00	0.00	41.0	100
10	44.04	32.50	13.27	8.46	1.15	0.19	0.00	0.00	0.38	0.00	0.00	56.0	100
11	47.85	26.07	10.89	12.21	2.31	0.00	0.00	0.66	0.00	0.00	0.00	52.1	100
Max	78.06	45.63	13.27	12.21	3.45	2.07	1.90	0.69	0.95	2.07	0.00	71.03	
Min	28.97	10.71	1.78	3.57	0.00	0.00	0.00	0.00	0.00	0.00	0.00	21.94	
Avg	52.49	30.32	6.03	8.07	1.67	0.29	0.48	0.21	0.25	0.19	0.00	47.51	
1- Naqus Fromation													
12	49.22	26.95	14.06	7.81	1.56	0.00	0.00	0.00	0.39	0.00	0.00	50.8	100
18	53.36	29.10	7.46	7.84	1.87	0.00	0.00	0.00	0.00	0.00	0.37	46.6	100
25	58.82	16.54	13.97	8.46	1.84	0.00	0.00	0.37	0.00	0.00	0.00	41.2	100
32	55.95	15.48	17.46	10.32	0.79	0.00	0.00	0.00	0.00	0.00	0.00	44.0	100
43	62.60	15.79	10.80	10.25	0.55	0.00	0.00	0.00	0.00	0.00	0.00	37.4	100
51	61.19	23.03	5.12	9.38	0.64	0.21	0.00	0.21	0.21	0.00	0.00	38.8	100
61	57.79	23.26	9.35	8.87	0.24	0.00	0.00	0.24	0.24	0.00	0.00	42.2	100
70	44.39	34.91	12.47	7.48	0.75	0.00	0.00	0.00	0.00	0.00	0.00	55.6	100
76	65.55	12.20	14.33	6.71	1.22	0.00	0.00	0.00	0.00	0.00	0.00	34.5	100
87	54.25	18.63	16.34	9.15	1.63	0.00	0.00	0.00	0.00	0.00	0.00	45.8	100
96	56.65	11.08	23.73	7.28	1.27	0.00	0.00	0.00	0.00	0.00	0.00	43.4	100
100	53.45	18.97	19.25	7.47	0.86	0.00	0.00	0.00	0.00	0.00	0.00	46.6	100
103	56.21	15.98	21.60	5.62	0.59	0.00	0.00	0.00	0.00	0.00	0.00	43.8	100
108	29.08	51.04	14.84	3.86	1.19	0.00	0.00	0.00	0.00	0.00	0.00	70.9	100
Max	65.55	51.04	23.73	10.32	1.87	0.21	0.00	0.37	0.39	0.00	0.37	70.92	
Min	29.08	11.08	5.12	3.86	0.24	0.00	0.00	0.00	0.00	0.00	0.00	34.45	
Avg	54.18	22.35	14.34	7.89	1.07	0.02	0.00	0.06	0.06	0.00	0.03	45.82	

Table 4.6: Average percentages of heavy minerals for different size classes.

Size	Opaques	Nonopaques	% Non Opaques									
			Zircon	Tourmaline	Rutile	Garnet	Epidote	Staurolite	Hornblende	Sphene	Monazite	Sillimanite
V.F	63.24	36.76	58.05	13.90	19.07	5.76	0.41	0.85	0.68	1.27	0.00	0.00
F.	50.98	49.02	56.20	20.73	19.29	2.26	0.32	0.45	0.35	0.15	0.24	0.00
M.	50.99	49.01	48.55	34.26	14.53	2.47	0.00	0.00	0.00	0.10	0.00	0.10

Table 4.7: Relative frequency distribution of non-opaque heavy minerals in the studied sandstones.

S. No	Non Opaques										Total
	Zircon	Tourmaline	Rutile	Garnet	Epidote	Staurolite	Hornblende	Sphene	Monazite	Sillimanite	
1- Araba Formation											
1	58.51	13.83	17.02	2.13	1.06	4.26	1.06	2.13	0.00	0.00	100
2	70.29	8.57	16.00	2.29	0.00	2.86	0.00	0.00	0.00	0.00	100
3	57.28	12.62	16.50	4.85	2.91	1.94	0.97	0.00	2.91	0.00	100
4	83.92	5.59	10.49	0.00	0.00	0.00	0.00	0.00	0.00	0.00	100
5	82.17	3.82	13.38	0.00	0.00	0.64	0.00	0.00	0.00	0.00	100
6	48.84	23.26	16.28	6.98	0.00	0.00	2.33	2.33	0.00	0.00	100
7	61.90	11.43	19.05	5.71	0.00	0.00	0.00	1.90	0.00	0.00	100
8	54.00	16.00	23.00	7.00	0.00	0.00	0.00	0.00	0.00	0.00	100
9	67.00	5.00	20.00	7.00	1.00	0.00	0.00	0.00	0.00	0.00	100
10	58.08	23.71	15.12	2.06	0.34	0.00	0.00	0.69	0.00	0.00	100
11	50.00	20.89	23.42	4.43	0.00	0.00	1.27	0.00	0.00	0.00	100
Max	83.92	23.71	23.42	7.00	2.91	4.26	2.33	2.33	2.91	0.00	
Min	48.84	3.82	10.49	0.00	0.00	0.00	0.00	0.00	0.00	0.00	
Avg	62.91	13.16	17.30	3.86	0.48	0.83	0.51	0.64	0.26	0.00	
2- Naqus Formation											
12	53.08	27.69	15.38	3.08	0.00	0.00	0.00	0.77	0.00	0.00	100
18	62.40	16.00	16.80	4.00	0.00	0.00	0.00	0.00	0.00	0.80	100
25	40.18	33.93	20.54	4.46	0.00	0.00	0.89	0.00	0.00	0.00	100
32	35.14	39.64	23.42	1.80	0.00	0.00	0.00	0.00	0.00	0.00	100
43	42.22	28.89	27.41	1.48	0.00	0.00	0.00	0.00	0.00	0.00	100
51	59.34	13.19	24.18	1.65	0.55	0.00	0.55	0.55	0.00	0.00	100
61	55.11	22.16	21.02	0.57	0.00	0.00	0.57	0.57	0.00	0.00	100
70	62.78	22.42	13.45	1.35	0.00	0.00	0.00	0.00	0.00	0.00	100
75	35.40	41.59	19.47	3.54	0.00	0.00	0.00	0.00	0.00	0.00	100
87	40.71	35.71	20.00	3.57	0.00	0.00	0.00	0.00	0.00	0.00	100
96	25.55	54.74	16.79	2.92	0.00	0.00	0.00	0.00	0.00	0.00	100
100	40.74	41.36	16.05	1.85	0.00	0.00	0.00	0.00	0.00	0.00	100
103	36.49	49.32	12.84	1.35	0.00	0.00	0.00	0.00	0.00	0.00	100
108	71.97	20.92	5.44	1.67	0.00	0.00	0.00	0.00	0.00	0.00	100
Max	71.97	54.74	27.41	4.46	0.55	0.00	0.89	0.77	0.00	0.80	
Min	25.55	13.19	5.44	0.57	0.00	0.00	0.00	0.00	0.00	0.00	
Avg	47.22	31.97	18.06	2.38	0.04	0.00	0.14	0.13	0.00	0.06	

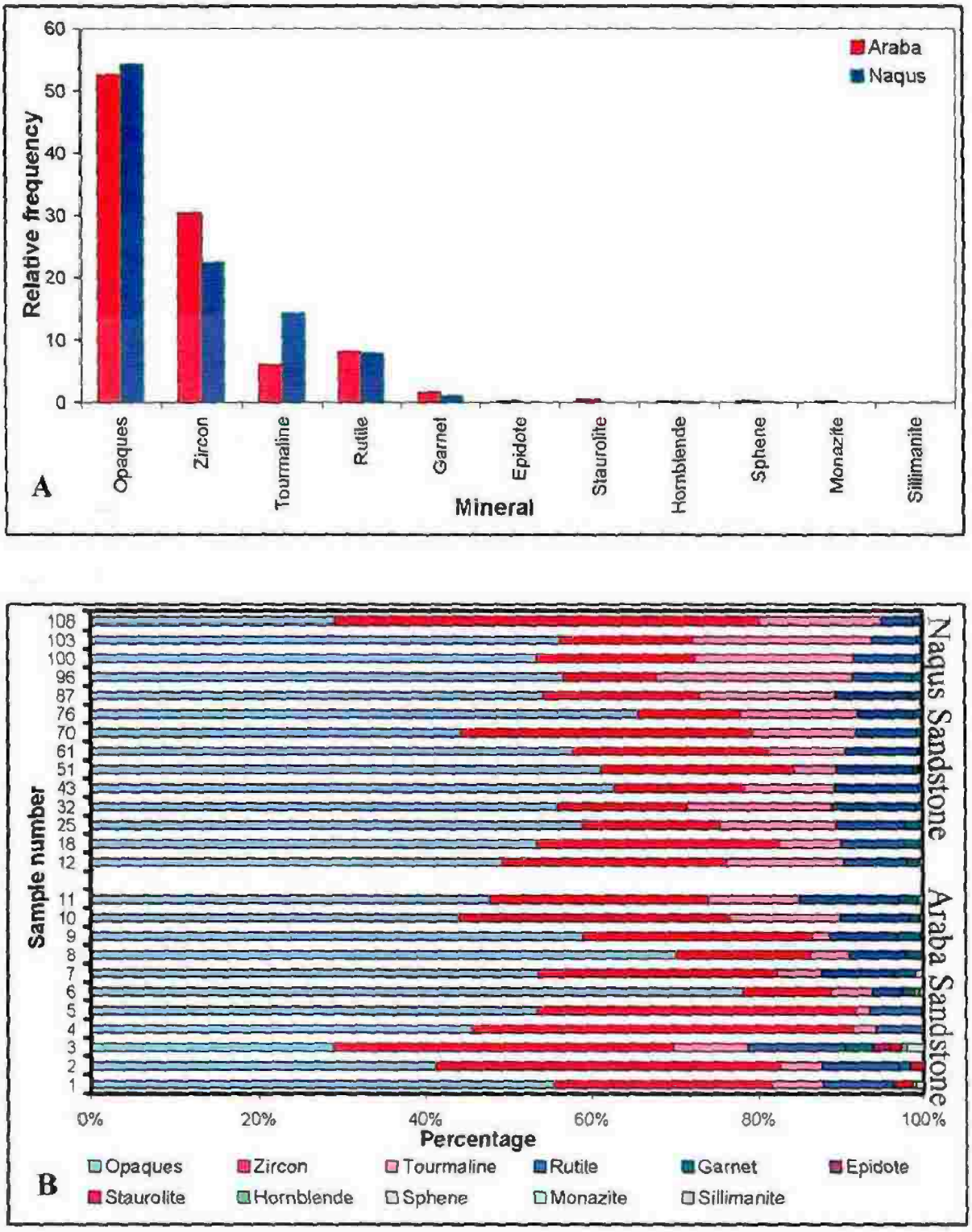

Fig. 4.2 (A, B): Frequency distribution of heavy minerals in Naqus and Araba sandstones.

diagnostic of zircon. It is regarded as one of the most stable minerals which persist through several sedimentary cycles and diagenesis, as well as through metamorphism. Different varieties of zircon are recognized in the studied sandstones (PL. 4.20). It is largely colorless, elongated, oval, rounded to subrounded, locally zoned and/or fractured and includes euhedral-subhedral crystals with singly or doubly terminated pyramids and to a lesser extent prismatic grains with well defined faces. Knee zircon twin with rounded terminatins is also recorded (PL. 4.20u). Vacuoles or bubbles may occur as inclusions in some zircon grains.

The shape of heavy minerals is generally a sensitive indicator to the intensity of abrasion (Folk, 1980). The euhedral crystals of heavy minerals in the sandstone indicate that they mainly represent the first cycle sediments. Euhedral zircon is generally derived from intrusive granitoids and may have a first-cycle origin, whereas rounded zircon, especially one with high rounding index, is regarded as a criterion of polycyclic origin with multiple stages of reworking and may be derived from sedimentary rocks or paraschists (Blatt, et al., 1980). Occasionally, it may be caused by magmatic corrosion (Mange and Maurer, 1992). Elongated zircon crystals occur in rapidly formed dykes (Claus, 1936 in Füchtbauer, 1974a). Zircon with a bipyramidal habit indicates extremely alkaline source rocks, whereas prismatic forms may originate from granites (Pettijohn et al., 1987). Idiomorphic zircon is an indicator of volcanism (Callender and Folk, 1958). All of these types are observed in the studied sandstone samples.

4.1.5.2.2 Tourmaline

Tourmalines are generally classified into: elbaite, schorlite and dravite (Deer et al., 1992). The elbaites are weakly pleochroic tourmalines, varying in color from green, blue, rosy ... etc. Members of the elbaites

are oftenly referred to as verdelite, indicolite, rubellite, etc., but in the present work, the writer uses the color in order to avoid any possible misunderstanding. Schorlites are very strongly pleochroic tourmalines (almost from black to colorless). Dravite is not a common tourmaline and is mainly formed in contact metamorphic zones. Detailed microscopic investigation for the sandstones under study revealed that toumaline is the second abundant nonopaque mineral. It comprises an average of 31.97 and 13.16 % of all nonopaques in Naqus and Araba formations, respectively (Table 4.7). In the studied sandstones, tourmaline is size dependent. Its relative abundance increases with increasing grain size. It accounts for 13.9 %, 20.73 % and 34.26 % of the total nonopaques in the very fine, fine and medium sand fractions, respectively (Table 4.6).

Many varieties of tourmaline with different colors are observed: yellowish brown, pale green, olive green, pink, blue, black and sometimes colorless (PL. 4.21). This color variation may be related to provenance. Tourmaline has strong and distinctive pleochroism mainly from pale yellow to brown and sometimes black (PL. 4.21a-o). Tourmaline occurs as subrounded to well rounded and sometimes euhedral prismatic grains with abraded pyramidal terminations and pronounced external striations (PL. 4.21x). Some tourmaline grains appear as curved near-triangular sections (PL. 4.21k, l, v) and as egg-shaped or long ellipsoidal grains (PL. 4.21p, r). Some grains show zoning and others appear to be homogeneous (PL. 4.21q). Few grains have authigenic overgrowths and show very poor cleavage (PL. 4.21o, q, s). Generally, tourmaline shape is quite sensitive to transport and also depends on the degree of authigenic overgrowth (Willner, et al., 2001).

Color and shape variations of the recorded tourmalines may be related to provenance. Well to very well rounded tourmalines are polycyclic

grains eroded from pre-existing siliciclastic deposits (Mange and Maurer, 1992). Brown tourmaline is believed to be diagnostic of metamorphic rocks (Blatt, 1992), however, brown or green tourmaline filled with inclusions and bubbles may indicate granitic source (Krynine, 1946). Blue and black tourmaline may indicate a pegmatitic origin (Pettijohn, 1975). Presence of angular and rounded tourmaline in the same specimen indicates a multiple source (sedimentary with contributions of igneous and metamorphic) (Folk, 1980). On the other hand, the abundance of subrounded to well rounded tourmaline may be due to a lower survival potential than zircon. Then, the high abundance of tourmaline may indicate derivation from metasomatized rich tourmaline source rock. The high abundance of tourmaline and zircon simultaneous with scarcity of other nonopaques may suggest prolonged abrasion and/or chemical weathering or the sediments are being reworked from older sediments (Folk, 1980).

4.1.5.2.3 Rutile and anatase

Rutile occupies the third order of abundance of the nonopaque minerals in the studied samples after zircon and tourmaline. It comprises an average of 18.06 and 17.3 % of all nonopaques in Naqus and Araba formations, respectively (Table 4.7). Rutile is present as elongated, subrounded to well rounded and sometimes euhedral prismatic grains with abraded bipyramidal terminations (PL. 4.22). The grains are characterized by their very high relief, reddish to opaque deep red-brown color, striations and extreme birefringence with slight pleochrism and twining (PL. 4.22). According to Füchtbauer (1974a), this type of rutile may suggest a pegmatitic origin or derivation from crystalline schists or contact metamorphic rocks. It has an extremely high resistance to weathering (Grim, 1973) and may develop a moderate roundness during

transportation (Dietz, 1973). The presence of rutile suggests that some of the source rocks were basic or reworked sedimentary rocks (Pettijohn, 1975). However, Force (1980) believed that most coarse detrital rutile is derived from high grade regional metamorphic terrains rather than from igneous rocks. Rutile may also be derived from *in situ* decomposition of ilmenite (Scholle, 1979). Banana rutile that indicates oriented pressure is also recorded in the investigated sandstone.

The studied samples contain some anatase grains (PL. 4.8B), which occur as well developed rectangular authigenic grains. The grains lie generally on the basal pinacoid (001) and may exhibit the inclined (111) faces. The color of anatase is generally yellow to brownish. Anatase is authigenic in origin, formed *in situ* from the decomposition of ilmenite or other titaniferous minerals (Milner, 1962a , b). In sandstones, anatase may be formed on the expense of rutile (Abdelwahab, 1972).

4.1.5.2.4 Garnet

Garnet occupies the fourth order of abundance of the nonopaque minerals in the studied sandstone after zircon, tourmaline and rutile. It comprises an average of 2.38 and 3.86 % of all nonopaques in Naqus and Araba formations, respectively (Table 4.7). Garnet is present as colorless, brownish, pinkish and greenish black grains that have an isotropic properties, high refractive index and different types of etching marks. Such grains have irregular, elongated and rounded to subrounded shapes (PL. 4.23a-j). Garnet indicates a high rank of metamorphism and is also present in pegmatites (Pettijohn, 1975). It is fairly resistant to abrasion and chemical attack (Deer et al., 1992). However, Morton (1987) mentioned that garnet with high calcium content (grossular) is unstable and dissolves completely at shallow depth. A minor iron-rich garnet

survives in the subsurface to a depth of about 3 km (Milliken, 1988; Milliken and Mack, 1990).

4.1.5.2.5 Other minerals

Sphene, epidote, staurolite, sillimanite, monazite and hornblende that belong to the metastable heavy minerals have been locally recorded. They constitute a minor amount of the total nonopaques, averaging about 1.45 % (Table 4.7).

Heavy minerals are strongly affected by chemical weathering both in source rocks and during transportation, especially in large region of low relief. The modification of heavy minerals by diagenetic processes (mainly intrastratal solution) has been accepted by many workers (Andel, 1959; Nickel, 1973). In the studied sandstone, it seems likely that diagenesis was so extensive to remove all the unstable and mostly the metastable minerals.

4.2 Classification and nomenclature

Dott's (1964) sandstone classification, based on three end-members: quartz, feldspar and rock fragments, was considered in this study. The compartmentalization of the classification triangle emphasizes feldspar and rock fragments, the more chemically unstable grains, making the classification useful in grouping sandstones as to their probable degree of reaction during diagenesis. It was also useful because chert is grouped with rock fragments instead of with quartz. Thin section examination reveals present-day quartz arenitic composition, although considerable amounts of unstable grains have been lost by dissolution. Ternary diagrams of quartz, feldspar and rock fragments (QFR) illustrate the compositional range of these sandstones from the different formations. The average present-day composition is $Q_{99.78}F_{0.0}R_{0.22}$ for Naqus Sandstone and is $Q_{99.82}F_{0.0}R_{0.18}$ for Araba Sandstone. On the other hand,

this average composition is $Q_{99.86}F_{0.0}R_{0.14}$ for the subsurface sandstone (Fig. 4.3).

The present composition of the studied sandstones is different- of course- from their composition at the time of deposition, because the sandstones have been subjected to later diagenetic processes and weathering. As a result, most of original feldspars, rock fragments, and possibly some other unstable detrital grains, have been completely eliminated. The presence of various stages of dissolution and replacement of feldspars, oversized pores and oversized pores filled with cement indicates that the studied sandstones were originally more feldspathic. By accounting for feldspar and rock fragment dissolution, the restored average original composition becomes $Q_{89.54}F_{8.22}R_{2.24}$ for Naqus Sandstone and $Q_{91.21}F_{6.9}R_{1.89}$ for Araba Sandstone. Similarly, this average composition becomes $Q_{98.70}F_{0.93}R_{0.37}$ for the subsurface sandstone (Fig. 4.3). This composition was determined by estimating the volume of framework grains (mostly feldspars and to a lesser extent rock fragments) that have been eliminated (dissolved) and/or replaced by authigenic minerals using the presence of skeletal grains and oversized pores or cement patches as evidences of the former existence of such grains.

Because the surface sandstone has not been deeply buried, there was little destruction of secondary pores by compaction and hence, most of the oversized pores are preserved. This indicates the ability to evaluate dissolved framework grains (mostly feldspars) and to correct the present-day modal composition of this sandstone. One can expect the restored framework composition to be very close to the depositional framework composition. On the other hand, the subsurface sandstone has undergone a considerable compaction and most of the oversized pores were lost. This results in underestimation of the original feldspar and rock fragment

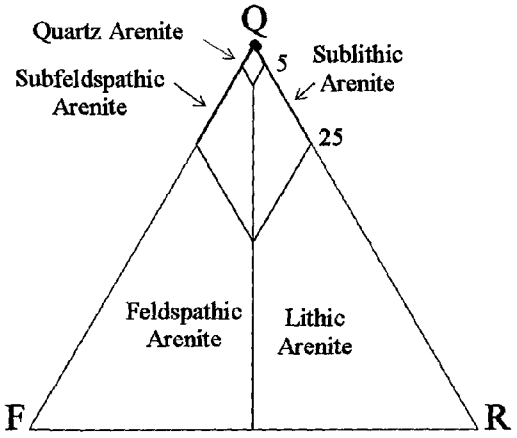

(Araba)

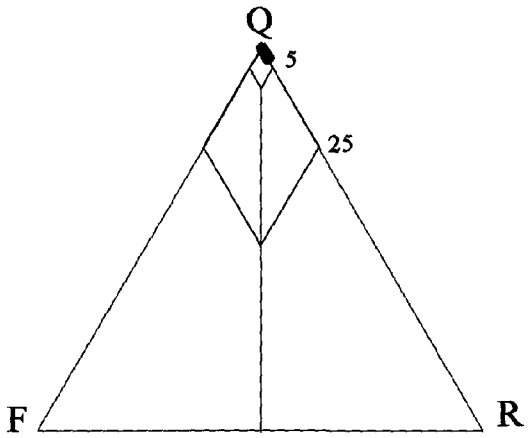

(Naqus)

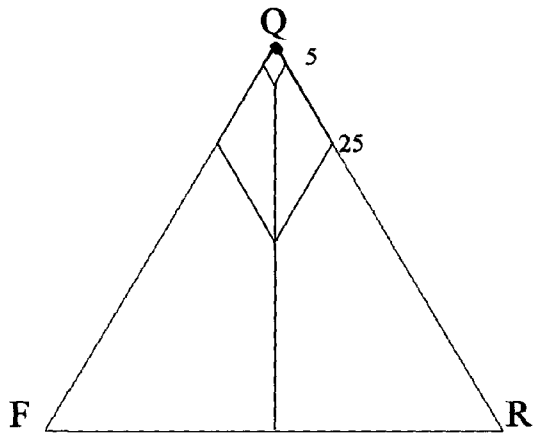

(Subsurface)

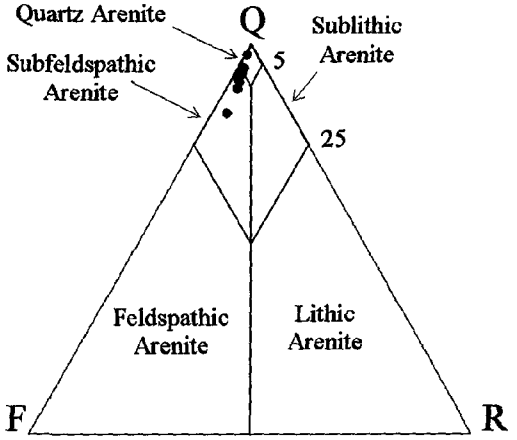

(Araba)

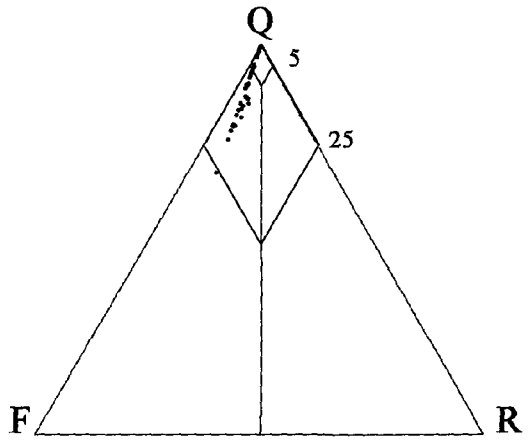

(Naqus)

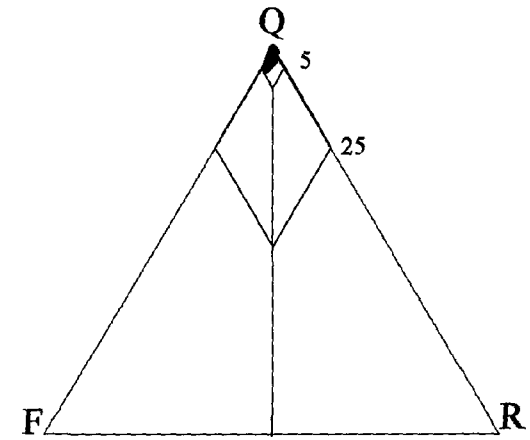

(Subsurface)

Fig. 4.3: Classification of the studied sandstones (Classification of Dott, 1964), the upper set shows the present day composition and the lower set refers to the initial composition. Q = quartz, F = feldspars, R = rock fragments.

contents. Therefore, the restored framework composition does not exactly mimic the depositional framework composition.

4.3 Cements and other authigenic minerals

Cements and replacement minerals in the studied sandstones vary in abundance. They make up to 42.50 % of the whole rock volume in Naqus Sandstone and up to 48.75 % of those in Araba Sandstone. The average values for cements and replacement minerals in the two formations are 12.94 and 34.27 %, respectively. On the other hand, cements and replacement minerals in the subsurface sandstone may reach 24.75 % with an average of 13.12 % of the whole rock volume (Table 4.1). Authigenic cements include quartz, K-feldspar, clays, iron minerals, calcite, gypsum and halite. On the other hand, allogenic cement is also recorded and is mainly represented by infiltrated clays (clay cutans). The generation of thin clay grain coats from mechanically infiltrated clays preceded the formation of other authigenic phases in most samples.

4.3.1 Quartz

The main factors that control the amount of quartz cement in sandstones are: framework composition, residence time in the "silica mobility window", and fluid composition, flow volume and pathways (McBride, 1989). Quartz cement makes up to 3.25 % of the whole rock volume of Naqus Sandstone and up to 2.50 % of those of Araba Sandstone. The average values for quartz cement in the two formations are 1.33 and 0.53 %, respectively. On the other hand, quartz cement in the subsurface sandstone makes up to 3.25 % with an average of 0.78 % of the whole rock volume (Table 4.1). Quartz cement is mainly represented by syntaxial overgrowths which are widely and uniformly distributed between samples of each unit. Microcrystalline quartz is another quartz

cement type that was recognized only in the silcrete of Naqus Formation. It occurs either as mosaic cement or as isopachous drusy coatings.

In the studied sandstones, quartz overgrowths form well developed crystal faces in optical continuity with detrital grains. In thin sections, the overgrowths or crystal faces are easily recognized outside the familiar "dust" line on detrital surfaces (PL. 4.24A, B), or as inclusion-free quartz that encrusts detrital grains containing abundant inclusions (PL. 4.24C, D). Some grains have two dust lines separating two layers of overgrowth (PL. 4.4C). These grains attest to two episodes of quartz cementation. Herein, quartz overgrowths precede most other diagenetic events (PLs. 4.25-2.27). The development of these overgrowths is governed by the atomic structure and crystallographic orientation of the detrital quartz grains. The stages of quartz overgrowth formation mentioned previously by Ernst and Blatt (1964), Waugh (1970) and Pittman (1972) and many of their described features are identified in the studied sandstones. Quartz overgrowths start as numerous oriented crystallographic projections, with rhombohedral and prismatic form, on grain surfaces. Overgrowths with well-defined crystal faces commonly grow until contact is made with another overgrowth (coaleasing) that nucleated elsewhere on the detrital surface (PL. 4.28A). The incipient minute projections become so numerous on grain surfaces that they merge and overlap with adjacent projections thus giving rise to the formation of larger rhombohedral or prismatic faces, if space and time permit (PL. 4.28B-D). In places, it is difficult to distinguish the boundary between the subunits because they are so tightly backed in crystallographic continuity. Such growth forms are locally visible under SEM, in which the outer crystal encloses underlying subunits (PL. 4.29A). Due to preferential growth of quartz cement in the c-axis direction (Waugh, 1970), rhombohedral faces are

invariably larger and more pronounced than prism faces. The final stage of overlapping produces almost perfectly formed authigenic quartz crystals that have the general appearance of hexagonal bipyramids (PL 4.29B-D).

Under normal conditions of cementation, adjacent grains compete for the diminishing pore space and interface with each other to produce a non-porous jigsaw puzzle interlock or mosaic of framework grains and their overgrowths (PLs. 4.24C, D; 4.25A).

Some quartz grains have two different sizes of overgrowths (PL. 4.29D). In the smaller mode, the crystals lack obvious crystal faces and form the same "bob-like" feature mentioned by Pittman (1972). In the larger mode, overgrowths have smooth, well-formed crystal faces. On polycrystalline quartz grains, each crystal unit has its own overgrowth in optical continuity with its subcrystal (PL. 4.30A, B; cf. Waugh, 1970). Some quartz overgrowths were formed at late stage postdating pressure solution. They mostly have no "dust" line (PL. 4.30C) and were formed around the grains subjected to pressure solution during compaction of the sediments. The well defined crystal faces of quartz of this stage confirm that overgrowth had taken place very late after leaching of calcite and initiation of appreciable oversized pores (PL. 4.30D). This is in a close agreement with Abdel-Wahab and Turner (1991), who considered the development of quartz overgrowth as a function of dissolved carbonate or unfilled pores. The studied sandstones are believed to be cemented by calcite at an early stage, and therefore the well developed quartz overgrowth resulted shortly after calcite dissolution, however insignificant amount of quartz overgrowths are present.

Quartzarenites and other quartz-rich sandstones occur chiefly in cratonic sequences tend to have the greatest amounts of quartz cement

(Pettijohn, 1975; Pettijohn et al., 1987). Sandstones of tectonically more active sedimentary basins are less quartz-rich and tend to have less quartz cement but have greater amount of clay minerals, carbonates and other cements. Quartz overgrowths in the studied sandstones are relatively volumetrically insignificant, although these sandstones are mostly quartzarenites. This may be attributed to quartz overgrowth inhibition. Several workers reported that mineral coatings on detrital quartz grains and entrapment of hydrocarbons in pores retard or inhibit quartz overgrowths by isolating detrital grains from water capable of precipitating quartz overgrowths (Füchtbauer, 1967; Pittman, 1972; Heald and Larese, 1974; McBride, 1989). Grain coatings have various origins, including emplacement of clays by infiltering near-surface ground water (Crone, 1975), formation of hematite as a near-surface oxidation product of Fe-bearing silicates (Walker, 1967), clay cements introduced during burial (Wilson and Pittman, 1977), and early diagenetic rim calcite (James, 1985). Coatings in the studied sandstones are, in decreasing order, infiltrated clays, hematite, calcite and opal (now dissolved or recrystallized to quartz). Where coatings have interfered with overgrowth and effectively inhibited enlargement, there are uneven quartz overgrowths in contact with portions of detrital grains (PL. 4.30C). Uneven quartz overgrowths are additional evidence of pre-existing grain coatings, which may be removed during diagenesis by solution or replacement. Clay coatings may have inhibited the precipitation of quartz cement in most samples in the manner described by Heald and Larese (1974). These coatings together with Iron minerals coatings and cements have both inhibited quartz overgrowth and resulted in incomplete (inhaled) crystals of the less advanced stages. The relatively high content of iron minerals and clays in Araba and subsurface sandstones might

explain their low quartz overgrowth content compared with Naqus Sandstone. Another factor might be the grain size; quartz cement has preference for coarse grained beds (McBride, 1984).

Authigenic quartz cement is also present in the form of silcrete. The term "silcrete" is applied to the highly siliceous indurated material formed at, or near, the earth's surface through the silicification of bedrock, weathering products, or other deposits by low temperature physico-chemical processes (Goudie, 1985). Silcretes occur often on the high parts of topography by silica deposition and removal of other elements. They form in many non-marine environments and range in age from Paleozoic to Holocene (Ollier, 1991). Herein, silcrete occurs as sandstone sheets of limited extension that range in thickness from 1 to 4 m and which have well developed vertical to subvertical joints giving rise to a columnar appearance (PL. 3.8B) that is typical of many silcrete occurrences elsewhere (cf. Smale, 1973; Langford-Smith, 1978; Summerfield, 1983b; Thiry and Millot, 1987; Ollier, 1991).

The studied silcrete is entirely composed of detrital quartz grains cemented by diagenetic quartz that reduced much of the primary porosity (PLs. 4.24C, D; 4.25A; 4.30C). The remaining porosity ranges from 1.8 % to 3.2 % with an average of 2.1 %. Two types of quartz cement were recognized: syntaxial quartz overgrowths and microcrystalline quartz. Syntaxial quartz overgrowths are by far the most common. They reach the highest degree of crystalline perfection where well-developed crystal faces completely enclose whole detrital grains (PLs. 4.7B; 4.24C, D; 4.25A; 4.30C). Most of the overgrowths exhibit successively zoned layers (PL. 4.31A). Microcrystalline quartz occurs in a considerable amount in the studied silcrete. Two modes of microcrystalline quartz cement are observed: microcrystalline drusy cement and microcrystalline mosaic

cement. The former occurs as isopachous fringes of equant quartz crystals covering syntaxial overgrowths and partially filling intergranular pores in the silcrete as the last incomplete stage of pore fill (PL. 4.31A, B). Microcrystalline mosaic texture was found as a part of the groundmass where the quartz grains, which are partially or completely enclosed by syntaxial quartz overgrowths, seem imbedded in it (PL. 4.31C, D). The SEM shows the material to be well developed, subhedral to euhedral microcrystalline quartz crystals (0.4-12 μm in diameter). These crystals almost fill the remaining pores (PL. 4.28C, D). Microscopic and SEM investigations revealed that syntaxial quartz overgrowth is the first silica phase to form in the studied silcrete. Thereafter, it is coated by either mosaic or drusy microcrystalline quartz (PLs. 4.28C, D; 4.31).

4.3.2 K-feldspar

Authigenic K-feldspar is present only as a minor constituent in the studied sandstones. It occurs as individual crystals partially filling pores (PLs. 4.32; 4.33). Such crystals lack detrital cores and are wholly authigenic. Some crystals show the typical adularia habit in which the (100), (001) and (101) forms are well developed (PL. 4.32C), other crystals were later subjected to dissolution (PL. 4.33B-D).

4.3.3 Clay minerals

Identifying and characterizing clay minerals is an important part of reservoir sandstone description. Clay minerals affect petrophysical characteristics by introducing considerable microporosity to the pore system, which, in turn, influences rugosity, saturation, and wetting characteristics. Diagenetic clay minerals are widespread in sandstones. They have been described by many authors (Wilson and Pittman, 1977). Common clay minerals occur not only as true cement from imported material precipitated from solution, but also as cement generated by

reaction between pore fluid and framework grains, and as a replacement of framework grains (e.g. kaolinization of K-feldspar and ferromagnesian minerals). They also occur as infiltrated particles transported physically in suspension in ground water. These various origins of clay minerals can be distinguished generally by textures seen in thin section, with the scanning electron microscope, or from X-ray diffraction data. Grain size and textural characteristics of clay minerals may vary considerably for any single mineral and between different minerals. Typically, the "clay" size fraction is defined as all particles with a mean spherical diameter (msd) of < 2 μm. Clay minerals, however, commonly may be finer grained, for example msd < 0.1 μm, or coarser grained, msd > 2 μm, and the clay-size fraction may include nonclay minerals. The studied sandstones contain both allogenic (infiltrated) and authigenic clays.

4.3.3.1 Allogenic (Infiltrated) clays

Clays introduced to the sediment shortly after deposition may occur as the result of mechanical infiltration of water containing suspended clay particles (Wilson and Pittman, 1977). Even though such clays are recognized as the earliest diagenetic event in many sandstones, generally they are not considered as authigenic. Herein, allogenic clays are found in minor proportions. They make up to 9.00 % of the whole rock volume of Naqus Sandstone and up to 11.75 % of those of Araba Sandstone. The average values for allogenic clays in the two formations are 1.21 and 1.80 %, respectively. On the other hand, the subsurface sandstone has infiltrated clays that may reach 21.50 % with an average of 4.42 % of the whole rock volume (Table. 4.1). The recorded infilterated clays occur as randomly distributed aggregates in pores and may fill to various extents the interstiatial voids (PL. 4.34A-C). In some samples, clay particles are oriented perpendicular to grain surfaces forming pore bridges (PL.

4.34D). The infiltrated clays in the studied sandstones are predominantly represented by kaolinite with traces of other clay minerals as was demonstrated by XRD and SEM.

4.3.3.2 Authigenic clays

The term authigenesis in sandstones was introduced by Heald (1950) to refer to the growth of new minerals by the *in situ* alteration of others after their deposition. Released ions from feldspars and rock fragments dissolution as well as replaced clay minerals, would be repricipitated as authigenic clay minerals. The newly formed clay species are functions of the environmental conditions such as Eh, pH and activities of other ionic species. Replacement clay, which considered authigenic (Willson and Pittman, 1977), plays an important role in changing the texture, mineral composition and the bulk chemistry of the sediments. This process is closely associated with dissolution and is responsible for the release of different chemical elements into the interstitial solution for development of authigenic minerals. Authigenic clay minerals have been described by many authors such as Willson and Pittman (1977), Hawkins (1978), Sommer (1978), Abdel-Wahab and Abu El-Maati (1989) and Abdel-Wahab and Turner (1991). All of them have confirmed the diagenetic origin of interstial clay and described different authigenic clay minerals.

Identification of clay minerals in the studied sandstones is mainly based on X-ray diffraction analysis, SEM observations, beside some pronounced features of clay minerals under high-power examination by using polarizing microscope investigations. Authigenic clays in the studied sandstones are represented mainly by kaolinite with minor amounts of illite, smectite, illite-smectite mixed-layer and chlorite. Such clays occur not only as as true cement from imported material precipitated from solution, but also as cement generated by reaction between pore

fluide and framework grains, and as a replacement of framework grains (e.g. kaolinization of K-feldspar and mica).

4.3.3.2.1 Kaolinite

Kaolinite occurs as authigenic grain attachments forming a weak grain cement. It is the most common authigenic clay mineral recognized in the studied sandstones. Kaolinite makes up 37.00 % of the whole rock volume of Naqus Sandstone and up to 24.00 % of those of Araba Sandstone. The average values of kaolinite in the two formations are 7.73 and 14.20 %, respectively. On the other hand, kaolinite in the subsurface sandstone may reach 10.00 % with an average of 1.29 % of the whole rock volume (Table 4.1). Values of kaolinite reported from point counts do not reflect the cryptic microporosity between clay platelets, which may reach 60 % of the kaolinite volume (cf. Hurst and Nadeau, 1995). Kaolinite varies largely in abundance among the studied sandstone units, and also in samples from the same unit. For example, it shows a remarkable decrease towards the topmost part of Naqus Sandstone. This remarkable decrease in kaolinite percentage is associated with better reservoir characteristics as will be discussed in chapter 6.

Scanning electron microscopy, backscattered electron imaging and high-power petrographic investigations show that diagenetic kaolinite in the studied sandstones display different morphologies. Kaolinite occurs typically as a pore-filling cement, but also as a replacement of feldspar grains and as an alteration product of muscovite and other ferromagnesian minerals (PLs. 4.35-4.38).

Pore-filling kaolinite is by far the most abundant, it makes up to 37.00 % of the whole rock volume of Naqus Sandstone and up to 23.75 % of those of Araba Sandstone. The average values for pore-filling kaolinite in the two formations are 7.14 and 12.35 %, respectively. On the other hand,

pore-filling kaolinite in the subsurface sandstone may reach 10.00 % with an average of 1.27 % of the whole rock volume (Table 4.1). It occurs in the form of face-to-face stacking of microporous pseudohexagonal plates (PLs. 4.26; 4.35D; 4.36) that have microporosities varying from 25.00 to 60.00 % (cf. Hurst and Nadeau, 1995). The micropores are largely hidden in thin sections, but they are recorded by SEM (PL. 4.36).

Vermicular kaolinite with a delicate vermicular form occurr as both isolated crystals and in clusters. The vermicular crystals exhibit a sequence of stacked pseudohexagonal plates that may extend the length of a pore and typically form curving, semicircular forms (PLs. 4.35D; 4.37A, B). Fine-grained masses of blocky crystals are another morphologic type of kaolinte (PL. 4.37C). Fan-shaped kaolinite is occasionally recorded (PL. 4.37D). Kaolinite also occurs as orderly stacked crystals where the individual cleavage plates tend to be aligned along the c-axis direction (PL. 4.36B, C).

Kaolinized K-feldspar and muscovite grains are the most common diagenetic textures of replacive kaolinite in the studied sandstones (PLs. 4.6D; 4.14B-D; 4.38). Kaolinite-replaced grains make up to 15.00 % of the whole rock volume of Naqus Sandstone and up to 7.50 % of Araba Sandstone. The average values for these grains in the two formations are 0.59 and 1.85 %, respectively. On the other hand, kaolinite-replaced grains in the subsurface sandstone may reach 0.75 % with an average of 0.02 % of the whole rock volume (Table 4.1). Partial or complete kaolinization of detrital K-feldspars is common (PLs. 4.14B-D; 4.38A, B). Some detrital muscovite grains (commonly termed "kaolinized" muscovite) have been extensively replaced by kaolinite at their splayed ends and along cleavage planes (PLs. 4.6D; 4.38C). On the other hand, few grains are completely neomorphosed to kailinite (PL. 4.38D).

It appears that the vermicular and pseudohexagonal plates of kaolinite are formed authigenically after burial of sand. Such textures could not have result from detrital sedimentation or infiltration.

4.3.3.2.2 Illite, Smectite and Illite-Smectite mixed-layer

Herein, these clays have a minor importance and are mainly recorded with SEM (PL. 4.39). However, illite and illite-smectite mixed-layer clays are recorded in a considerable amount in some subsurface sandstone samples from wells RB-A1 and RB-C2 as indicated by XRD analysis (Table 4.8).

4.3.3.2.3 Chlorite

Traces to minor quantities of authigenic chlorite have been detected in the subsurface sandstone. Authigenic chlorite was noted with the SEM (PL. 4.39D) and was not detected by XRD analysis, this is most likely due to its insignificant content. However, one sample from RB-A3 well (depth 12432 feet) is found to have an exceptionally large quantity of Fe-rich chlorite (up to 7 % of the whole rock volume).

4.3.4 Iron minerals

Iron minerals are abundant and ubiquitous cement in the studied sandstones. They vary largely in abundance among the studied sandstone units, and in samples from the same unit. They may comprise up to 6.50 % of the whole rock volume of Naqus Sandstone and up to 32.25 % of those of Araba Sandstone. The average values of iron minerals cement in the two formations are 1.55 and 17.22 %, respectively. On the other hand, iron minerals cement in the subsurface sandstone may reach 13.50 % with an average of 4.04 % of the whole rock volume (Table 4.1). Some subsurface sandstone samples have more than 70 % by volume of iron minerals cement (mainly hematite), such samples were not included in the point counting.

Identification of iron minerals was mainly based on petrographic and SEM observations. X-ray diffraction analysis of iron-rich sandstone samples was of little value due to the amorphous or cryptocrystalline nature of the recorded iron minerals. In the studied sandstones, iron minerals are mainly represented by hematite, with some goethite. Under sedimentary conditions, goethite is unstable with respect to hematite (Berner, 1969; Langmuir, 1971). Thus thermodynamically, any sediment containing sufficient FeO(OH) might eventually end up as a red bed.

Iron minerals display different textural varieties as revealed by petrographic examination of thin sections. Hematite-nodule-bearing sandstones are one type. The hematite nodules are composed of hematite and quartz grains. They have a homogenous simple fabric of sand or silt-sized grains set in a well cemented hematite zone (PL. 4.18C). In some instances, iron-bearing solutions infiltrated along fractures, bedding planes, solution seams and sutured contacts between grains to develop hematite-rich zones (PL. 4.40A-C). Iron minerals were also found completely or partially filling fracture planes which resulted from either compaction or shuttering of detrital quartz grains (PL. 4.2C, D).

The iron minerals also occur as evenly distributed grain coats. The absence of iron minerals coating at grain contacts indicates late stage diagenetic origin for those iron minerals (PL. 4.27A). In other cases they may occur in the interstitial and secondary pore spaces as pore-filling cement which completely destroys both the primary and secondary porosity (PLs. 4.40D; 4.41).

In many studied samples, more than one generation of hematite was identified. It may coat both detrital quartz grains and authigenic quartz overgrowths (PL. 4.41B). This suggests that the hematitic pigment, in case of lowering the water table, may begin to form from reactions with

the oxidizing alkaline ground water, shortly after deposition and continue to develop over a long time. Walker (1976) suggests that the earliest pigment forms by alteration of clay-sized goethite, and that later pigment forms by neoformation following dissolution of iron-rich minerals. A multistage of oxidation has been reported also by Abdallah et al. (1993) in several ferruginous horizons, a primary oxidizing condition having a continuous Fe-oxide impregnation that coats quartz grains, and a secondary one having Fe-oxide cement generations that postdate earlier cements and compaction. In the present sandstones, iron minerals may fill the intercrystalline boundaries of polycrystalline grains (PL. 4.41C, D).

SEM study revealed many textural varieties that could not be distinguished by using the polarizing microscope. These different textures have no distinctive colors. Botryoidal and cellular textures of hematite as grain coating, pore-filling, pore-lining and coating quartz overgrowths (PLs. 4.29C; 4.42; 4.43A) are common. Hematite rosettes are also recorded. The crystals are elongated (rod-like) or blade-like in shape (PL. 4.43B-D). They occur as interstitial pore-filling, pore-lining and as drusy coatings on the surface of both detrital quartz grains and quartz overgrowths.

Sometimes iron minerals occur as extensive pore fill in sufficient abundance to warrant the term ferricrete (PL. 4.41C). The term "ferricrete" was coined by Lamplugh (1902) for material cemented by iron oxides and was reviewed by Ollier and Galloway (1990). Ferricretes can form either by pedogenic processes or by the precipitation of iron minerals from laterally flowing surface or ground water (Ollier and Galloway, 1990). The simple textural and mineralogical forms of iron concentrations described in the current study agree with the ground water ferricretes (cf. Milnes et al., 1987; Wright et al., 1992; Abdallah et al.,

1993) and should not be confused with compositionally and structurally complex iron concentrations which are typically found in pedogenic laterites (cf. Tardy and Nahon, 1985; Milnes et al., 1987; Nahon, 1991). The studied ground water ferricretes are also compatible with Blodgett et al. (1993), who concluded that many sedimentary beds with red pigmentation do not show evidence of pedogenesis, and the formation of pigment in red beds is generally not an outcrop weathering phenomenon.

Field observations show different varieties of ferricrete facies including liesegang bands and color mottling (PLs. 3.1A-D; 3.2A, B). The yellow, brown, red and purplish red colors of sandstones are attributed to different iron oxide minerals in these rocks. The yellow color is produced by goethite, dark brown by maghemite, red and purplish red by hematite (c.f. Blodgett et al., 1993). However, the degree of "purpleness" imported by hematite increases clearly with particle size and clustering of hematite crystals (Torrent and Schwertmann, 1987). Different sandstone samples with gradations in color from bright red through darker red were studied by SEM. The study shows that the larger the crystal size and more dense the crystal cluster, the darker the red color in the studied sandstones.

4.3.5 Calcite

Non-ferroan calcite is the main carbonate mineral present as a cement in the studied sandstones. Calcite cement makes up to 2.00 % of the whole rock volume of Naqus Sandstone and up to 0.75 % of those of Araba Sandstone. The average values of calcite cement in the two formations are 0.12 and 0.10 %, respectively. On the other hand, calcite cement in the subsurface sandstone may reach 2.25 % with an average of 0.17 % of the whole rock volume (Table 4.1).

Based on petrographic and SEM observations, calcite is mainly present as poikilotopic spar with individual crystals reaching several millimeters

in diameter. However, very fine disseminated relics of micritic to fine sparry calcite (grains of 0.5 to 20 μm) can be occasionally seen, such relics could be considered as an early stage calcite. Both forms of calcite fill both intergranular primary pores and oversized secondary pores (PL. 4.44A-C). Oversized patches of calcite were formed by replacing feldspar grains with no preserved ghosts or by filling the pores formed where feldspars dissolved after burial. SEM examination reveals that poikilotopic calcite cement occurs as blocky mosaic forms surrounding detrital grains and filling pore spaces (PLs. 4.44D; 4.45A). Also, calcite crystals with a euhedral rhombic outlines are frequently recorded (PL. 4.45B, C).

Herein, calcite cement has a patchy distribution (PLs. 4.45D; 4.46A) and is not observed in all samples, however, the abundance of large, oversized pores, floating grains, corroded and etched quartz grains (PL. 4.46B-D) may suggest that calcite cement was once widespread but was subsequently dissolved.

4.3.6 Halite

Halite occurs in both surface and subsurface sandstones. It makes up to 7.00 % of the whole rock volume of Naqus Sandstone and up to 3.00 % of those of Araba Sandstone. The average values of halite in the two formations are 1.01 and 0.52 %, respectively. In the subsurface sandstone, halite may reach 7.75 % with an average of 2.30 % of the whole rock volume (Table 4.1). Because halite is presently undergoing dissolution, its original extent is unknown.

In the studied sandstones, halite occurs mainly as a pore-filling cement and fills oversized areas (PL. 4.47A-C). Also it fills the fracture planes of detrital quartz grains (PL. 4.47D). Such planes may result from either compaction or shuttering. SEM observations indicate that halite also

occurs as small cubic crystals with rounded corners due to dissolution (PL. 4.48A, B), and as massive, waxy coatings on detrital grains and other authigenic cements (PL. 4.48C, D). Textural relationships and the fresh surfaces of halite crystals indicate that halite cement is a late diagenetic event.

4.3.7 Gypsum

Gypsum forms scattered patches of cement in few samples. Most patches are at the millimeter scale, but locally, they may be at the centimeter scale (PL. 4.27C, D). Quartz grains contained within and/or contacted gypsum cement, usually display deeply embayed margins and eroded edges due to peripheral replacement (PL. 4.27C, D). Such replacement is either the product of a pre-existing calcite or the present sulphate minerals. Textural relationships and the fresh surfaces of gypsum crystals indicate that gypsum cement is a late diagenetic event.

4.4 X-ray diffraction analysis

X-ray diffraction analysis was carried out on selected samples to identify the clay mineral species and shed light on their possible sources and to get an idea about the diagenetic history of the studied sandstones. The results of X-ray diffraction analysis are broadly in accordance with the results of the petrographic examination. These results show that quartz is the only detrital mineral of significant amount in the studied sandstones, also indicate the presence of the same suite of authigenic minerals except for iron minerals that are believed to be cryptocrystalline or amorphous. XRD analysis of the clay fraction indicate that the authigenic clay mineral suite in the studied sandstones are mainly represented by kaolinite with traces or minor quantities of illite, illite-smectite mixed layer and chlorite, particularly in the subsurface sandstone. A semi-quantitative estimation of the mineral composition of

the bulk samples and the oriented clay fractions was performed (Table 4.8 and Fig. 4.4).

4.5 Porosity

Porosity is the third architectural component of the studied sandstones. It may reach 27.75 % of the whole rock volume of Naqus Sandstone and 11.50 % of those of Araba Sandstone. The average values of thin section porosity in the two formations are 17.57 and 3.45 %, respectively. On the other hand, thin section porosity in the subsurface sandstone may reach 14.75 % with an average of 4.86 % of the whole rock volume (Table 4.1).

From petrographic investigation, porosity was divided into four categories: 1) intergranular pores (PL. 4.49A, B), 2) oversized pores (PL. 4.49C, D), 3) intragranular pores (PL. 4.50A) and 4) fracture porosity (PL. 4.50B-D). Intergranualr pores are the most dominant, oversized pores have a considerable contribution, whereas, intragranular and fracture porosities are of less extent.

Herein, the term "secondary porosity" refers to percent of intragranular porosity plus percent of oversized pores and percent of fracture porosity, whereas intergranular porosity refers to all porosity between grains, whether it is primary or has resulted from the dissolution of pore-filling cement. This intergranular porosity is termed "primary porosity" taking in consideration neglecting of intergranular cement dissolution in the reported percentage (PL. 4.49B). Of the total present thin section porosity, primary porosity averages 75.06, 54.75, 95.70 %, and secondary porosity averages 24.94, 45.25 and 4.3 % in the Naqus, Araba and subsurface sandstones, respectively (Table 4.4). Most of the secondary porosity appears to have resulted from the partial to complete dissolution of unstable detrital grains, particularly feldspars, based on the remnants found within some secondary pores (PLs. 4.15C, D; 4.16). However,

dissolution of calcite cement in some samples contributes to that population of secondary porosity (PL. 4.49C). Porosity, together with other important petrophysical parameters of the studied sandstones, will be considered in chapter 6.

4.6 Depositional environment of the studied sandstones

The sediments of Naqus Formation, which are formed of non-fossiliferous white quartizitic sand and pebbles, are believed to have a non-marine mode of deposition. The numerous quartz pebbles found distributed randomly in Naqus Sandstone or in fining upward sequence along its cross-bedding suggest a high energy shallow agent of transportation, probably a meandering fluvial system. The streams were probably very erratic and intermittent with coarse load at the bottom followed by the finer sediments with the diminishing of the flood. The proposed fluvial origin for Naqus Sandstone is strengthened by the presence of convolute bedding and recumbent foresets.

Araba Formation represents an aqueous environment. The presence of cross-bedding, carbonate cement and fossil tracks of *Cruziana* and *Skolithos* as well as the traces of burrowing organisms at the base of the formation may support a shallow marine depositional environment. The *Skolithos* ichnofacies clearly indicates clean, well-sorted near-shore sands with high levels of wave and current energy (intertidal zone). The varicoloration of the sandstone beds could be the result of oxidation processes due to the wind activation of oxygen dissolved in the sea water or the alteration of iron bearing minerals such as mica and feldspars. Biotite and hornblende may have been altered by weathering to hematite and goethite, which give the red coloration. The dominant sedimentary structure in the varicolored sandstones is conventional horizontal bedding, which also suggests a quite water agent. The observed small scale cross-beds with horizontal planes in between could be due to an abrupt decrease in the current velocity and increase of the water depth (cf. McKee, 1962).

Table 4.8: XRD data for the studied sandstones.

S. No.	Kaolinite %	Quartz %	Halite %	Gypsum %	Calcite %	Total Non Clays %
1- Araba Formation						
1	26.33	65.72	2.85	5.10	0.00	73.67
2	8.15	83.86	4.16	2.50	1.33	91.85
4	5.49	92.58	1.92	0.00	0.00	94.51
5	17.42	82.58	0.00	0.00	0.00	82.58
7	21.40	71.34	7.26	0.00	0.00	78.60
7D	18.91	66.28	0.00	0.00	14.81	81.09
9	25.48	62.26	0.00	9.09	3.17	74.52
10	22.52	71.78	2.52	3.18	0.00	77.48
Min	5.49	62.26	0.00	0.00	0.00	73.67
Max	26.33	92.58	7.26	9.09	14.81	94.51
Avg	18.21	74.55	2.34	2.48	2.41	81.79
2- Naqus Formation						
12	10.52	88.26	1.22	0.00	0.00	89.48
18	12.24	87.76	0.00	0.00	0.00	87.76
26	6.68	69.36	23.96	0.00	0.00	93.32
35	15.93	71.24	10.18	2.65	0.00	84.07
39	25.13	74.87	0.00	0.00	0.00	74.87
43	37.30	58.47	4.23	0.00	0.00	62.70
51	18.51	81.49	0.00	0.00	0.00	81.49
61	18.96	74.41	6.64	0.00	0.00	81.04
70	11.88	88.12	0.00	0.00	0.00	88.12
79	5.79	94.21	0.00	0.00	0.00	94.21
87	7.76	92.24	0.00	0.00	0.00	92.24
98	10.43	89.57	0.00	0.00	0.00	89.57
103	3.54	96.46	0.00	0.00	0.00	96.46
108	2.00	98.00	0.00	0.00	0.00	98.00
111	1.70	98.30	0.00	0.00	0.00	98.30
Max	37.30	98.30	23.96	2.65	0.00	98.30
Min	1.70	58.47	0.00	0.00	0.00	62.70
Avg	12.66	84.18	3.08	0.18	0.00	87.44

S. No.	Kaolinite %	Illite %	Illite-Smectite Mixed Layer %	Quartz %	Hematite %
3- Subsurface					
A1-12335.5	8.00	1.00	0.00	91.00	0.00
A1-12340	4.00	3.00	1.00	92.00	0.00
A1-12462	7.00	1.00	0.00	92.00	0.00
A5-12222	7.00	0.00	0.00	93.00	0.00
A5-12257	6.00	0.00	0.00	94.00	0.00
A5-12296	13.00	0.00	0.00	81.00	6.00
A5-12618	8.00	0.00	0.00	92.00	0.00
A5-12634	5.00	0.00	0.00	95.00	0.00
B3-12356	5.00	0.00	0.00	95.00	0.00
B3-12370	7.00	0.00	0.00	93.00	0.00
B3-12390	1.00	0.00	0.00	99.00	0.00
B3-12893	6.00	0.00	0.00	94.00	0.00
B3-12404	1.00	0.00	0.00	99.00	0.00
C2-12260	7.00	0.00	0.00	93.00	0.00
C2-12270	1.00	0.00	0.00	99.00	0.00
C2-12293	18.00	2.00	0.00	80.00	0.00
C2-12298	18.00	2.00	0.00	80.00	0.00
C2-12299	10.00	1.00	0.00	89.00	0.00
C2-12308	7.00	0.00	0.00	93.00	0.00
Max	18.00	3.00	1.00	99.00	6.00
Min	1.00	0.00	0.00	80.00	0.00
Avg	7.32	0.53	0.05	91.79	0.32

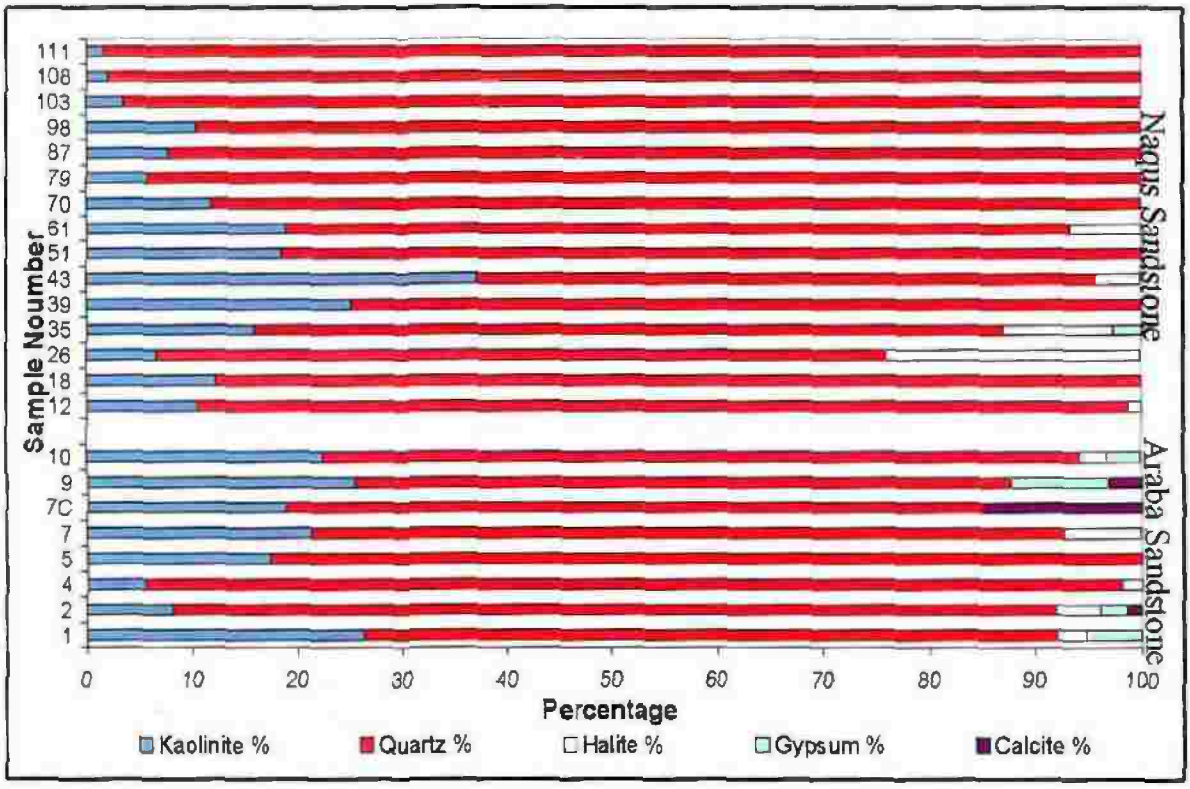

Fig. 4.4a: XRD data for the analyzed surface sandstone samples.

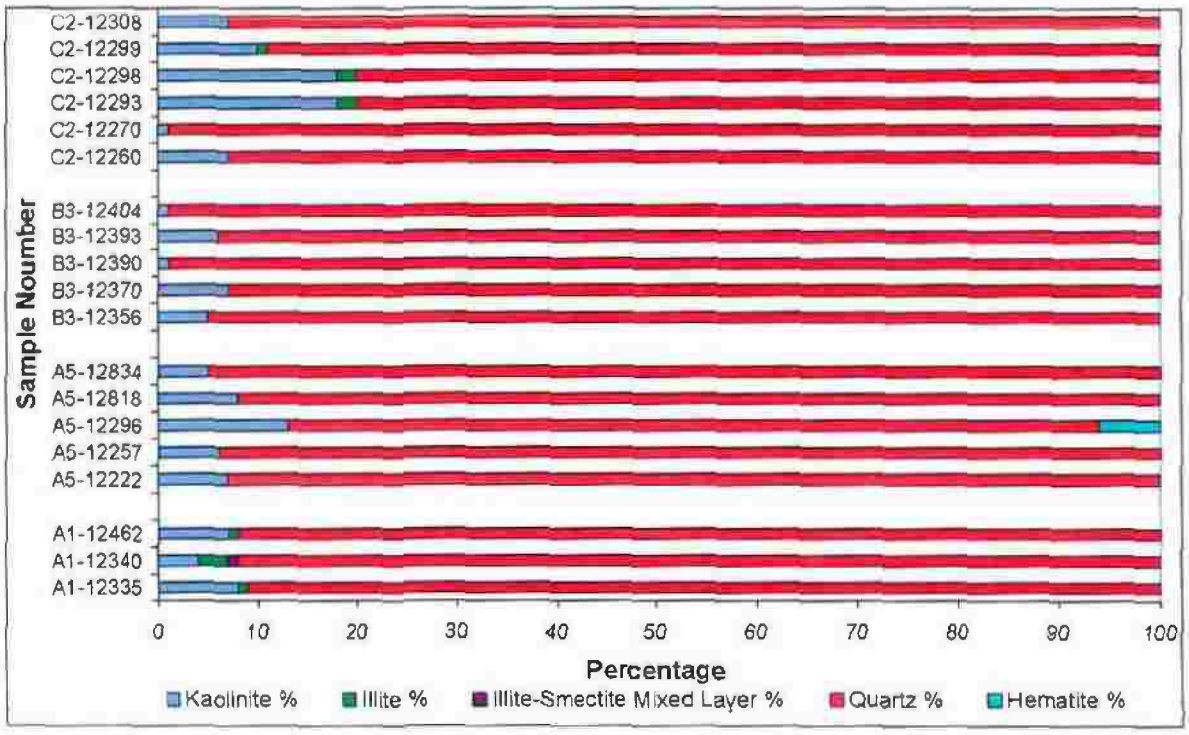

Fig. 4.4b: XRD data for the analyzed subsurface sandstone samples.

Plate 4.1

A) Monocrystalline detrital quartz displaying straight (nonudulose) extinction. Sample also shows closed packing and remnant porosity (blue stain). Plane light, sample RB-C2 (12290 ft).

B) A in crossed polarizers.

C) A textural inversion- a polymodal grain size distribution. Coarse sand grains are mixed together with very fine sand grains with some fragments in the intermediate size ranges. Such a texture can be produced by burrowing or other *in situ* mixing processes. Crossed polarizers, sample RB-B4 (12420 ft).

D) Same as C. Plane light, sample RB-A1 (12340 ft).

Plate 4.1

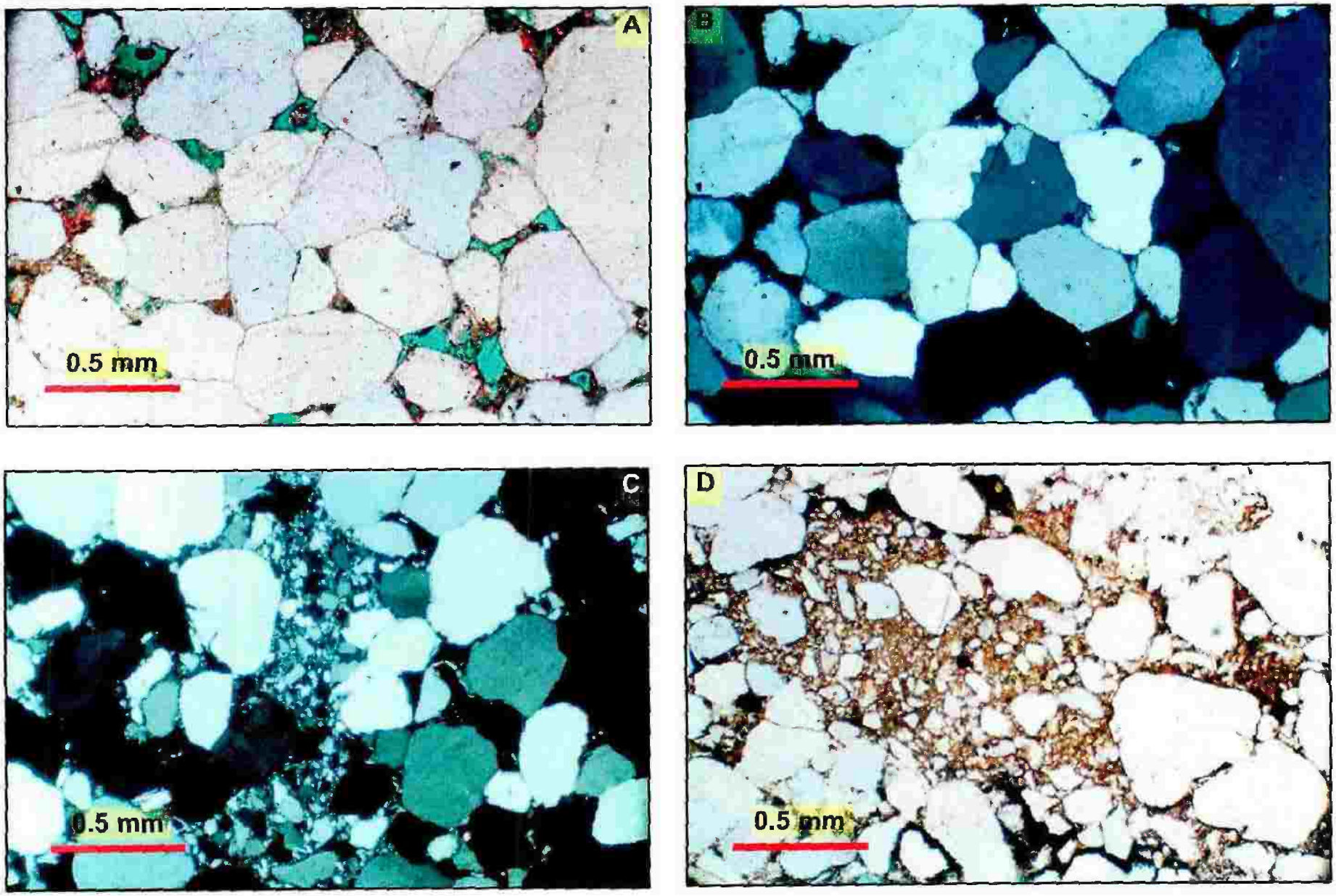

Plate 4.2

A) A textural inversion- well rounded but poorly sorted (possibly polymodal) grains. Crossed polarizers, sample RB-A1 (12460 ft).

B) Banding on the scale of a thin section. Crossed polarizers, sample Na-61.

C) Authigenic pore and fracture- filling hematite (Hm). Plane light, sample Na-35.

D) Close up view of C.

Plate 4.2

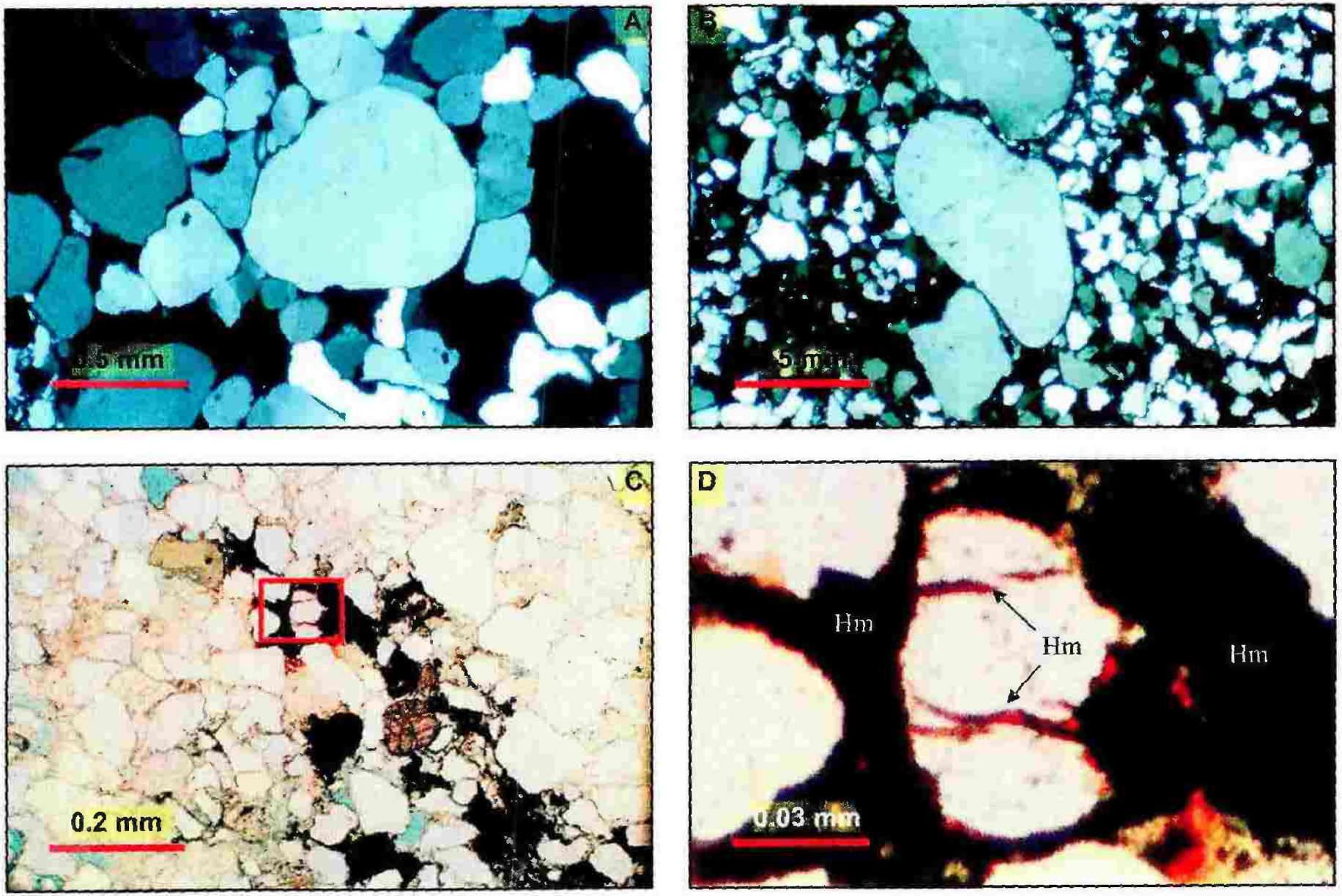

Plate 4.3

A) Intraparticle porosity (arrows) represented by microfractures in a detrital quartz grain. Microfractures can be very effective in improving permeability of tight sandstones. Slightly oversized pores (OSP) are also developed. Plane light, sample Na-18.

B) Monocrystalline quartz with elongate shape indicating either schistose or hydrothermal origin within relatively open quartz veins. Crossed polarizers, sample Ar-10.

C) Same as B. Plane light, sample Na-12.

D) Detail of volcanic quartz crystal (upper left). This grain has straight extinction, a euhedral outline, and a large "negative crystal" or vacuole. The vacuole has the same crystallographic orientation as the complete quartz grain, hence the term "negative crystal". This feature is common but not ubiquitous in quartz of volcanic origin. Plane light, sample Ar-9.

Plate 4.3

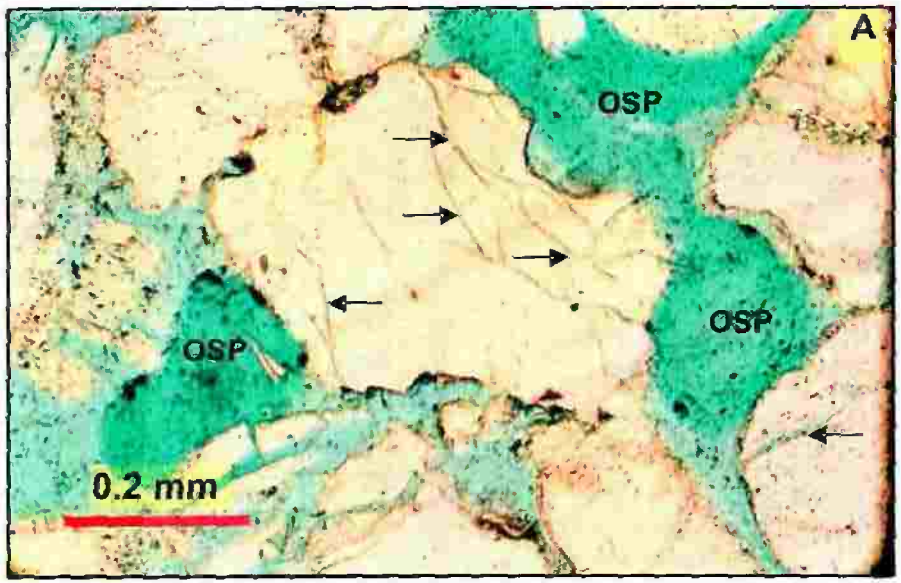

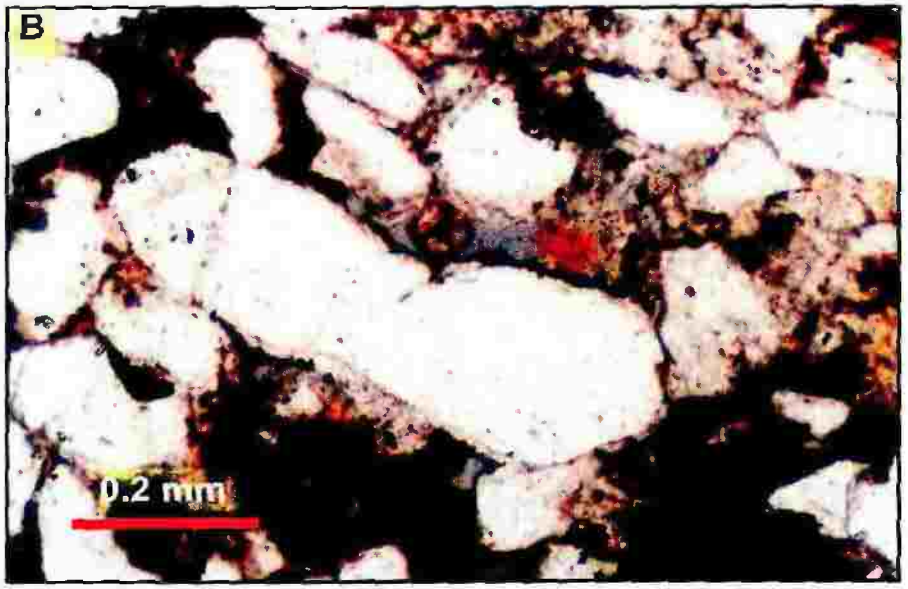

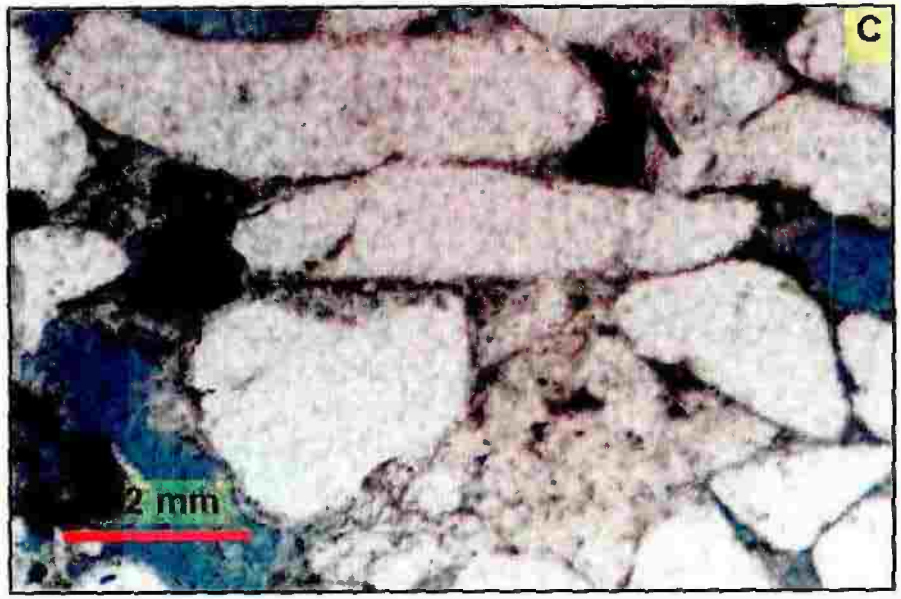

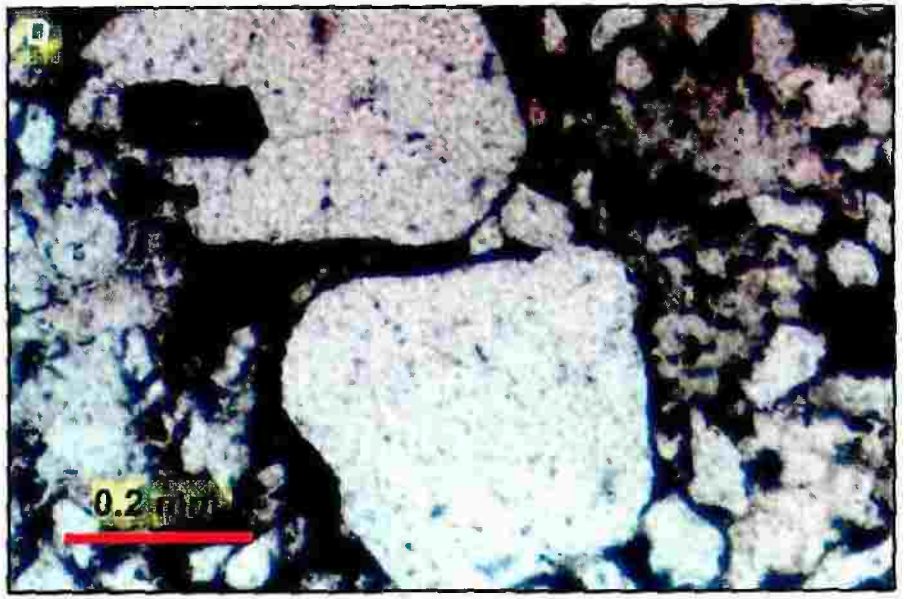

Plate 4.4

A) Monocrystalline quartz having idiomorphic hexagonal shape with perfectly straight sides, rounded corners and nonundulose extinction. This type is referred to as volcanic quartz and is derived from erosion of volcanic and shallow intrusive rocks. Crossed polarizers, sample Na-112.

B) A volcanic (β) quartz with euhedral, bipyramidal outline and straight extinction. The dark inclusion (blue arrow) is probably altered glass. Note the concavo-convex contact between grains (black arrow). Plane light, sample Na-112.

C) Monocrystalline detrital quartz with rounded overgrowth (R) of reworked origin (worn overgrowth). Plane light, sample RB-B3 (12401 ft).

D) Monocrystalline detrital quartz (upper left) showing regular segmented undulosity. Crossed polarizers, sample Na-112.

Plate 4.4

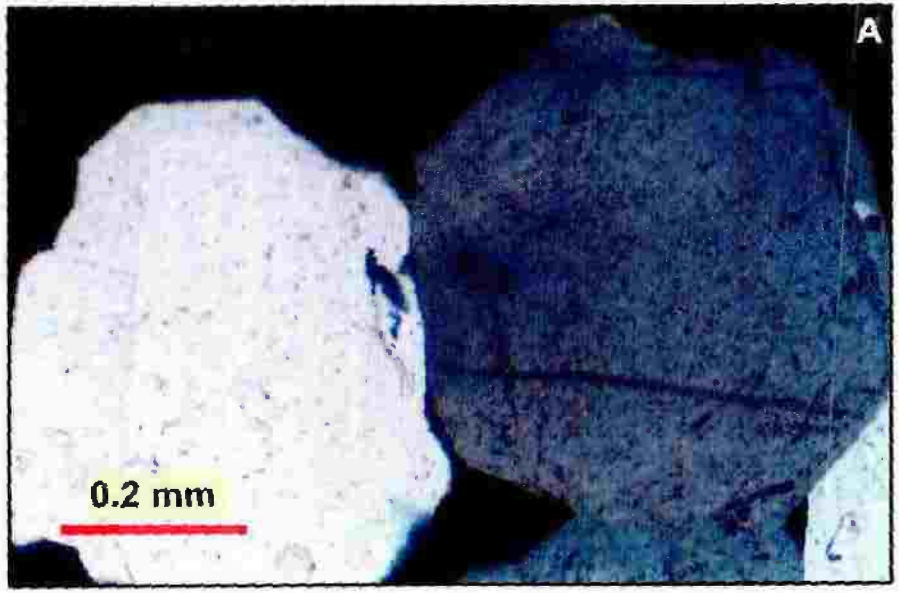

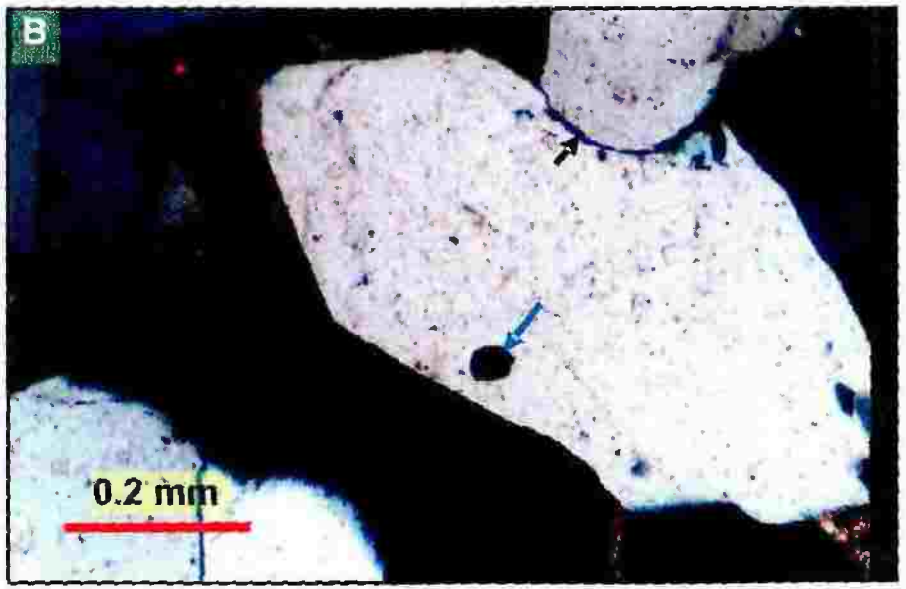

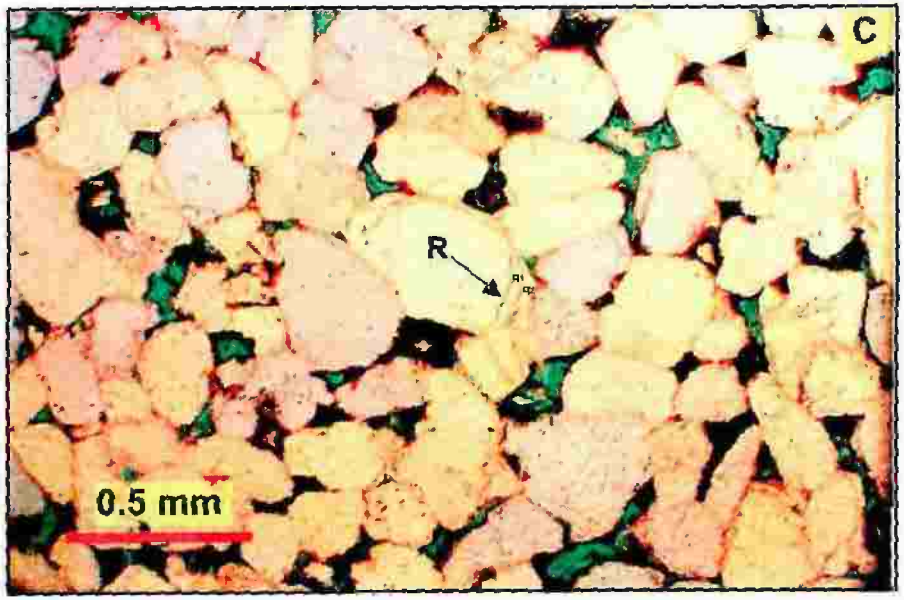

Plate 4.5

A) Monocrystalline detrital quartz (center) showing regular segmented undulosity. Crossed polarizers, sample RB-A1 (12460 ft).

B-D) Monocrystalline detrital quartz grains (center) showing irregular segmented undulosity. Crossed polarizers, samples RB-B7 (12251 ft), Na-28 and RB-A1 (12460 ft), respectively.

Plate 4.5

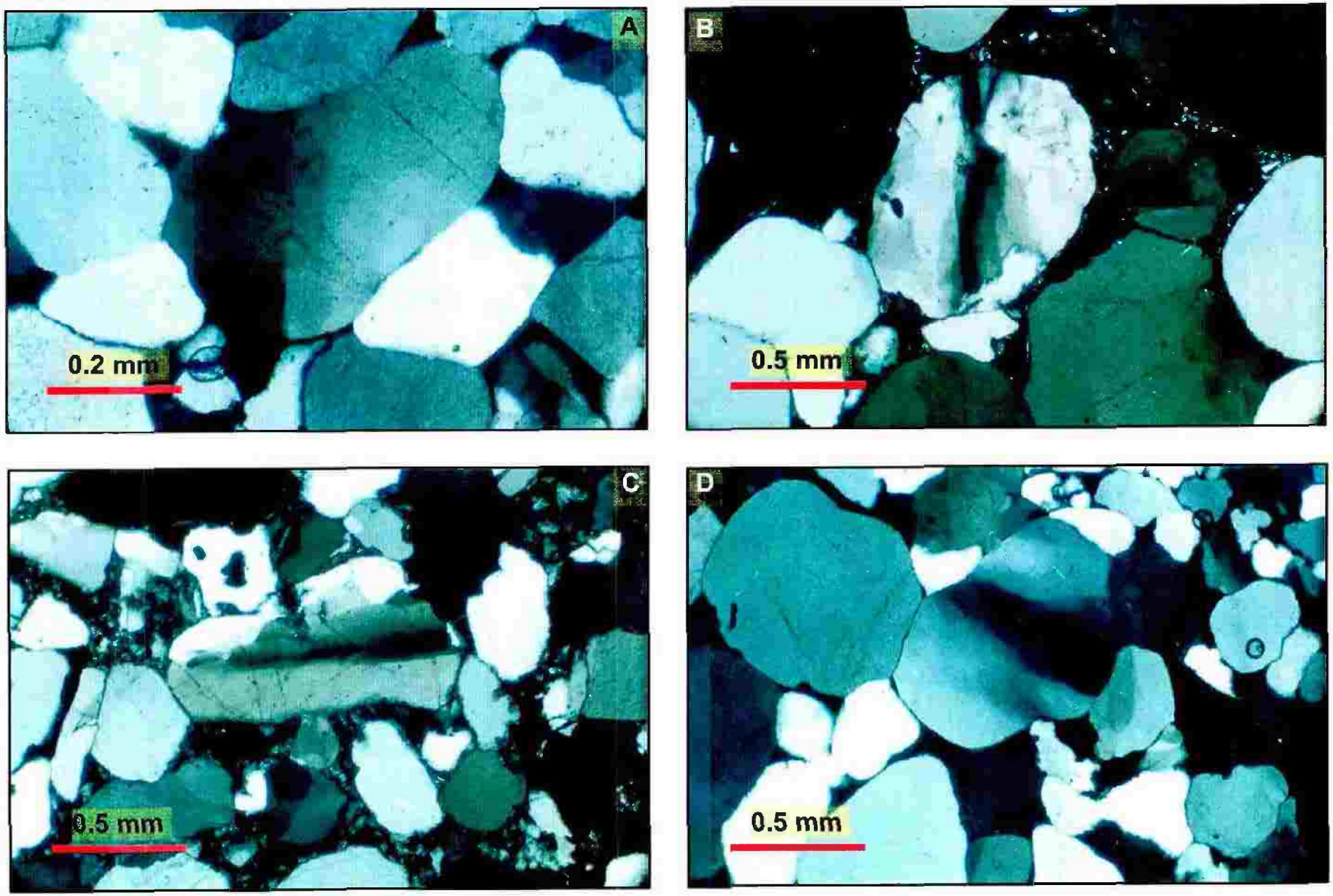

Plate 4.6

A) Strained quartz grain (lower left) showing extinction in the form of gradational bands. Crossed polarizers, sample RB-A5 (12305 ft).

B) A single-crystal quartz grain with strongly undulose extinction. Grain extinguishes completely with more than 5 degrees of stage rotation. Such grains may be more abundant in strained source rocks (especially metamorphics), but evidence is still incomplete. Crossed polarizers, sample Ar-9.

C) Boehm lamellae in a detrital quartz grain (center). Crossed polarizers, sample RB-A5 (12208 ft).

D) Monocrystalline quartz (lower right) with abundant vacuoles, probably gas and liquid trace. A Mica flake (M) was deformed between quartz grains and altered at its splayed ends. Crossed polarizers, sample Ar-10.

Plate 4.6

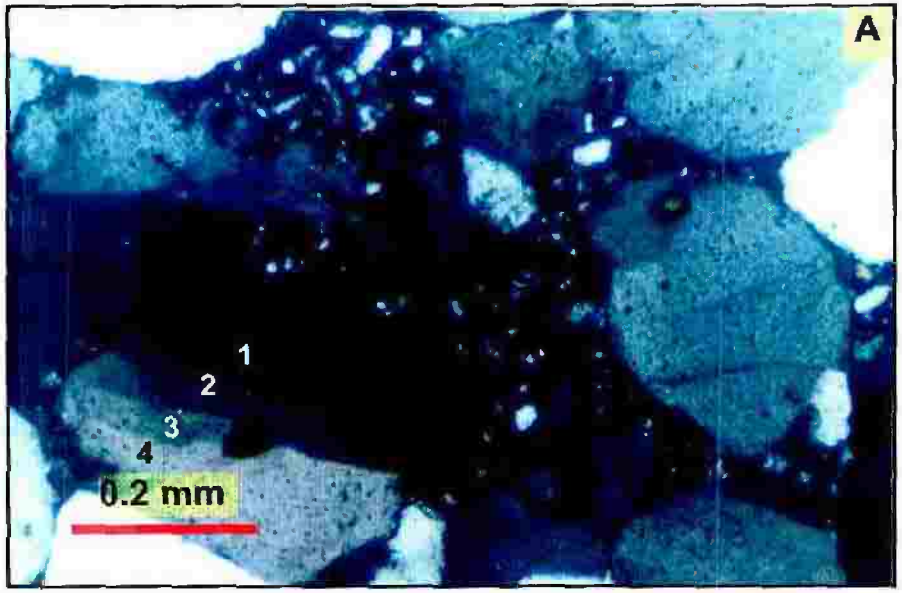

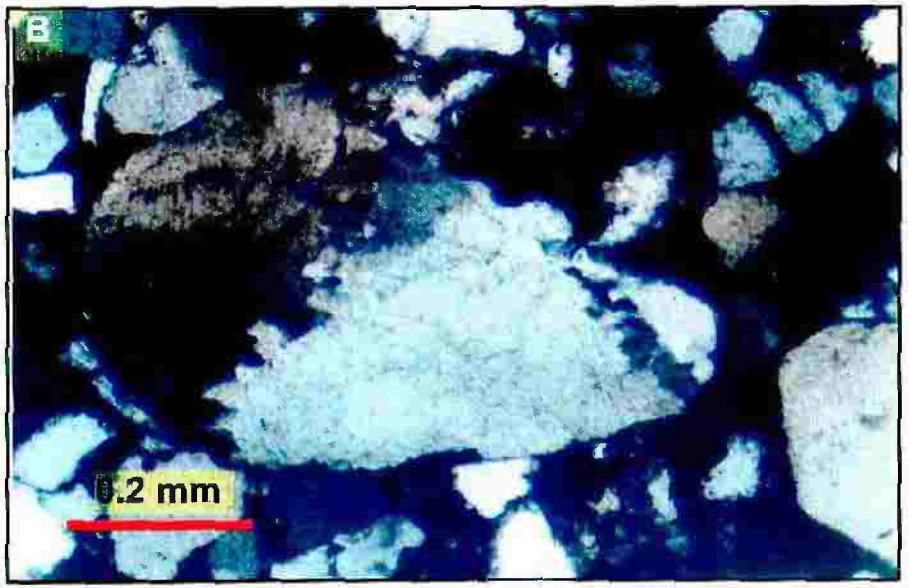

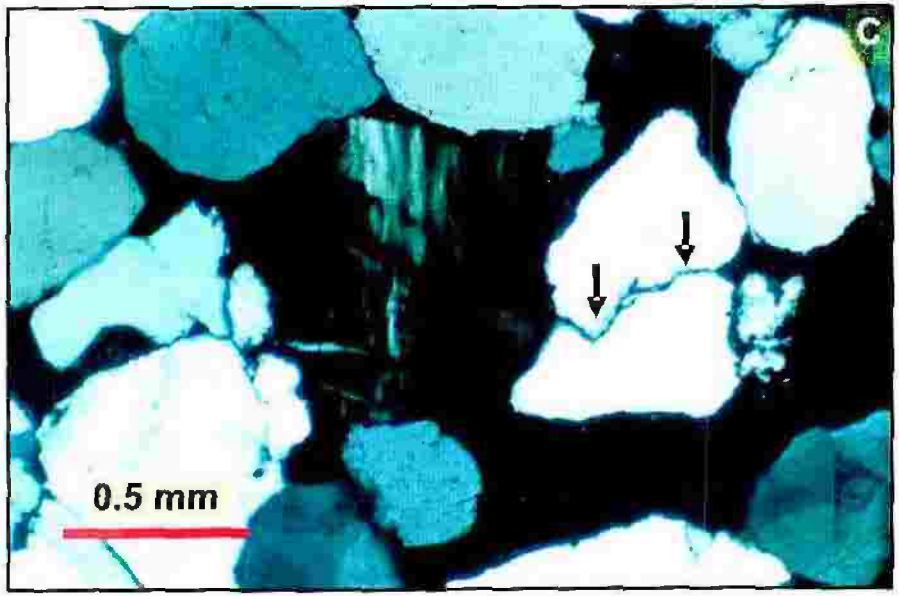

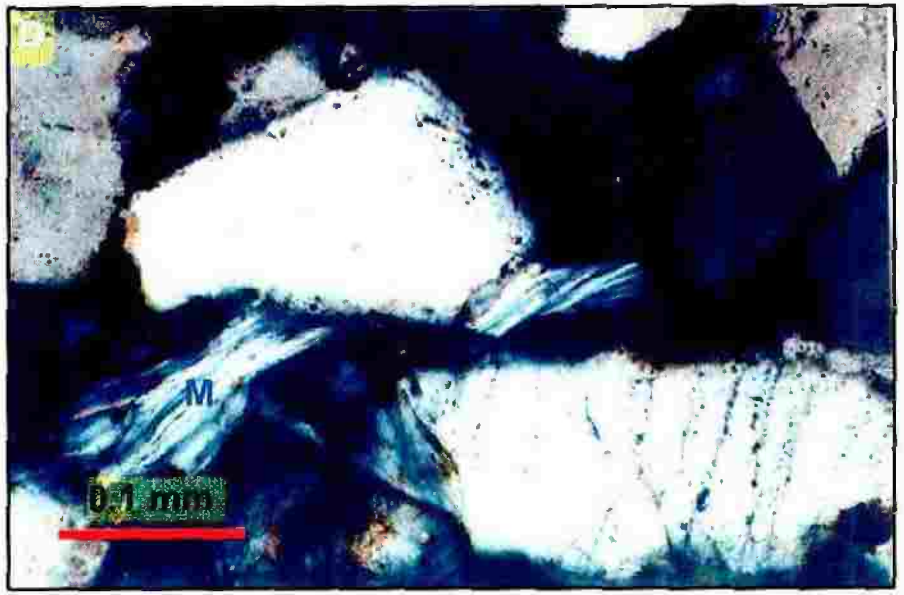

Plate 4.7

A) Monocrystalline quartz with bipyramidal zircon inclusion. Plane light, sample Na-12.

B) Monocrystalline quartz (center) with bipyramidal zircon inclusion. Quartz overgrowth with well-formed crystal faces (q) completely enclose whole detrital grain showing the highest degree of crystalline perfection. Crossed polarizers, sample Na-112.

C) Monocrystalline quartz (center) containing subhedral prismatic zircon (Z) and blue prismatic tourmaline (T) inclusions. Crossed polarizers, sample Ar-8.

D) Monocrystalline quartz (center) with green platy tourmaline inclusion. Note concavo-convex and sutured grain contacts. Crossed polarizers, sample RB-B3 (12368.7 ft).

Plate 4.7

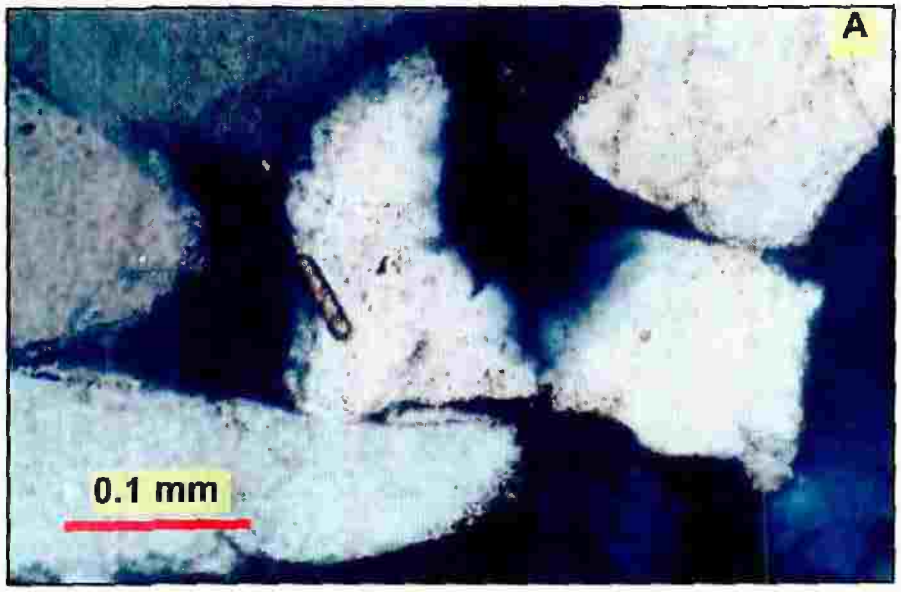

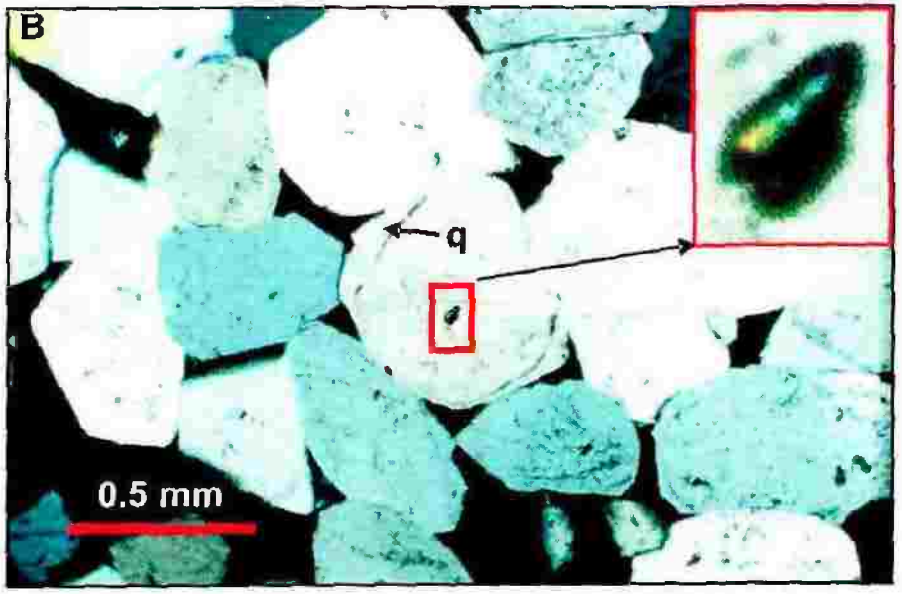

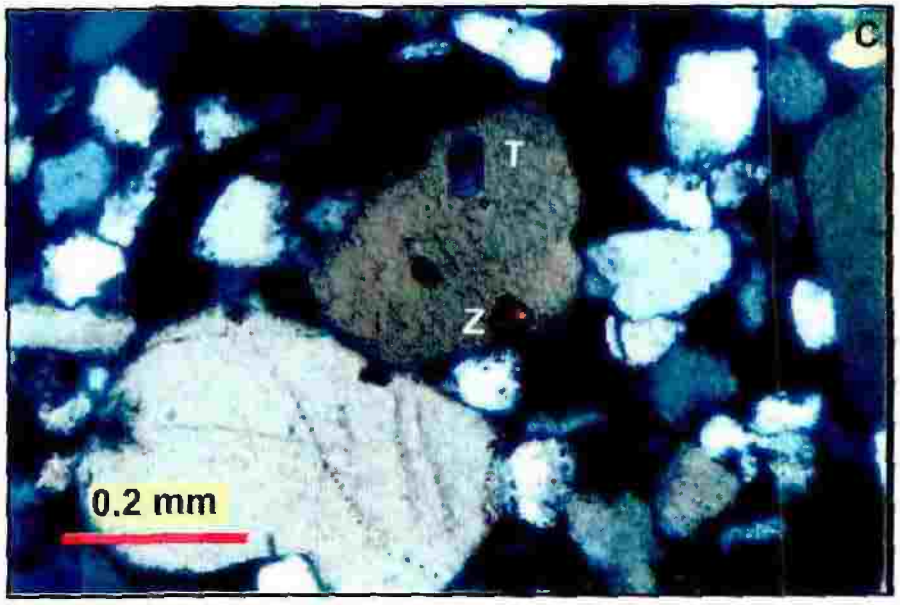

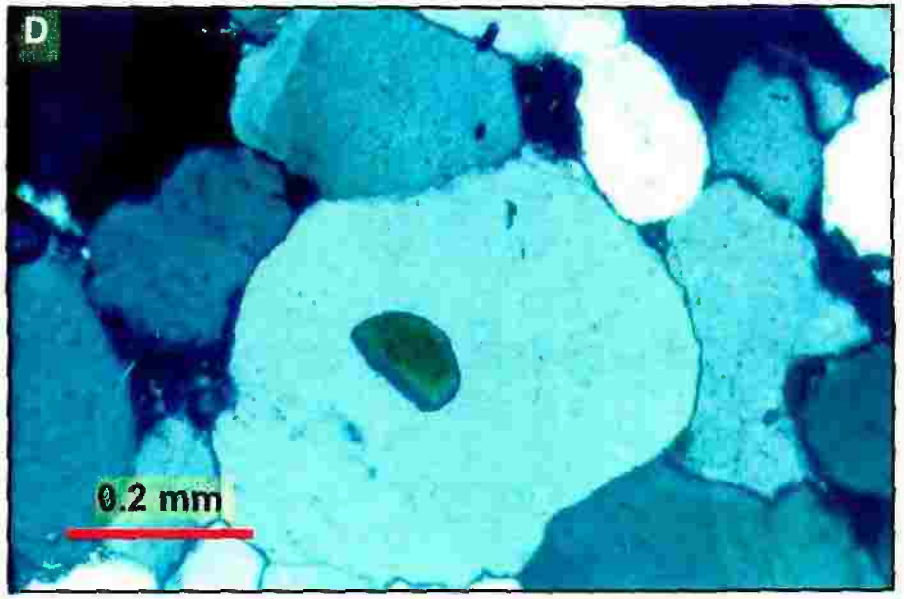

Plate 4.8

A) Monocrystalline quartz (center) with brown subhedral prismatic tourmaline inclusion inclosing opaque inclusions. Plane light, sample RB-B3 (12368.7 ft).

B) Monocrystalline quartz with a brown rectangular anatase inclusion. Plane light, sample Na-76.

C) Monocrystalline quartz with abundant needle-shaped (fibrolite) sillimanite inclusions (arrows). Detrital quartz grains with sillimanite inclusions are excellent evidence for a metamorphic source area. Plane light, sample RB-A1 (12340 ft).

D) Close up view of C.

Plate 4.8

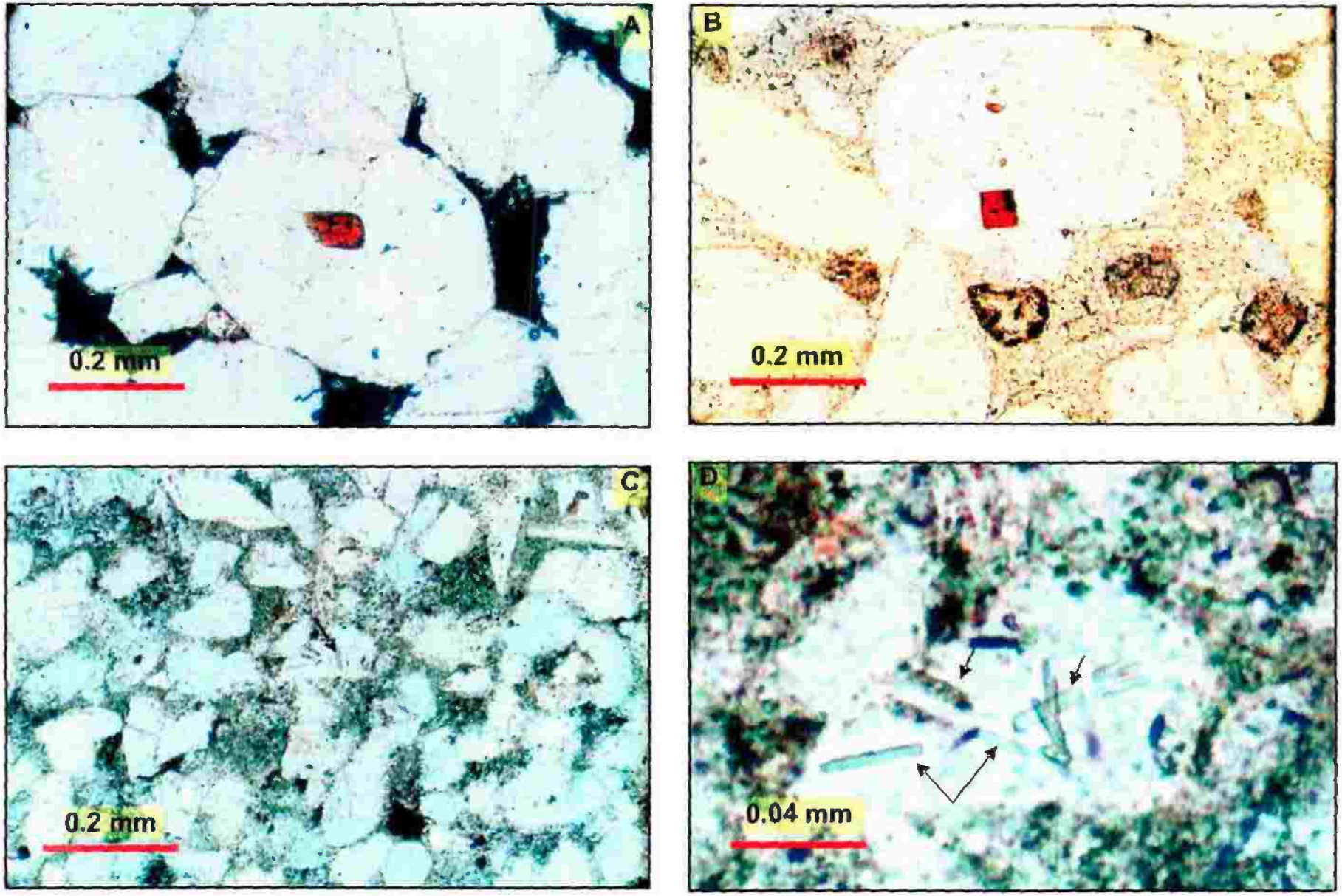

Plate 4.9

A) Monocrystalline quartz with prismatic sillimanite inclusion. Crossed polarizers, sample RB-A5 (12208 ft).

B) Monocrystalline quartz with abundant acicular sillimanite inclusions. Plane light, sample RB-B3 (12382.6 ft).

C) Monocrystalline quartz with abundant acicular rutile inclusions. Plane light, sample RB-A5 (12825 ft).

D) Monocrystalline quartz with muscovite (Mu) and kyanite (Ky) inclusions. Crossed polarizers, sample RB-B3 (12368.7 ft).

Plate 4.9

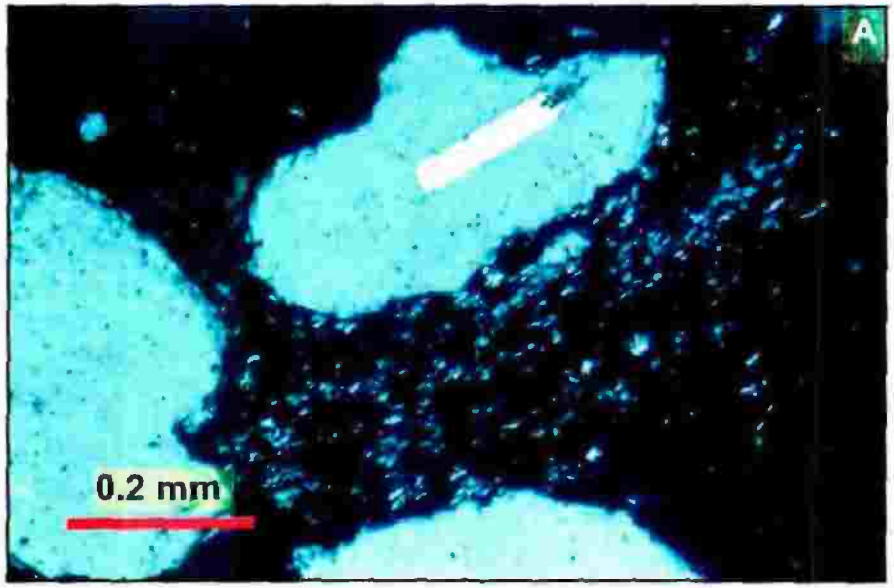

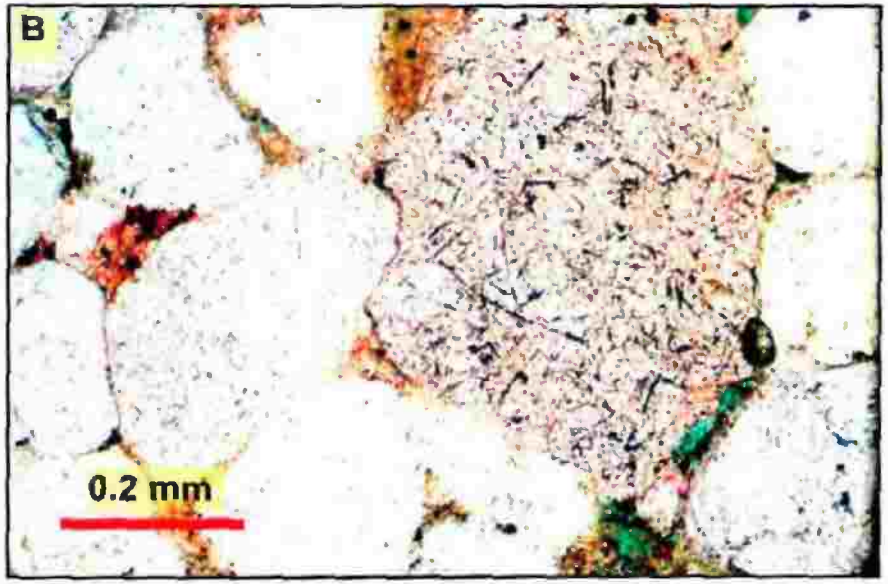

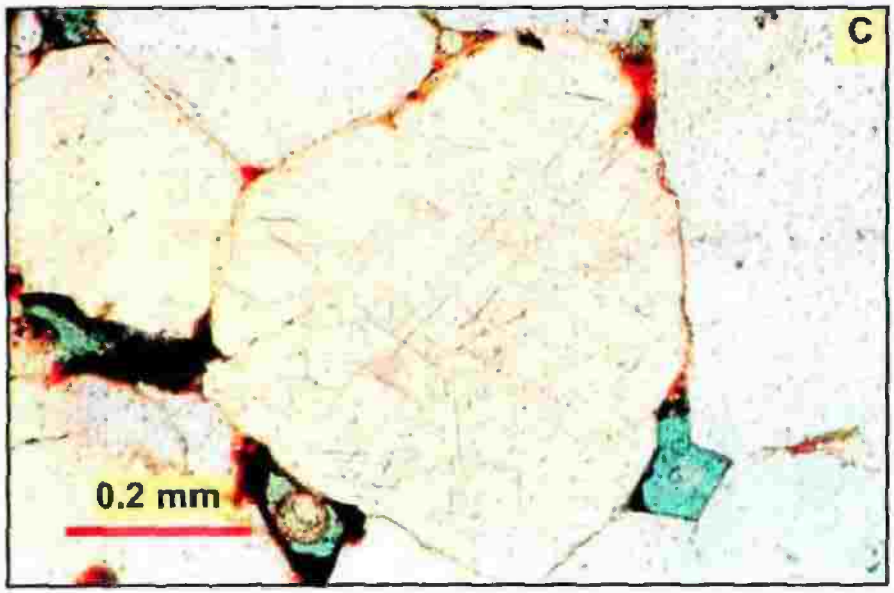

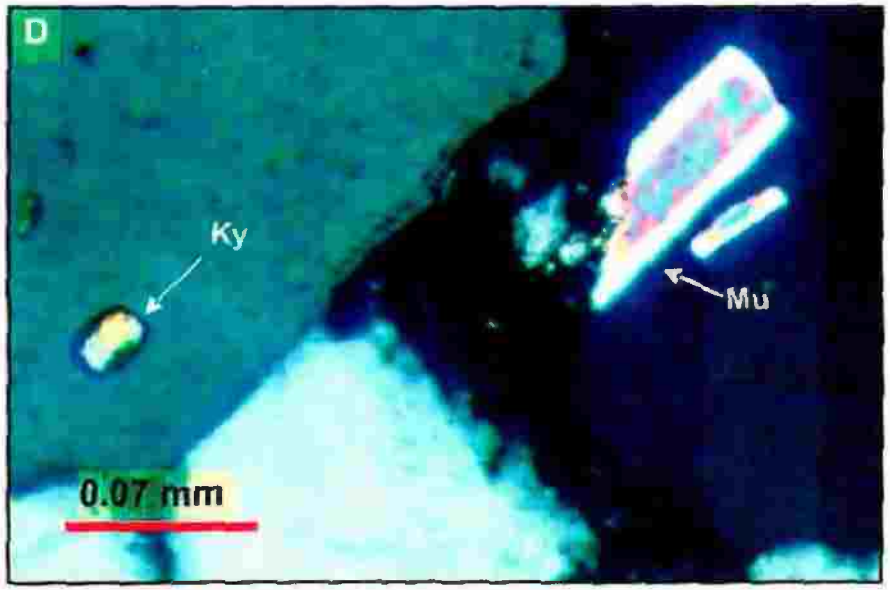

Plate 4.10

A) Polycrystalline quartz of two crystals with almost smoothed intercrystalline boundary. Crossed polarizers, sample Na-31.

B) Polycrystalline quartz of four crystals with almost smoothed intercrystalline boundaries. Crossed polarizers, sample RB-B3 (12382.6 ft).

C) Polycrystalline quartz (a) of two crystals with sutured intercrystalline boundary. Note polycrystalline quartz (b) of numerous elongated crystals indicating a metamorphic origin. Crossed polarizers, sample RB-A1 (12341 ft).

D) Polycrystalline quartz of two crystals with sutured intercrystalline boundary. Crossed polarizers, sample RB-A1 (12460 ft).

Plate 4.10

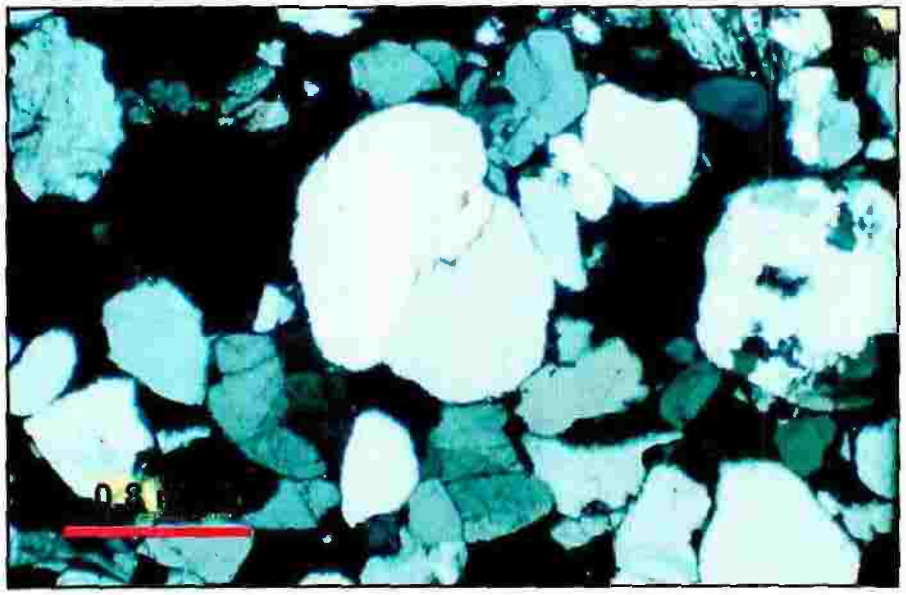

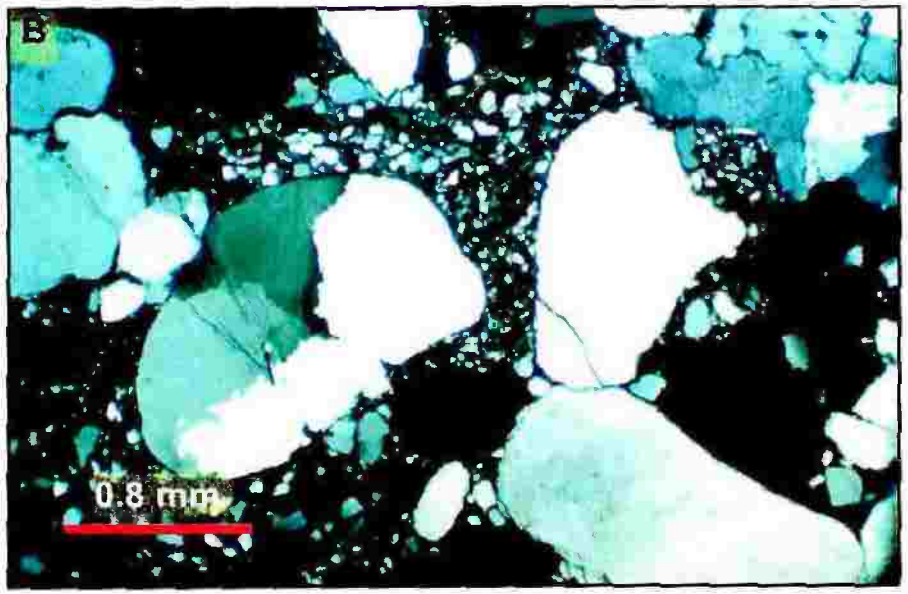

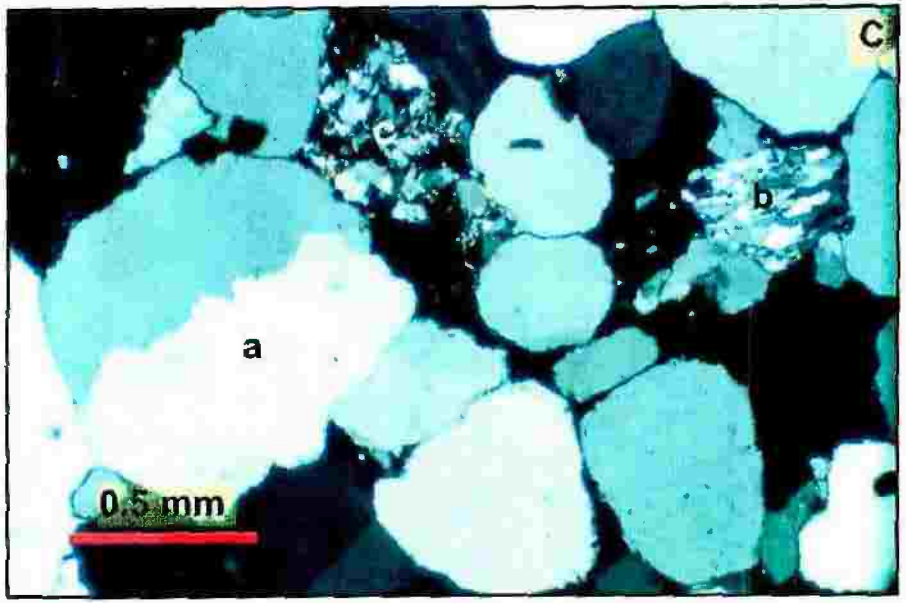

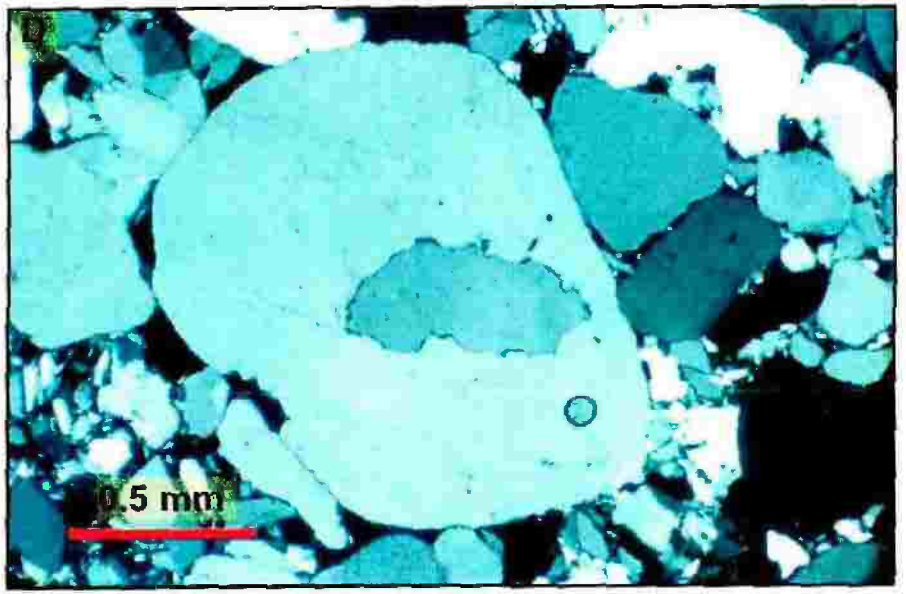

Plate 4.11

A) Polycrystalline quartz of five crystals with sutured intercrystalline boundaries. Crossed polarizers, sample Na-79.

B) Polycrystalline quartz (a) with almost perfect orientation of elongated and crenulated crystals, having sutured intercrystalline boundaries indicating a metamorphic origin. Crossed polarizers, sample Na-31.

C) Same as B. Sample Na-33.

D) Polycrystalline quartz with numerous crystals, having sutured intercrystalline boundaries indicating a metamorphic origin. Crossed polarizers, sample Na-31.

Plate 4.11

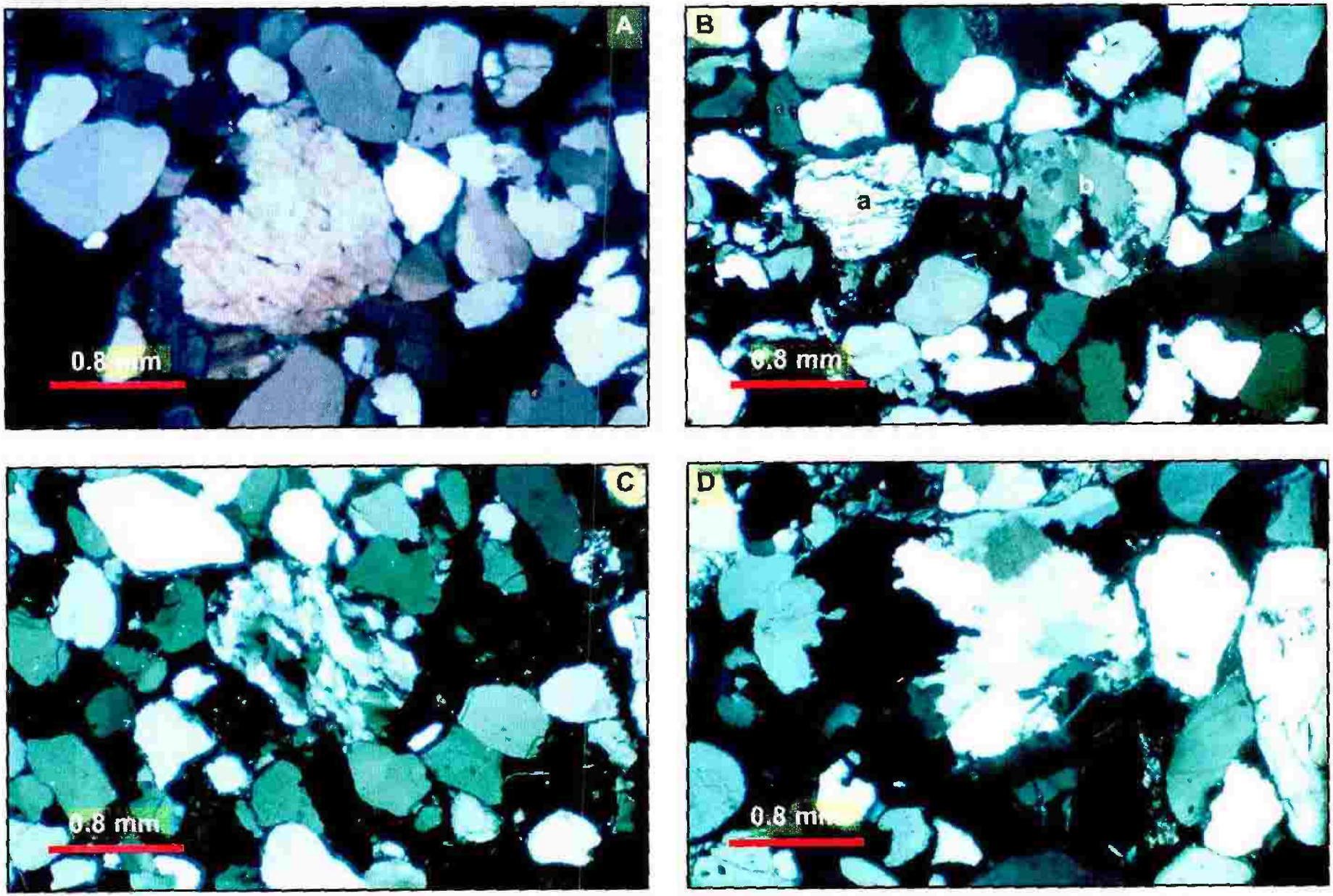

Plate 4.12

A) Polycrystalline quartz, from a metamorphic rock, having a bimodal distribution of crystal sizes illustrating a recrystallization "caught in the act". Crossed polarizers, sample Ar-9.

B) Polygonized quartz. The polygonal units tend to meet at 120° angles at triple junctions of crystal boundaries indicating a probable metamorphic origin. Crossed polarizers, sample Na-13.

C) Polycrystalline quartz having straight intercrystalline boundaries rather than intercrystalline suturing indicating schistose origin. Crossed polarizers, sample Na-79.

D) Polycrystalline quartz with numerous silt-sized individual crystals. Crossed polarizers, sample Na-85.

Plate 4.12

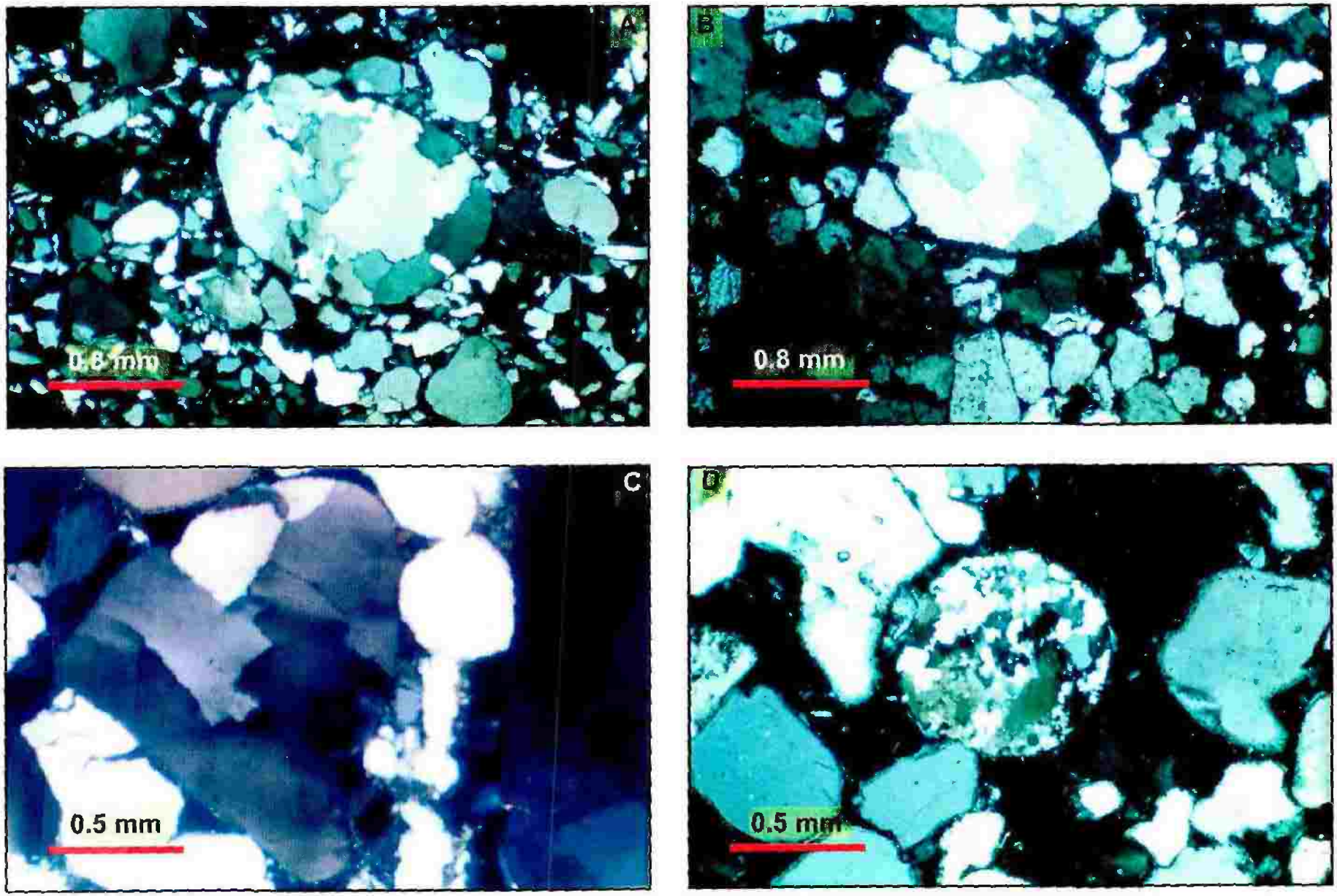

Plate 4.13

A, C) Polycrystalline quartz with well-defined dust lines (arrows) that define undulose boundaries. Plane light, samples Na-79 and RB-A5 (12208 ft), respectively.

B, D) A and C in crossed polarizers.

Plate 4.13

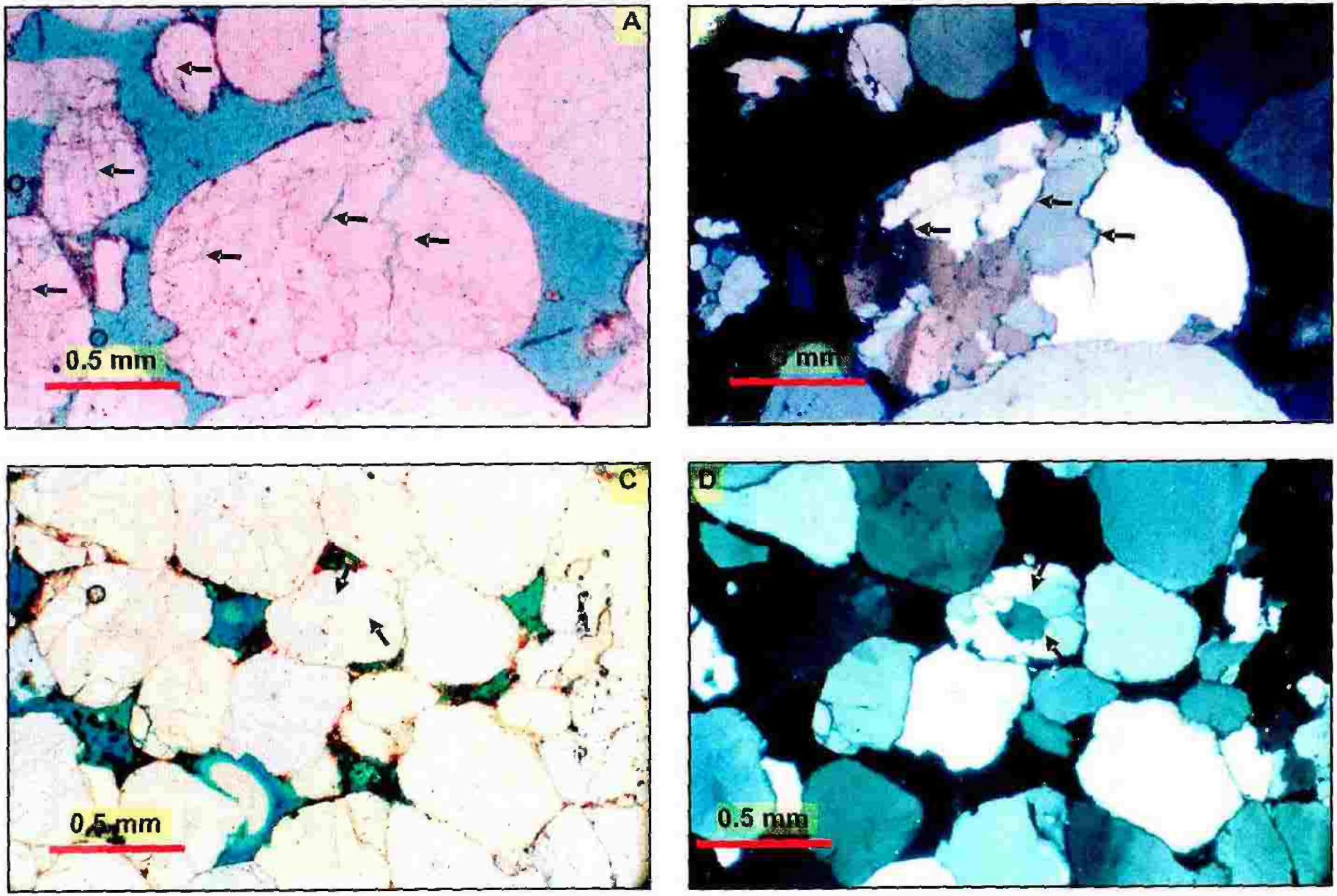

Plate 4.14

A) A semicomposite quartz grain with a slightly undulose extinction. Grain consists of a number of individual quartz crystals with very closely aligned optic c-axes. Crossed polarizers, sample Na-112.

B) Alteration of detrital K-feldspar. Crossed polarizers, sample Ar-10.

C) Alteration of detrital K-feldspar into clay minerals. Plane light, sample Na-13.

D) C in crossed polarizers.

Plate 4.14

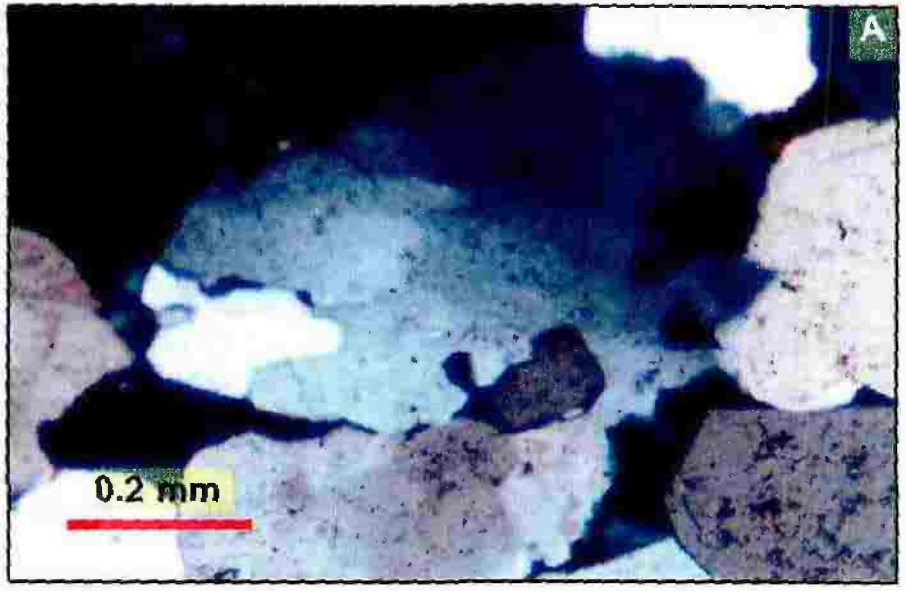

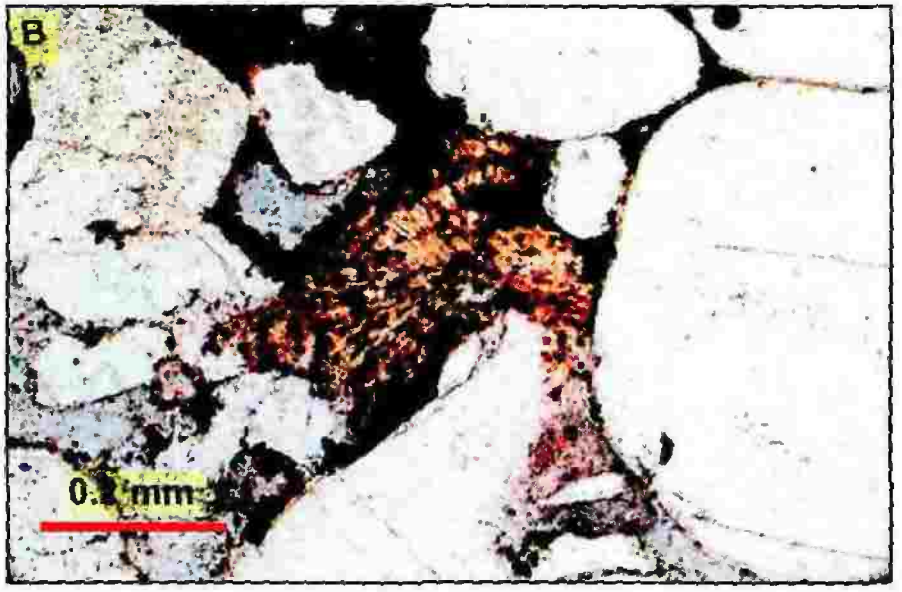

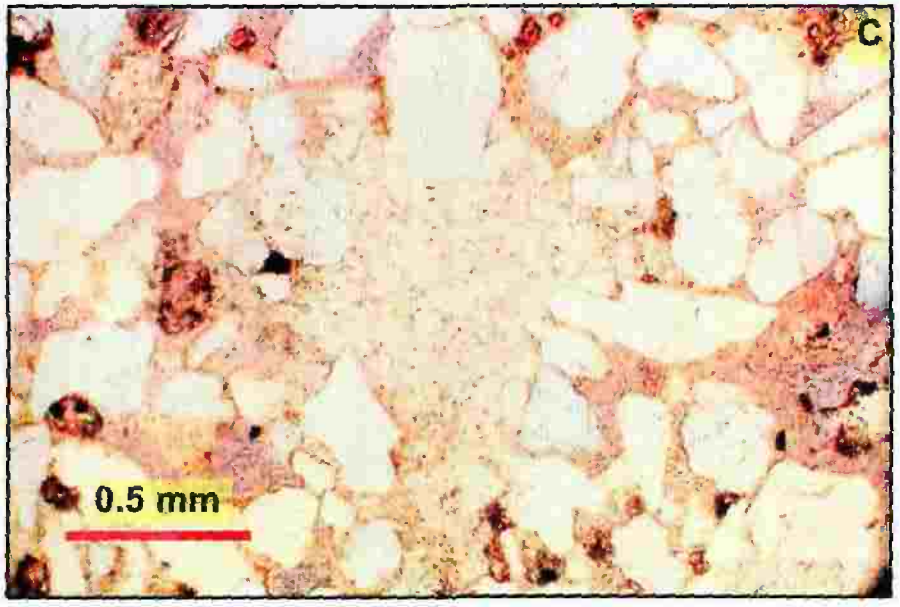

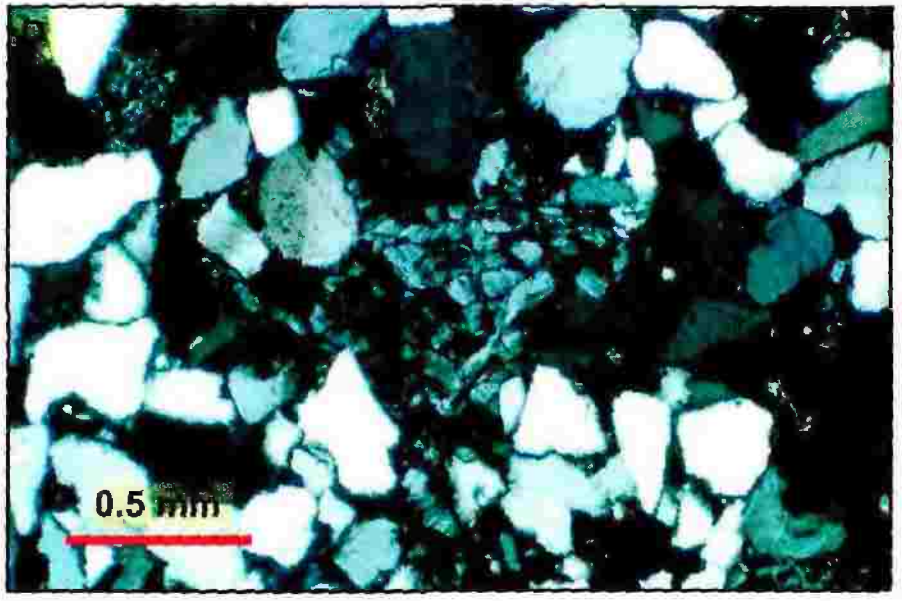

Plate 4.15

A) Alteration of detrital K-feldspar (arrow). Plane light, sample Ar-7c.

B) A in crossed polarizers.

C, D) Initial stages of K-feldspar dissolution. Plane light, samples Ar-3 and Na-12, respectively.

Plate 4.15

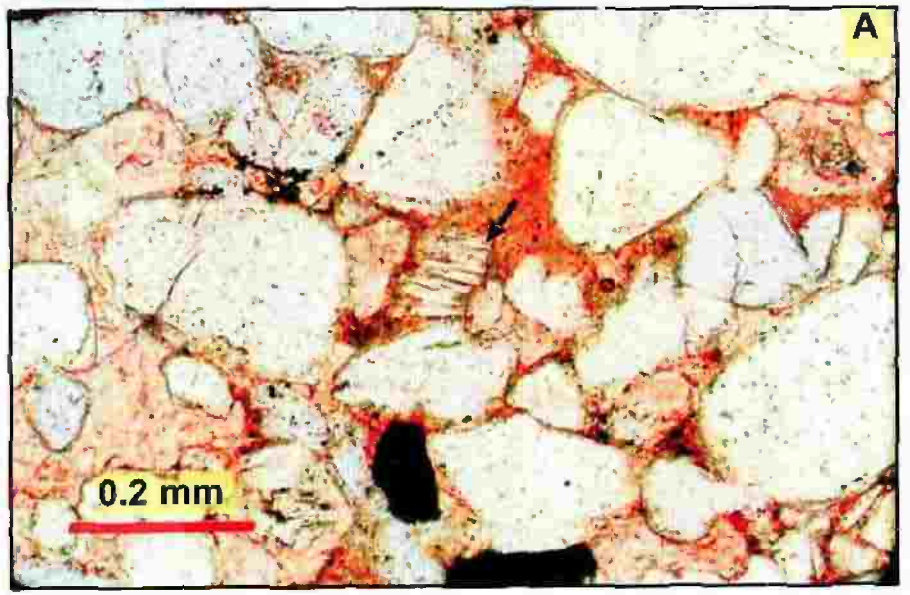

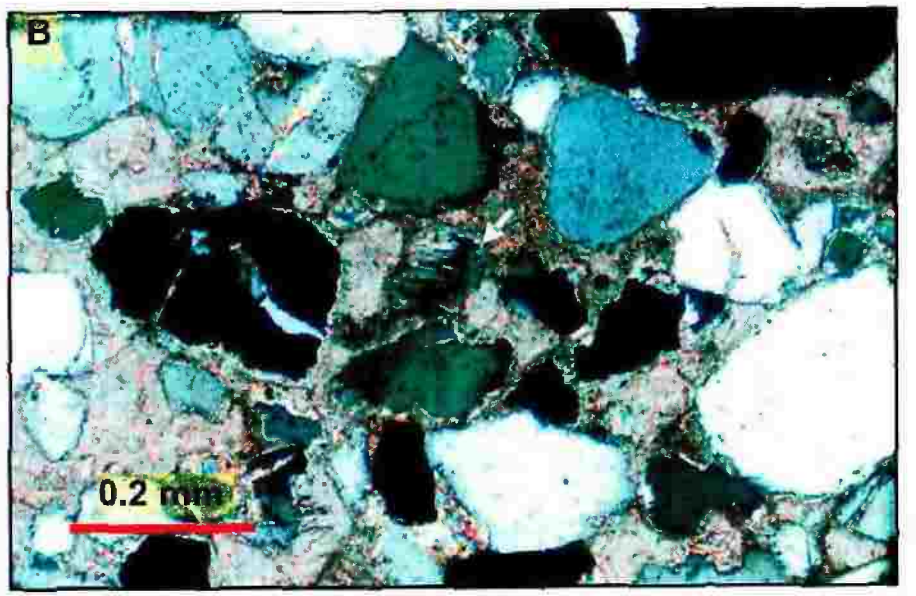

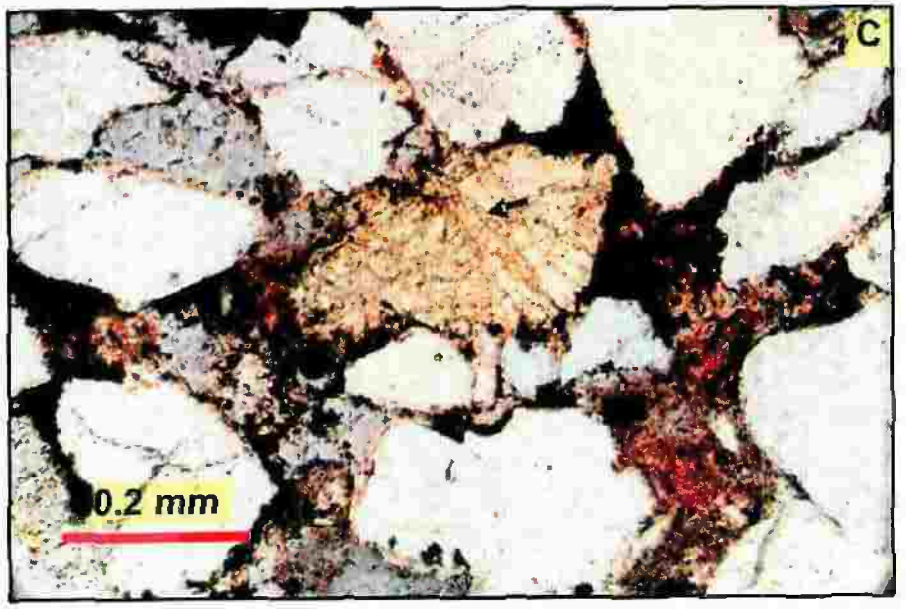

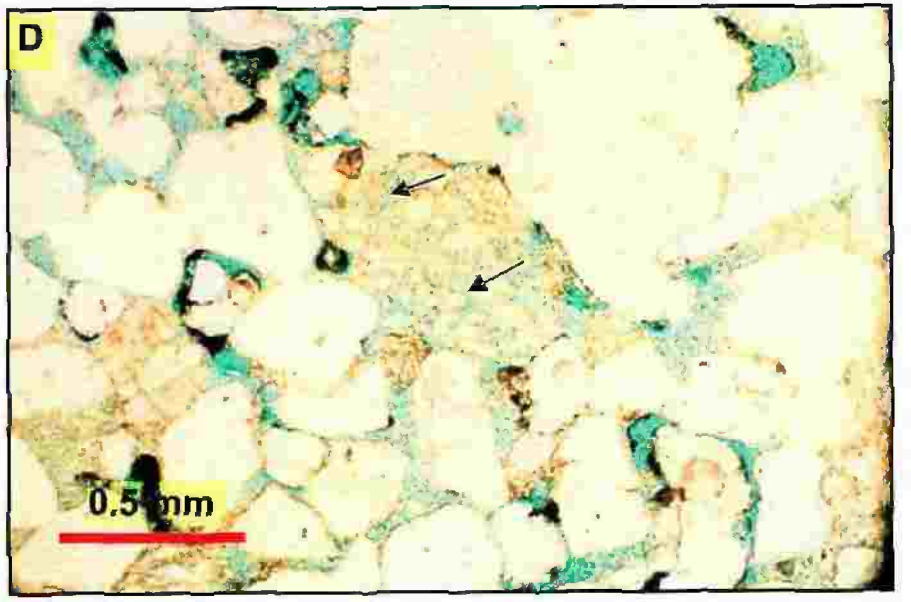

Plate 4.16

Progressive stages of K-feldspar dissolution. Stages C and D are extreme case where the entire grain was dissolved and leached leaving behind an oversized pore space (OSP). In stage C the iron and/or clay rim (arrow) marks the original grain boundary. Arrows (photos A and B) point to intragranular pores. All in plane light exposure, samples Na-31, Na-94 and Na-12, respectively.

Plate 4.16

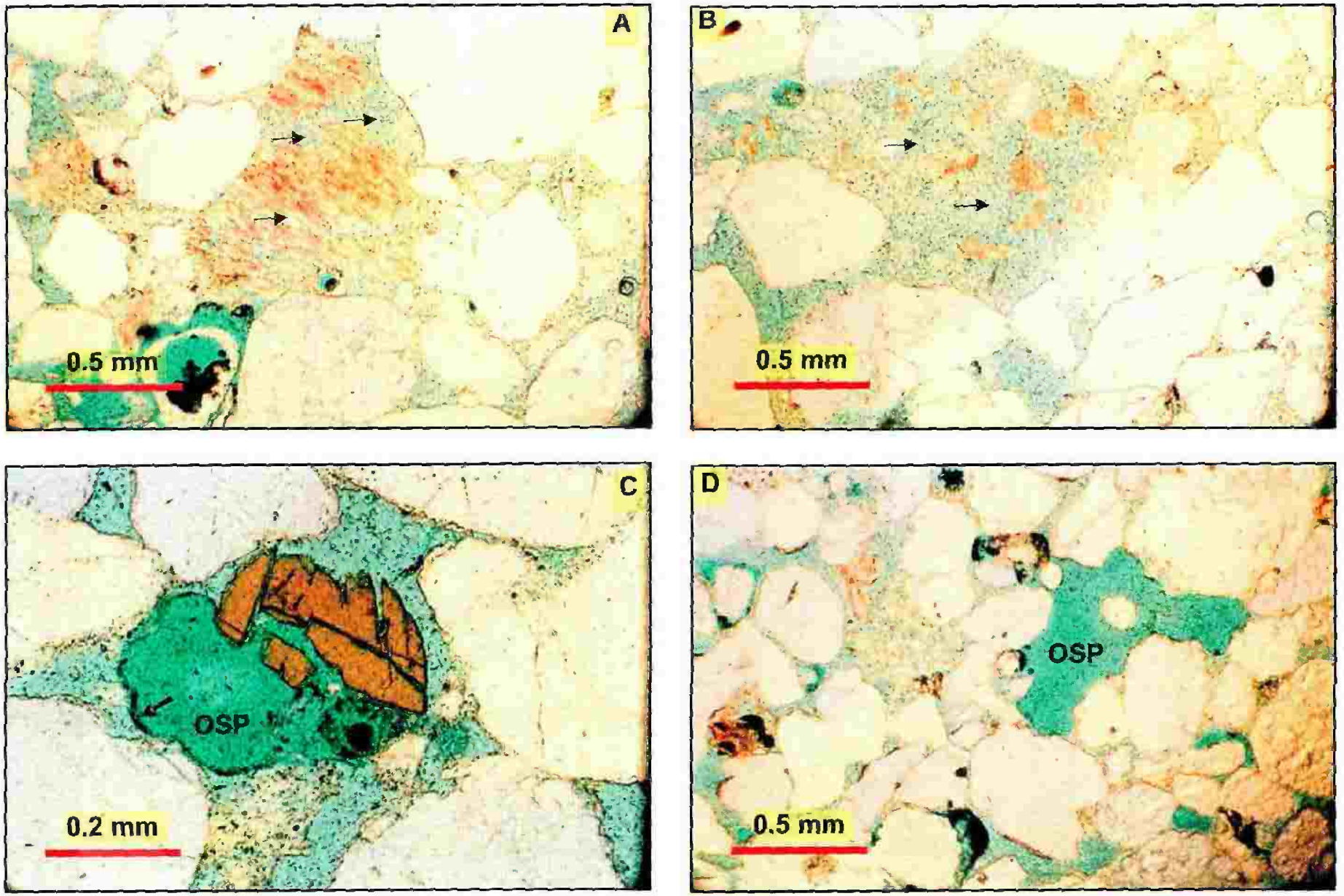

Plate 4.17

A) Subrounded chert grain of a sedimentary origin. Crossed polarizers, sample RB-A5 (12268 ft)

B) Large chert accumulation between quartz grains of different shapes and sizes. Crossed polarizers, sample RB-A1 (12341 ft).

C) Coarse chert fragment composed of a mosaic of interlocking quartz crystals. Crossed polarizers, sample Na-13.

D) Chert grain displaying sign of dissolution as indicated by intragranular porosity (arrows). Plane light, sample RB-C2 (12290 ft).

Plate 4.17

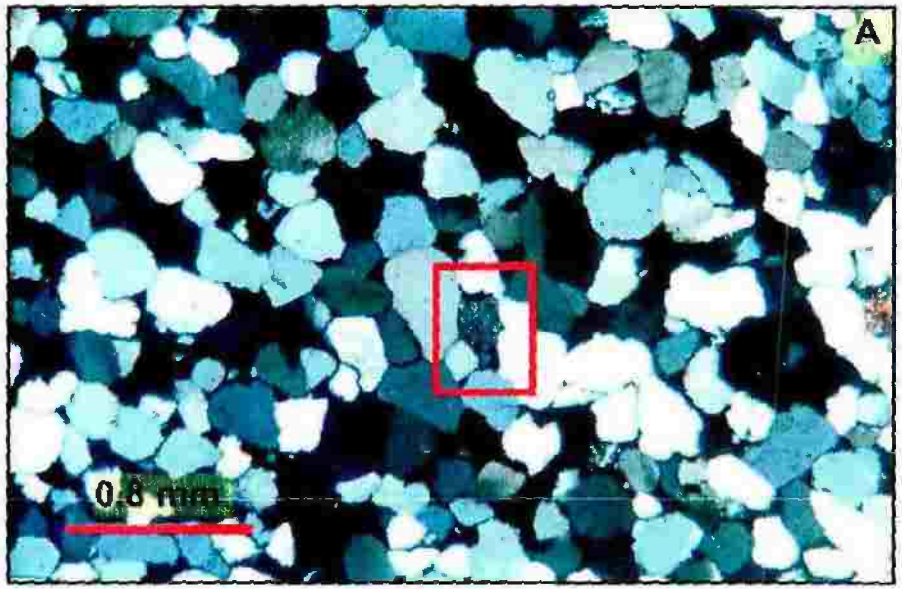

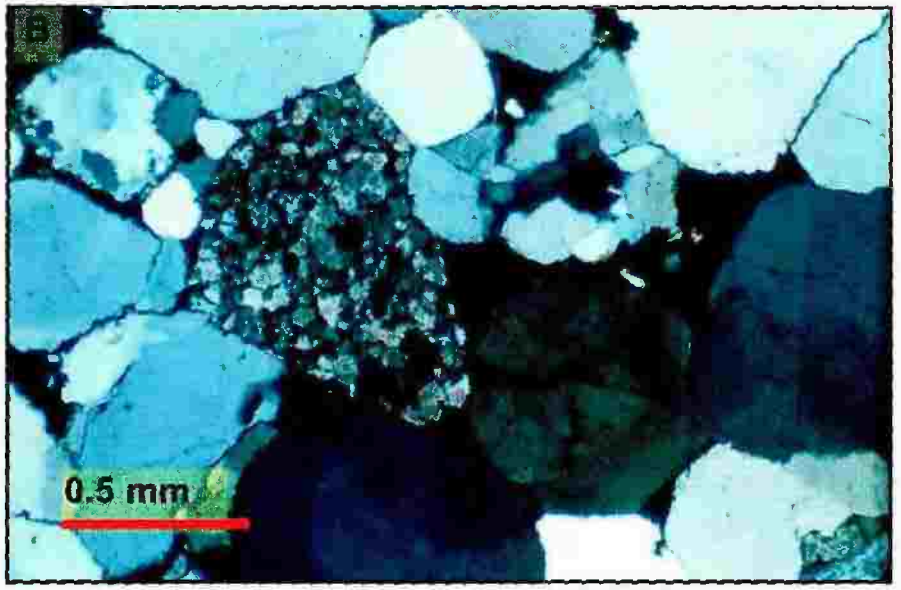

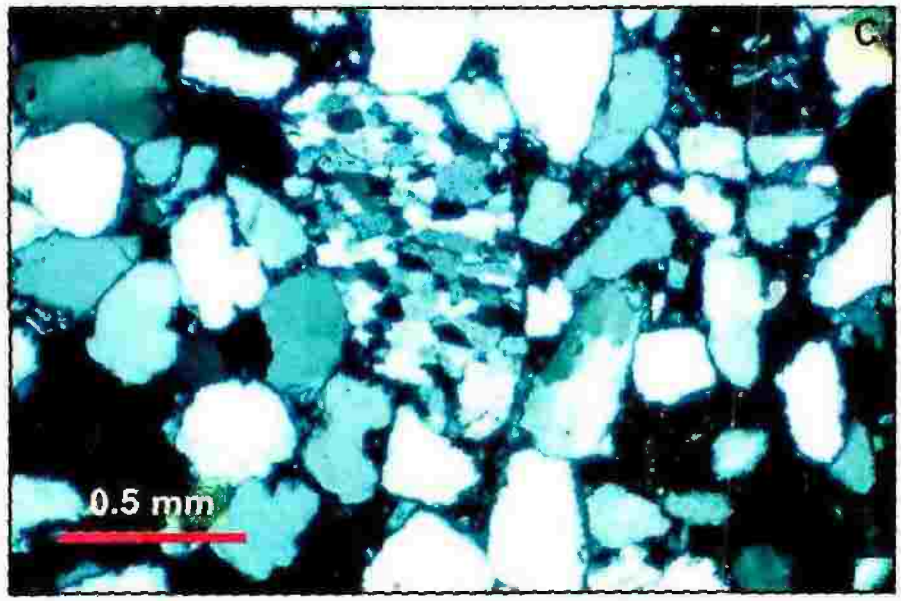

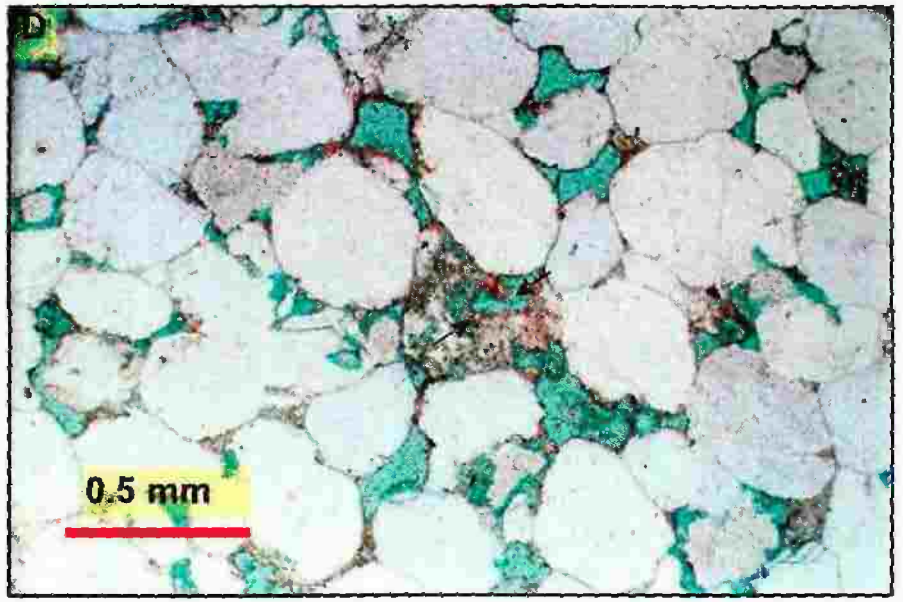

Plate 4.18

A) Silica-cemented siltstone clast. Plane light, sample Na-13.

B) Silica-cemented sandstone clast. Plane light, sample RB-B4 (12479 ft).

C) Hematite-cemented sandstone clast in a hematite-cemented sandstone. Plane light, sample RB-A5 (12297 ft).

D) Clay clast plastically deformed between rigid quartz grains. Plane light, RB-B3 (12401).

Plate 4.18

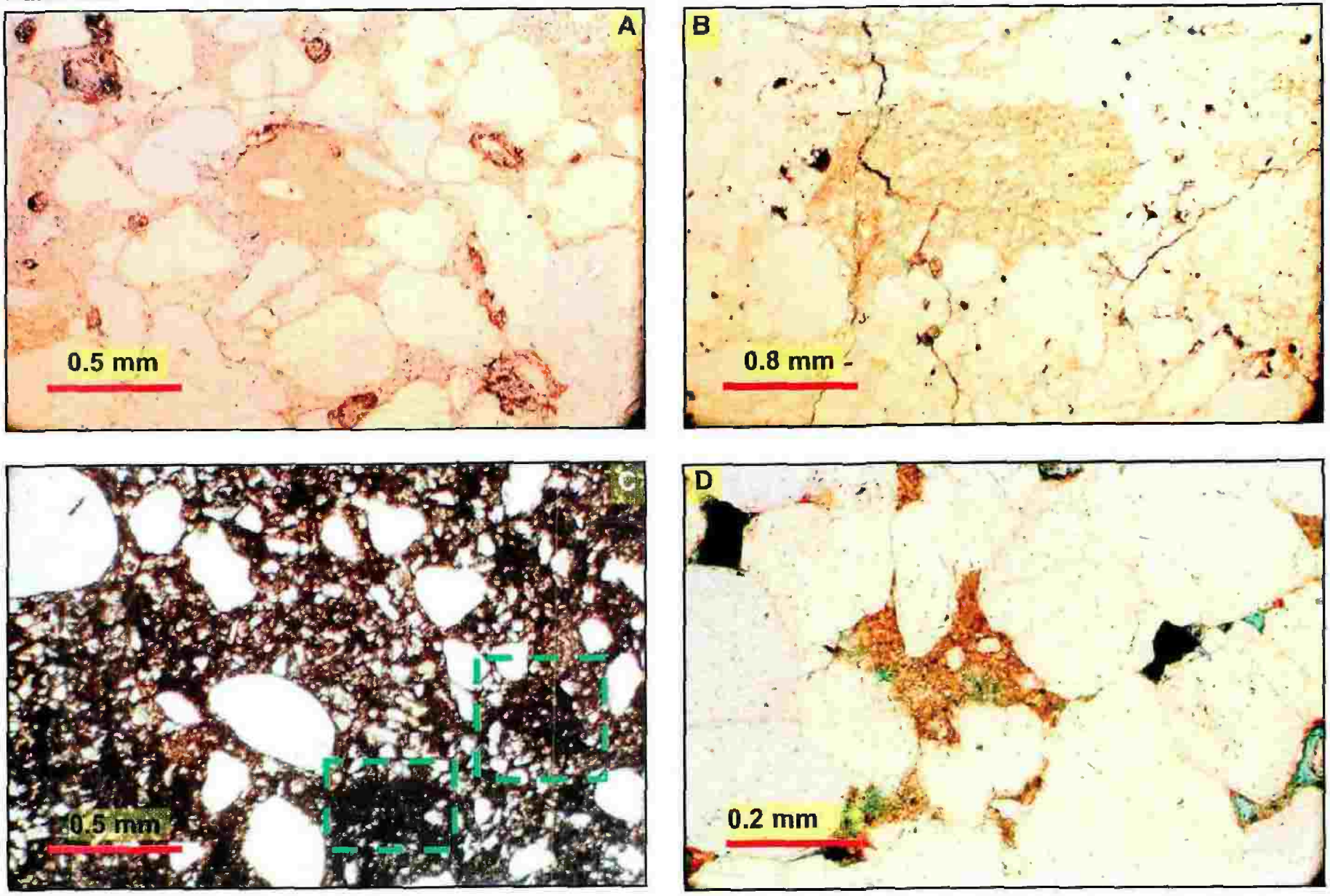

Plate 4.19

A) Metamorphic rock fragment, probably quartz mica schist. Crossed polarizers, sample RB-B3 (12368.7 ft).

B) Deformed mica flake (arrow) between quartz grains. Note alteration of the flake started along the cleavage planes and the outer rim. Crossed polarizers, sample Ar-9.

C) Gypsum flake (arrow) deformed between quartz grains. Plane light, sample Ar-11.

D) C in crossed polarizers.

Plate 4.19

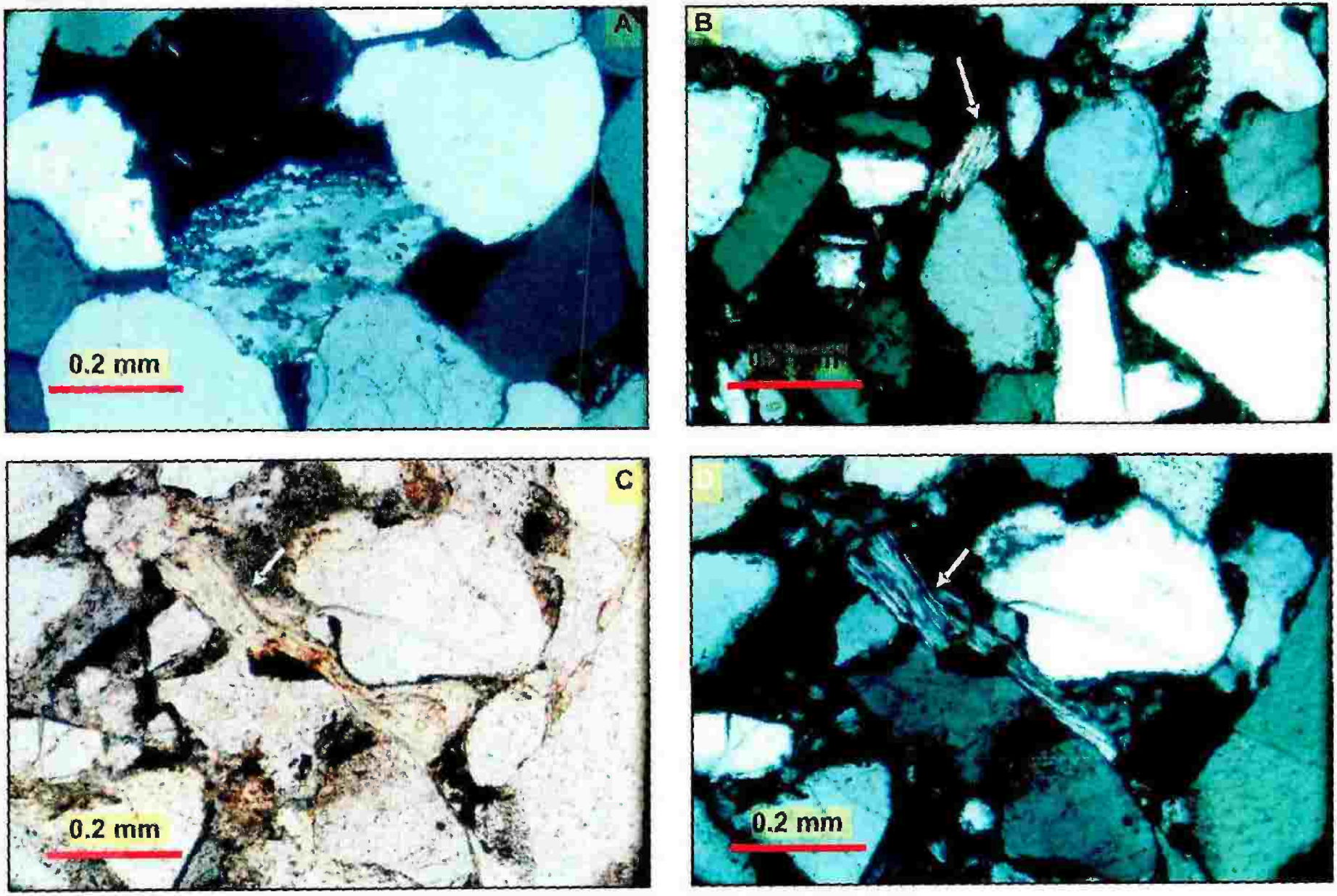

Plate 4.20

Different varieties of zircon in the studied surface sandstone.

Plate 4.20

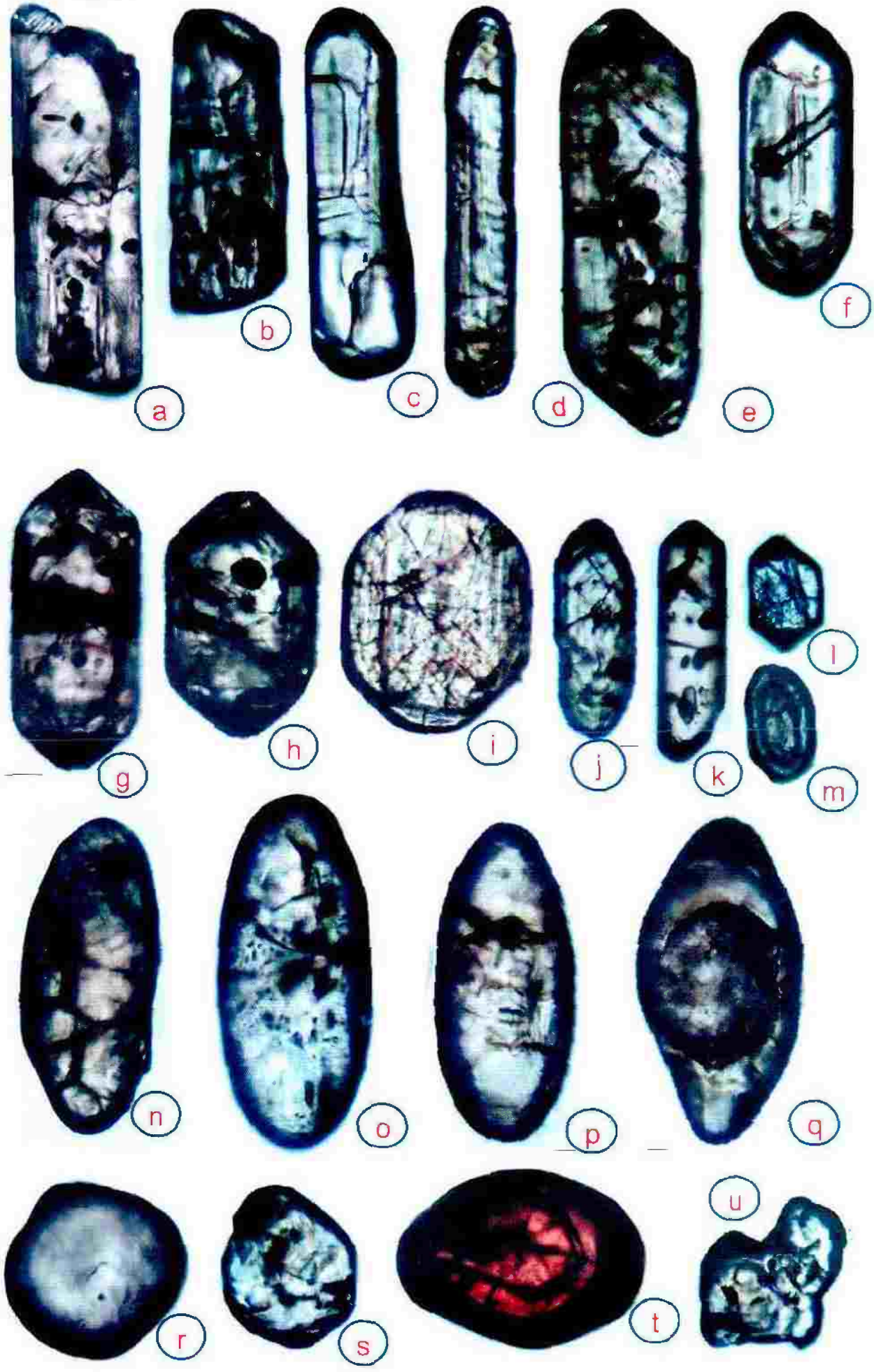

Plate 4.21

Different varieties of tourmaline in the studied surface sandstone

Plate 4.21

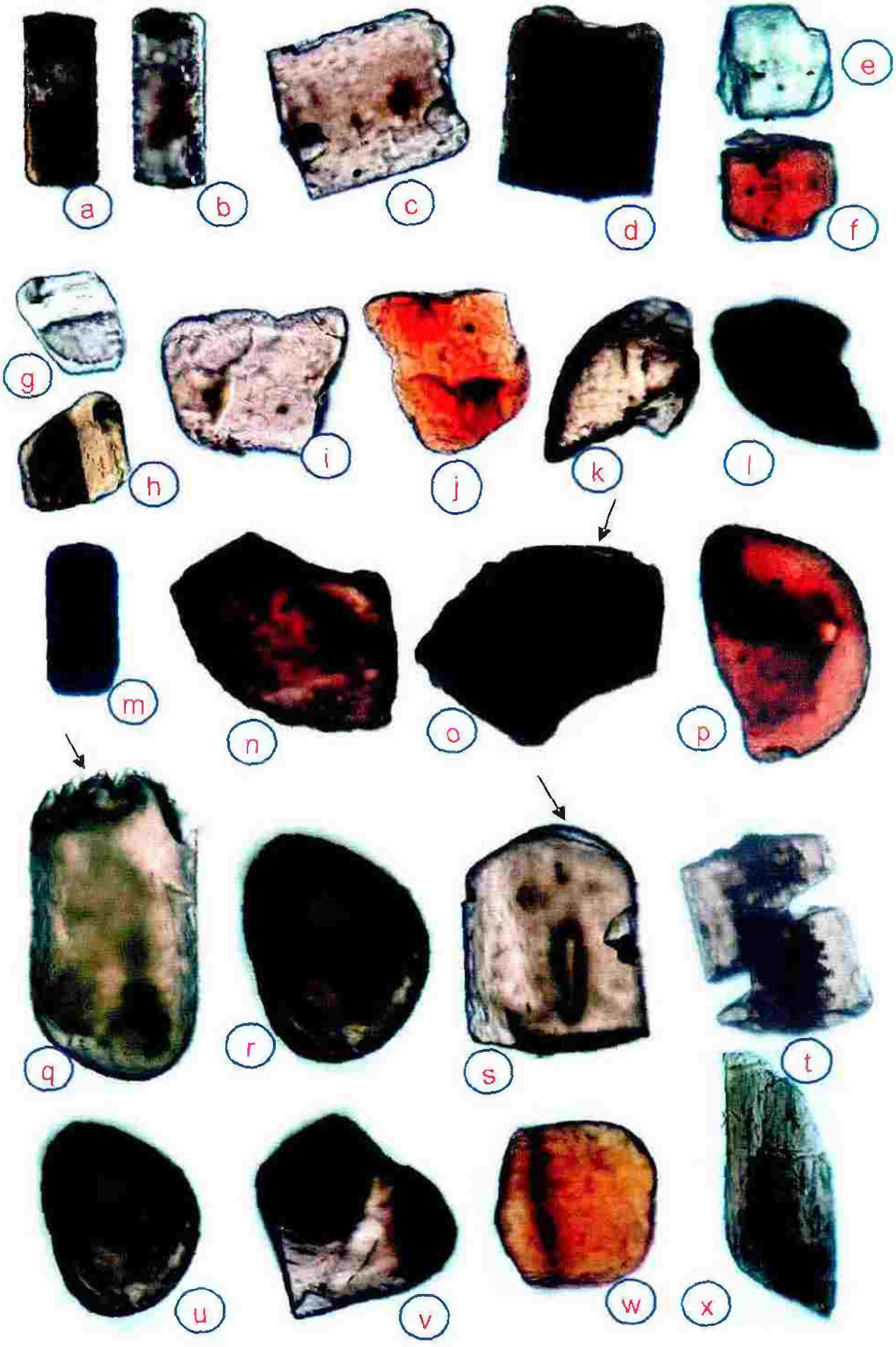

Plate 4.22

Different varieties of rutile in the studied surface sandstone.

Plate 4.22

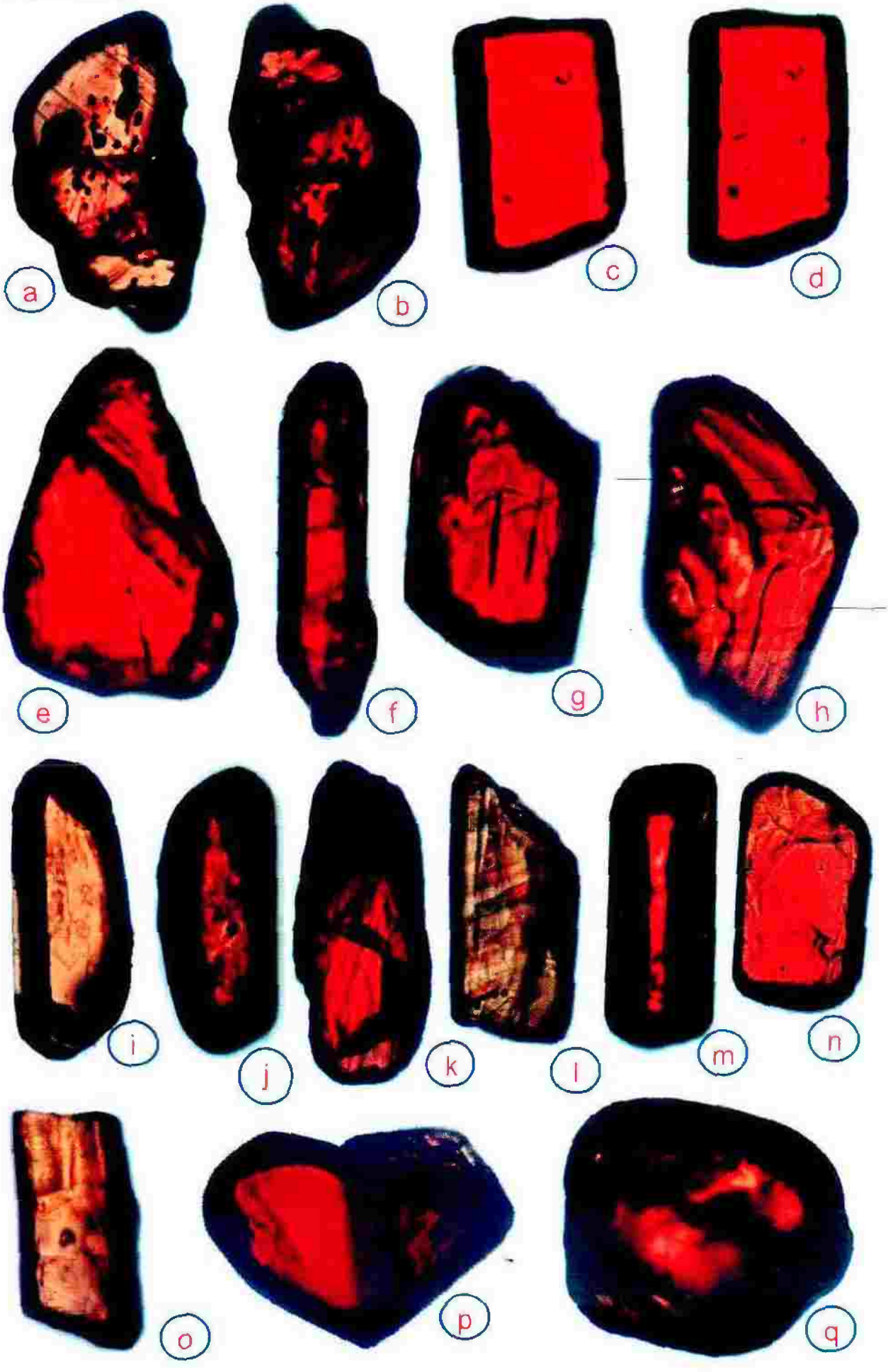

Plate 4.23

Different varieties of garnet (a-j), staurolite (k-l) and chlorite (m-n) in the studied surface sandstone.

Plate 4.23

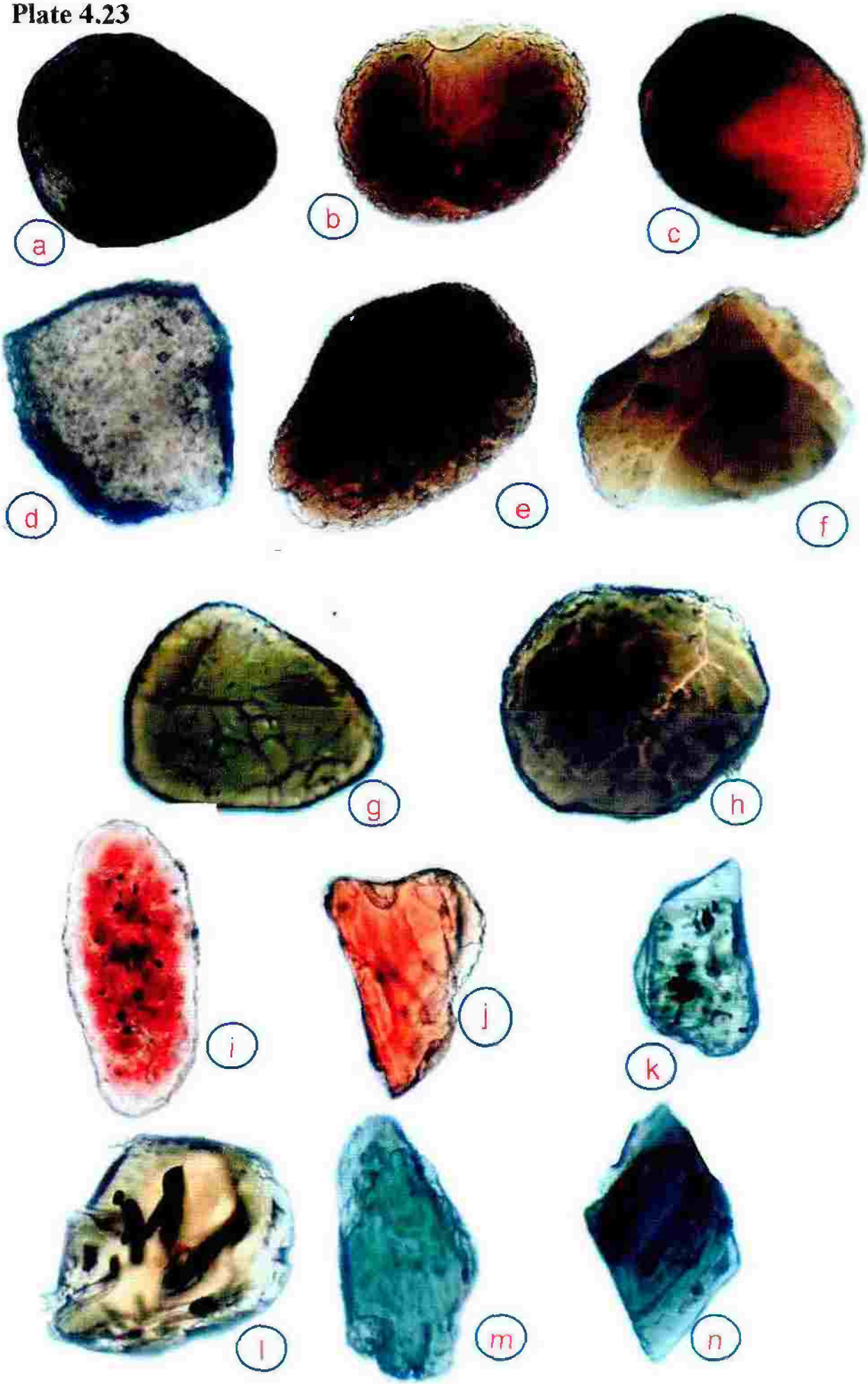

Plate 4.24

A, B) Dust lines (arrows) mark the boundary of detrital quartz grains with their overgrowths (q). Plane light, sample RB-A5 (12305 ft).

C) Quartz overgrowth with well-formed crystal faces that is free of inclusions (q) encrusts a detrital core (Q) containing abundant inclusions (arrows). Overgrowths almost enclose the whole detrital grains showing the highest degree of crystalline perfection. Most of pore spaces were occluded by interlocking quartz cement (blue epoxy fills remnant pore space P). Plane light, sample Na-112.

D) C in crossed polarizers.

Plate 4.24

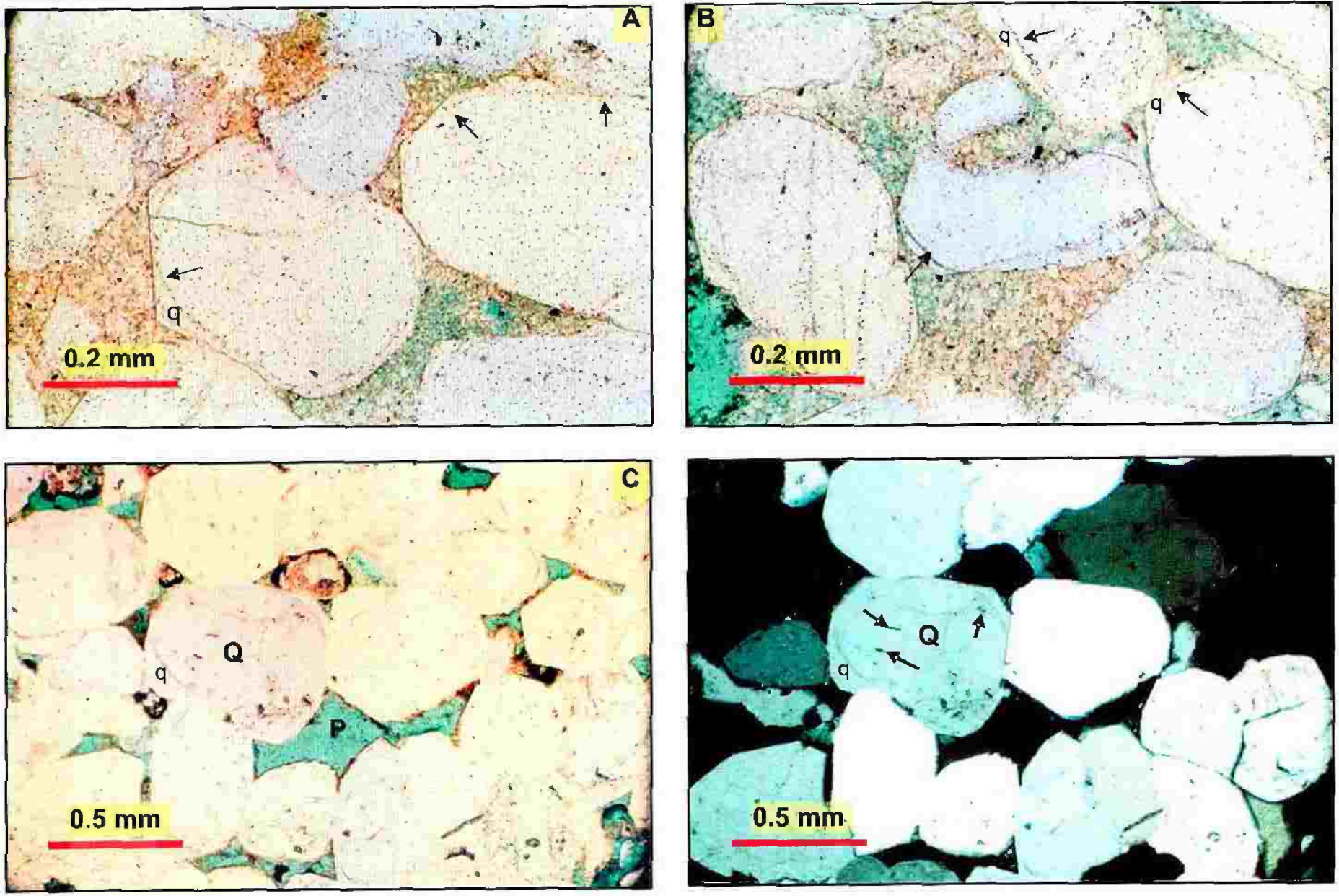

Plate 4.25

A) Quartz overgrowth with well-formed crystal faces (q) preceded compaction. Overgrowths almost enclose whole detrital grains showing the highest degree of crystalline perfection. Crossed polarizers, sample Na-112.

B) Quartz overgrowth with well-formed crystal faces (q) preceded calcite cement (Ca). Corrosion (arrows) on both detrital quartz grains and their overgrowths is due to dissolution. Plane light, sample RB-B4 (12492 ft).

C, D) SEM micrographs showing a well-developed euhedral calcite crystals (Ca) the formation of which post-dated quartz overgrowth (q). Fracturing (Fr) post-dated quartz overgrowth. Samples RB-A5 (12825 ft) and Ar-4, respectively.

Plate 4.25

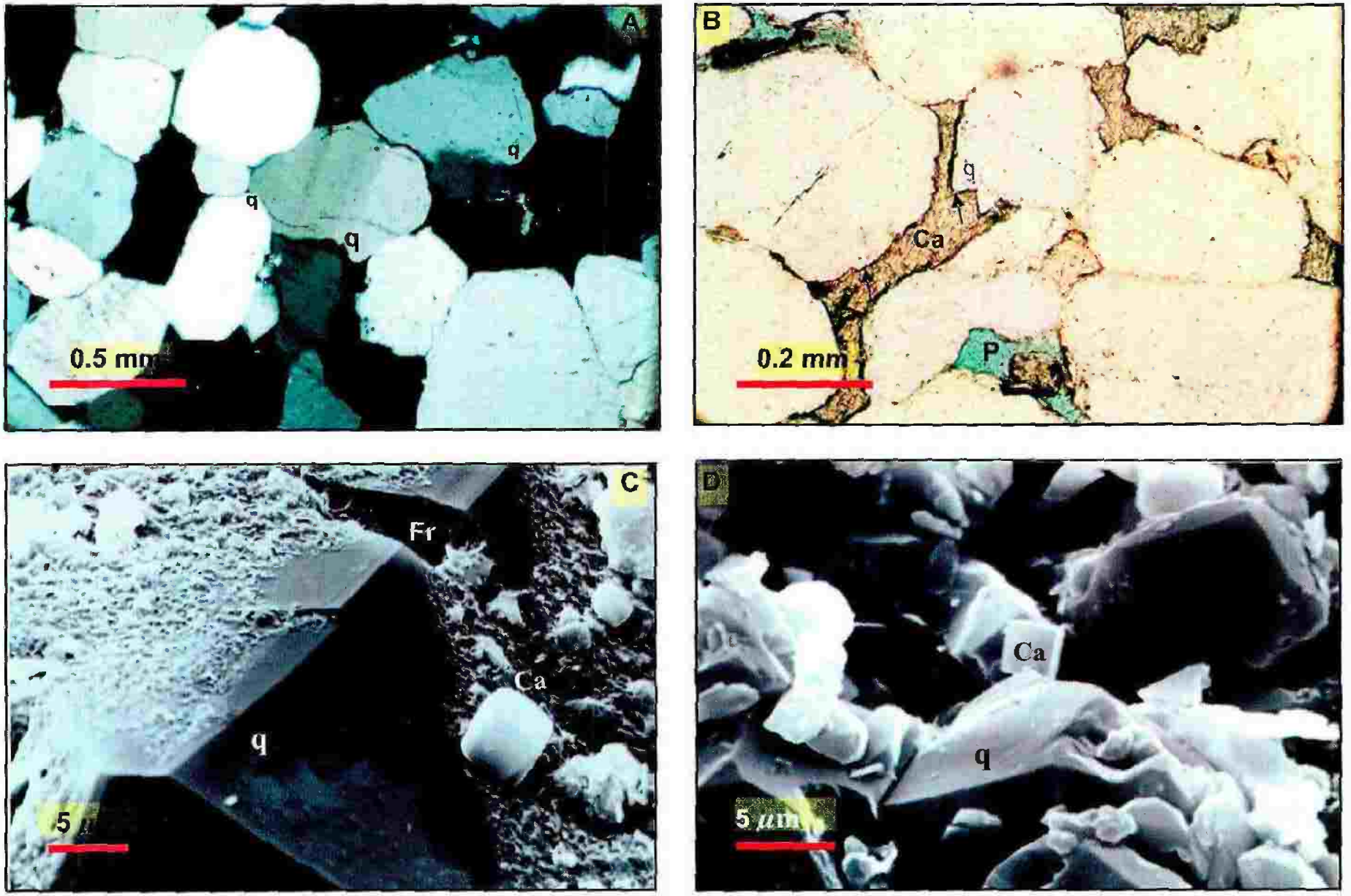

Plate 4.26

A, B) SEM micrograph showing quartz overgrowth (q) and pore-filling kaolinite (Ka). Quartz overgrowth predates kaolinite. Samples RB-A5 (12825 ft) and RB-B3 (12357 ft), respectively.

C) SEM micrograph showing kaolinite (Ka) setting on the surface of quartz overgrowth (q), i.e. quartz overgrowth predates kaolinite. Sample RB-B3 (12357 ft).

D) SEM micrograph showing quartz overgrowth (q) predating kaolinite (Ka). Sample RB-A1 (12341 ft).

Plate 4.26

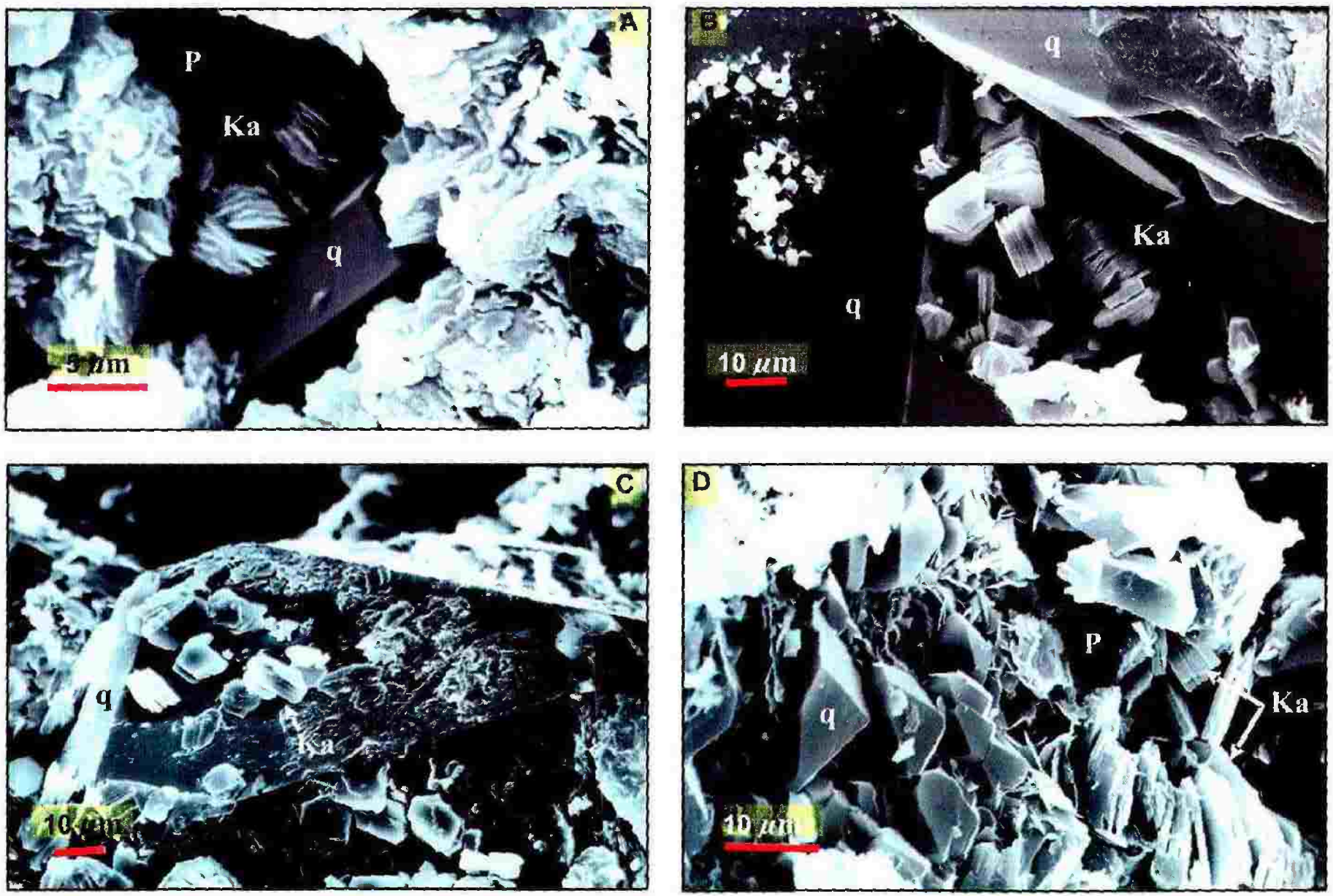

Plate 4.27

A) Quartz overgrowth with well-formed crystal faces (q) preceded hematite cement (Hm). Plane light, sample RB-C2 (12290 ft).

B) Quartz overgrowth with well-formed crystal faces (q) preceded halite cement (Ha). Plane light, sample RB-A1 (12341 ft).

C) Quartz overgrowth preceded gypsum cement (Gy). Note traces of anhydrite within gypsum. Plane light, sample RB-B3 (12357 ft).

D) C in crossed polarizers.

Plate 4.27

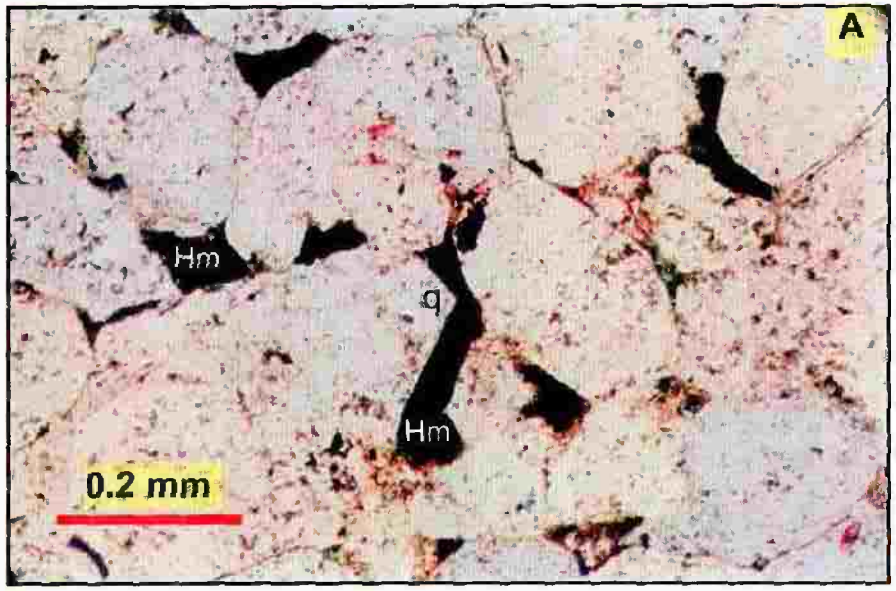

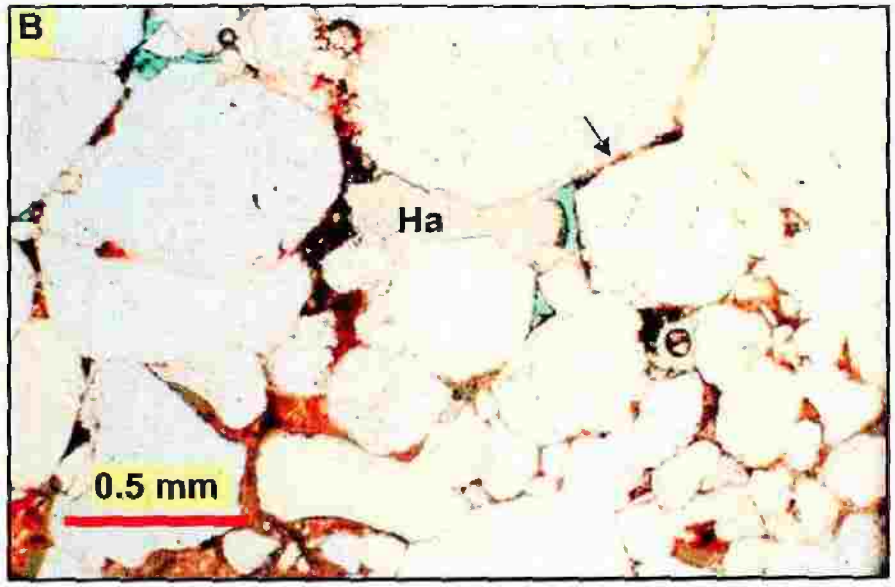

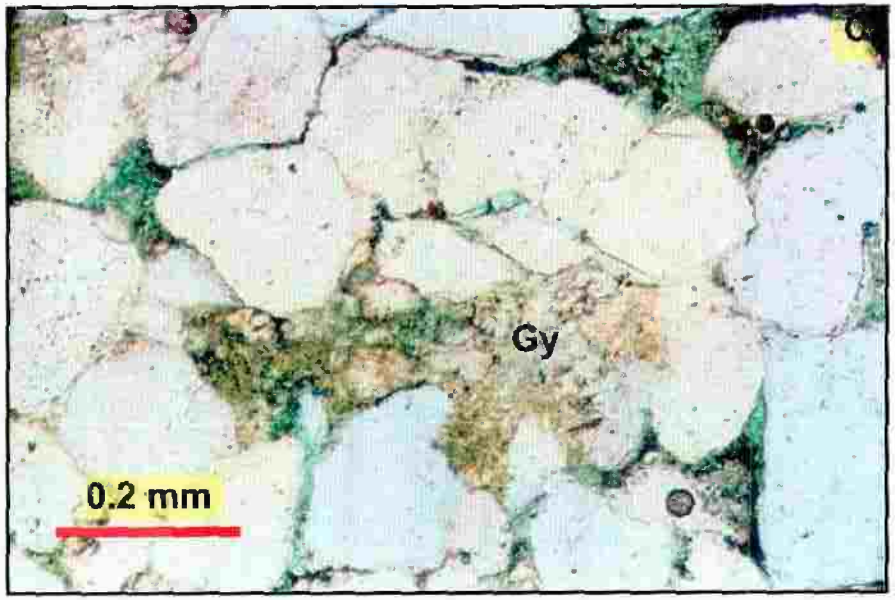

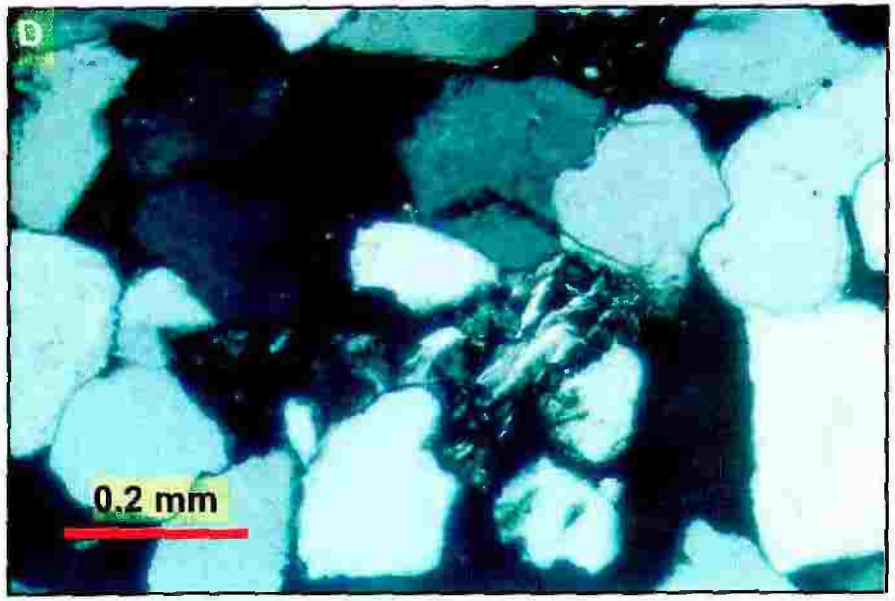

Plate 4.28

A) Quartz overgrowth with well-defined crystal faces grow and meet adjacent overgrowths on the same detrital grain. SEM, sample RB-B3 (12357 ft).

B, C) Concentration of oriented rhombohedral projections on a unicrystalline grain. Note microcrystalline quartz (arrows) on photo C. SEM, samples, RB-A5 (12825 ft) and Na-112, respectively.

D) Overlap of prismatic projections on a unicrystalline grain. Note microcrystalline quartz (arrows). SEM, sample Na-112.

Plate 4.28

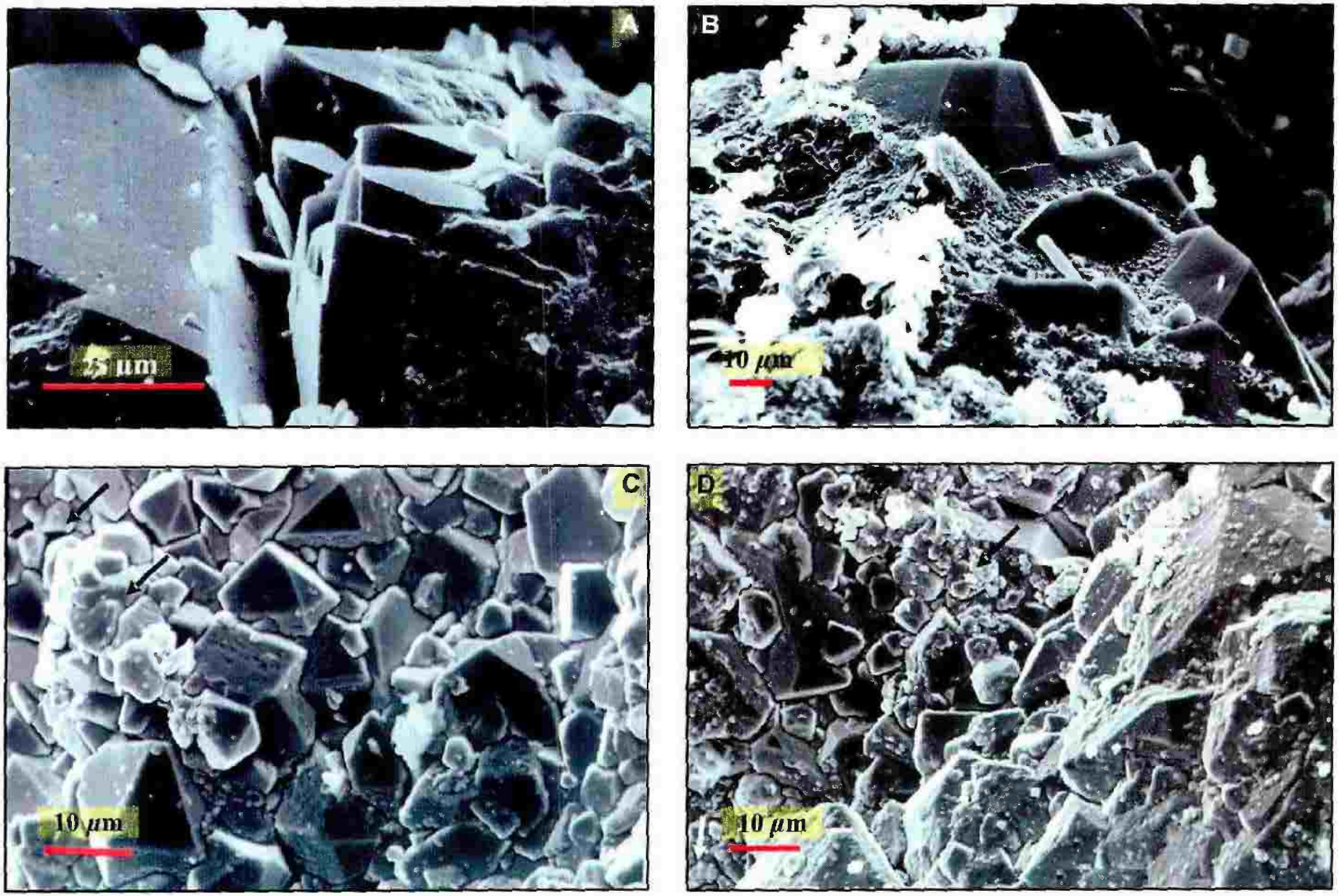

Plate 4.29

A) A faster growing overgrowth (q_1) nearly encloses slower growing subunits (q_2 and q_3). SEM, sample Na-112.

B) Authigenic euhedral prismatic bipyramidal quartz crystals which grow in open pore. SEM, sample Na-112.

C) Same as B. Note authigenic botryoidal hematite (Hm) postdating quartz overgrowth. SEM, sample Na-112.

D) Neoformed quartz overgrowths display both prismatic double pyramidal (Pr) and rhombohedral (Rh) perfect crystal faces in open pore. These crystals have no detrital quartz nucleolus. Note the smaller mode of quartz overgrowth (arrows) that lack obvious crystal faces. SEM, sample Na-112.

Plate 4.29

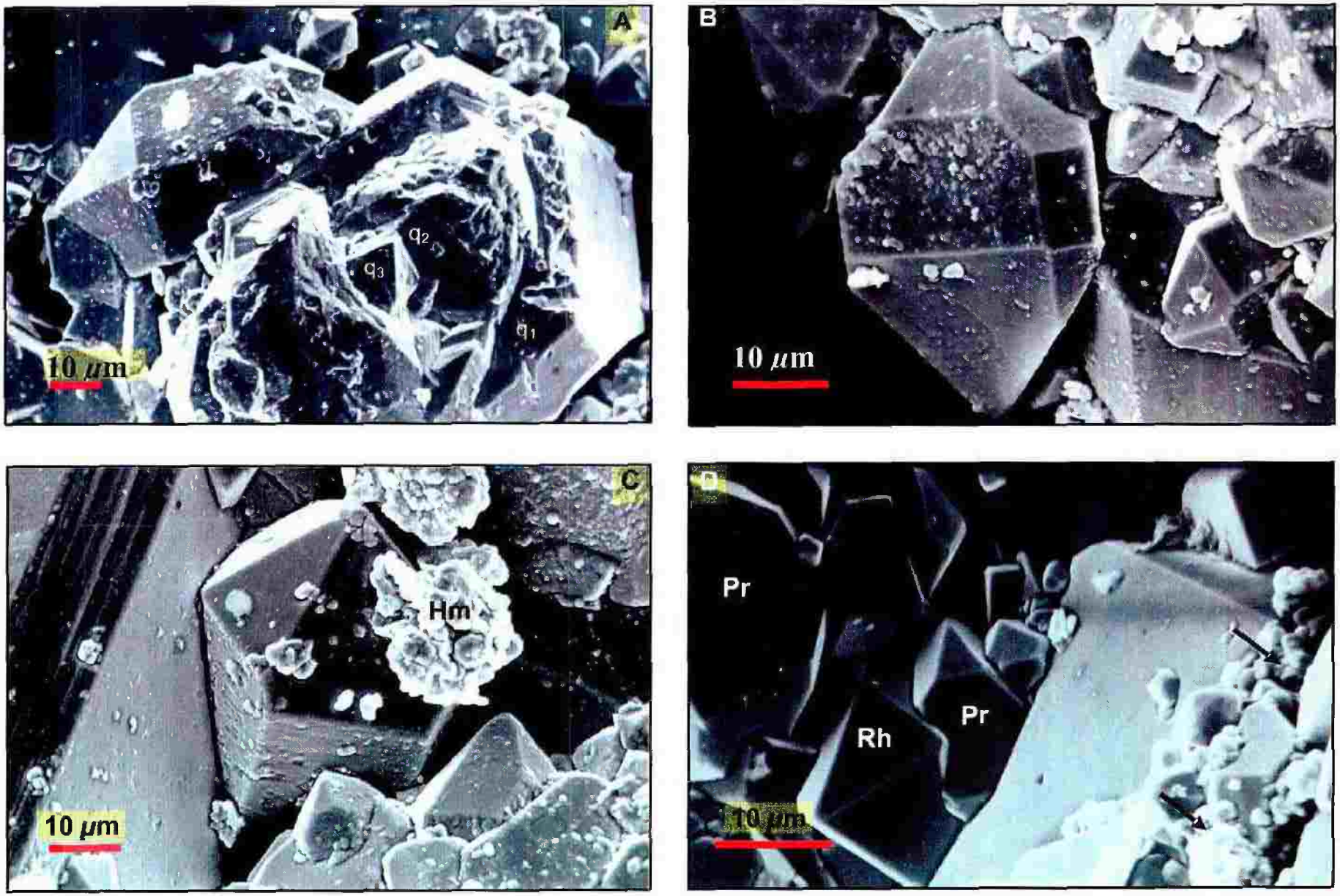

Plate 4.30

A) Quartz overgrowths (arrows) on polycrystalline grain. Each subcrystal displays its own overgrowth in optical continuity. Plane light, sample RB-A1 (12341 ft).

B) A in crossed polarizers.

C) Quartz overgrowths (q) formed at late stage postdating pressure solution and have no "dust" line. Such overgrowths are recognizable primarily because of their euhedral crystal terminations. Note uneven quartz overgrowth (q_1) in contact with portions of detrital grains (Q) that had partial coatings at the time of cementation. SEM, sample Na-112.

D) Neoformed authigenic quartz crystals of perfect faces formed as a void filling rather than as a replacement. Note orientation of crystals and increase of crystal size toward viewer (cavity center). SEM, sample RB-A1 (12341 ft).

Plate 4.30

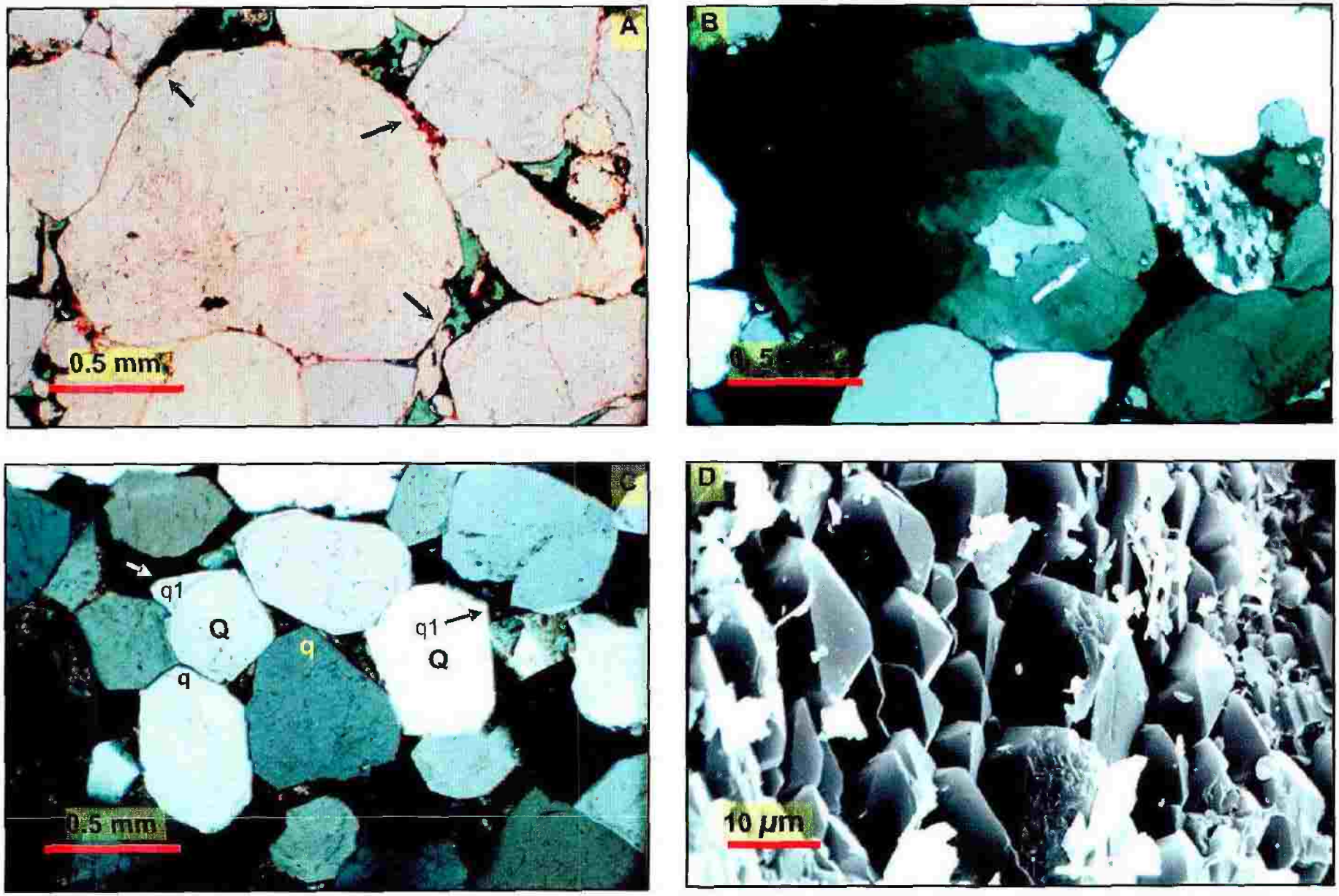

Plate 4.31

A) Syntaxial quartz overgrowth showing high degree of crystalline perfection with zoned layers. SEM, sample Na-112.

B) Syntaxial quartz overgrowth coated by drusy microquartz cement (arrows). SEM, sample Na-112.

C, D) Detrital quartz grains with their syntaxial quartz overgrowth (q) seem imbedded in microcrystalline quartz crystals (Mq). SEM, sample Na-114.

Plate 4.31

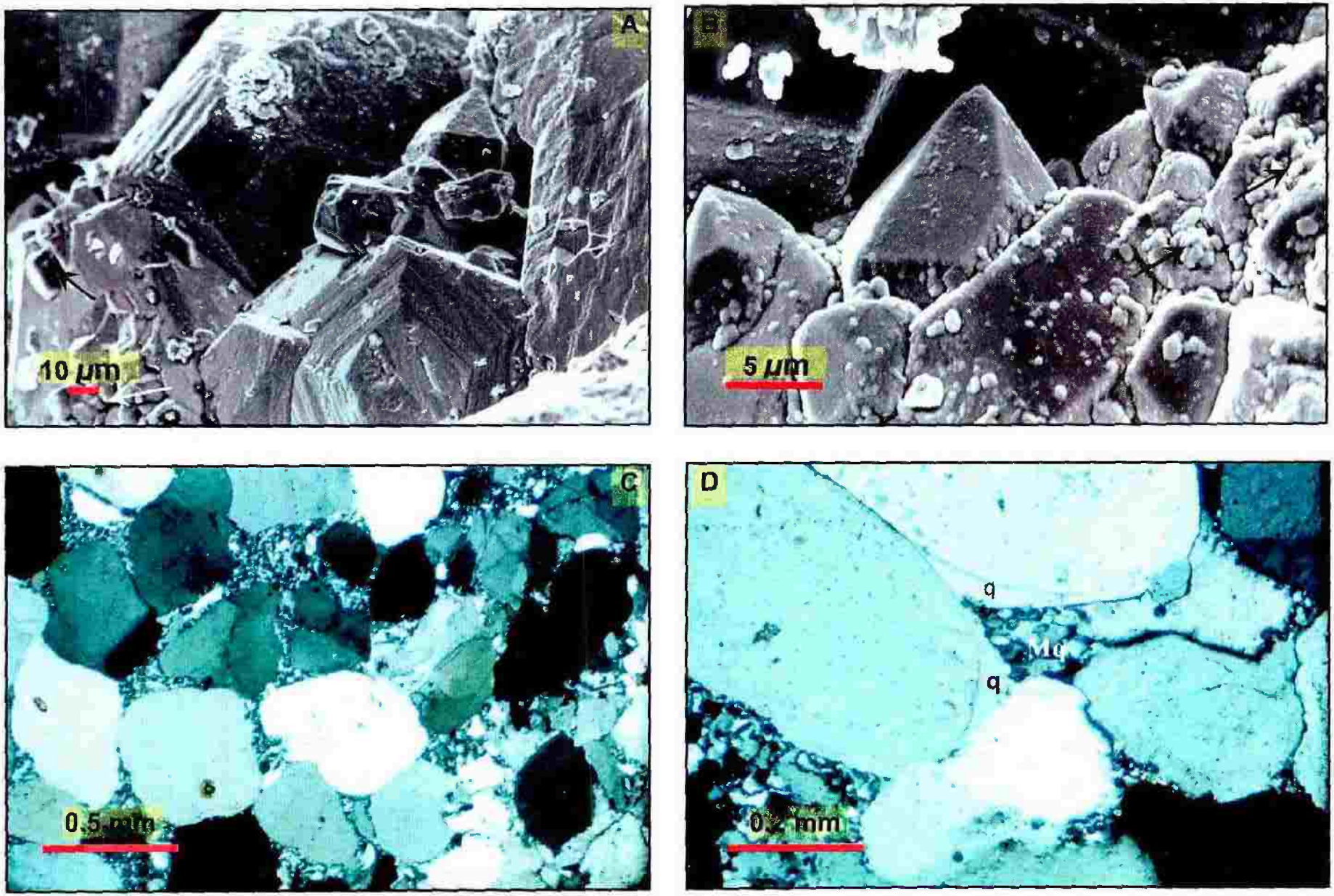

Plate 4.32

A) Authigenic K-feldspar crystal. SEM, sample Ar-7.

B) Close up view of A.

C, D) Authigenic K-feldspar crystals having smooth crystal faces typical of adularia. SEM, sample RB-B3 (12357 ft).

Plate 4.32

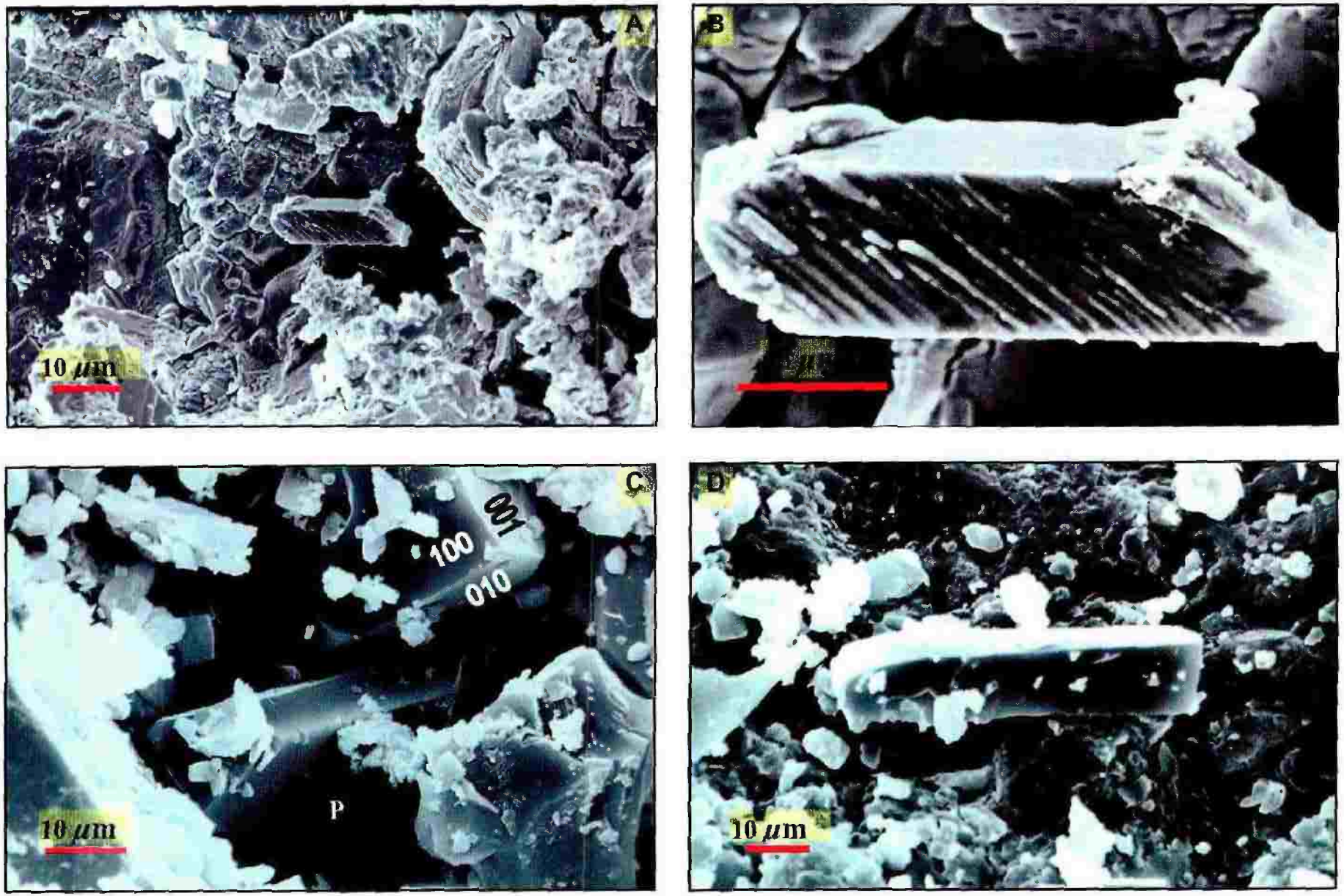

Plate 4.33

A-C) Authigenic K-feldspar crystals having smooth faces typical of adularia, partially fills pore spaces. SEM, sample Ar-7.

D) Coarse authigenic K-feldspar crystal (K-f) subjected to dissolution (arrow). SEM, sample RB-B3 (12357 ft).

Plate 4.33

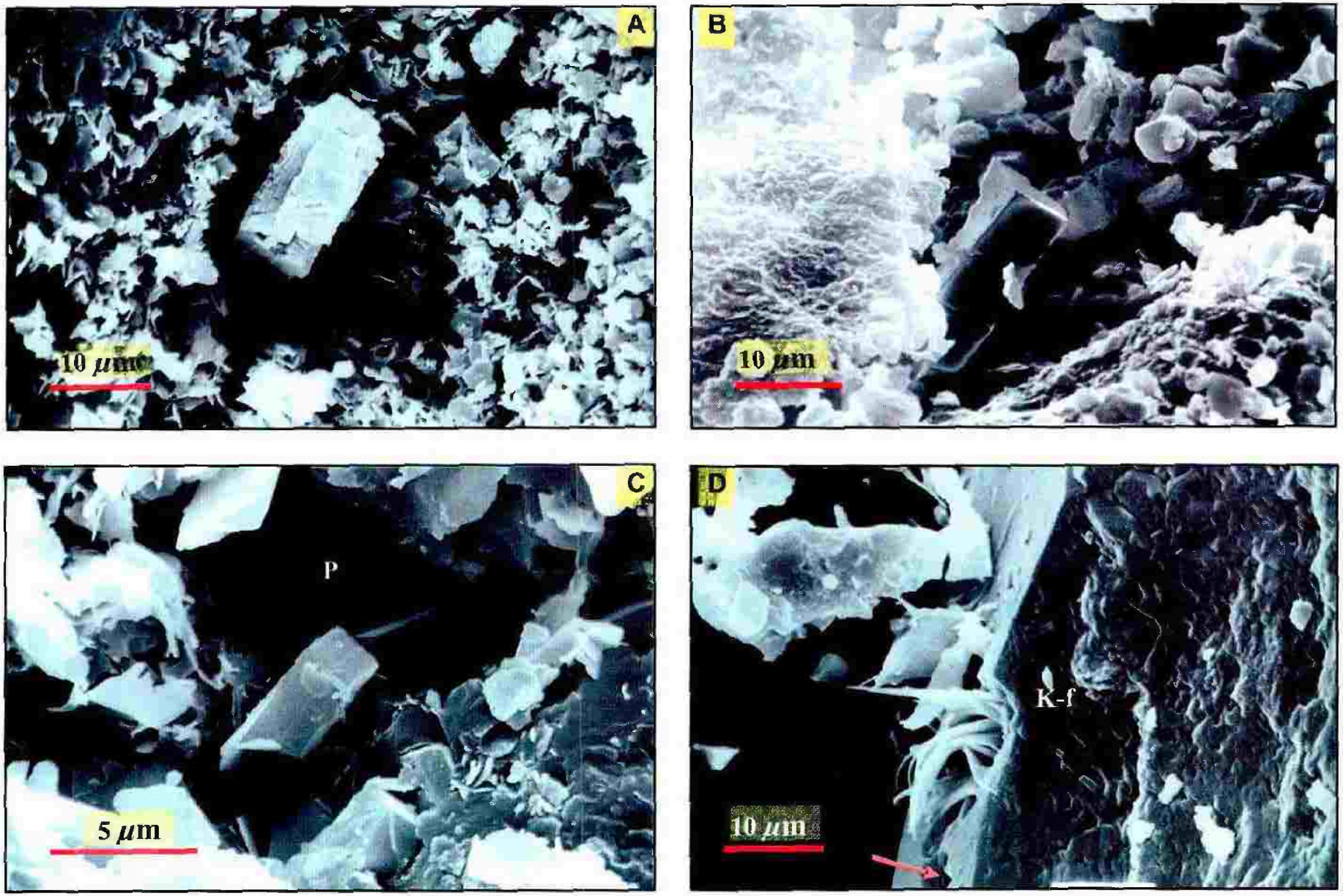

Plate 4.34

A, B) Photomicrographs showing mechanically infiltrated clays as pore-filling cement. Framework grains exhibit normal packing and quartz overgrowths are entirely absent. Plane light, samples RB-A5 (12287 ft) and RB-B7 (12205 ft), respectively.

C) SEM micrograph of allogenic clay particles having ragged outlines. Sample Ar-7c.

D) SEM micrograph of allogenic clays forming pore bridge (arrow). Sample Ar-7c.

Plate 4.34

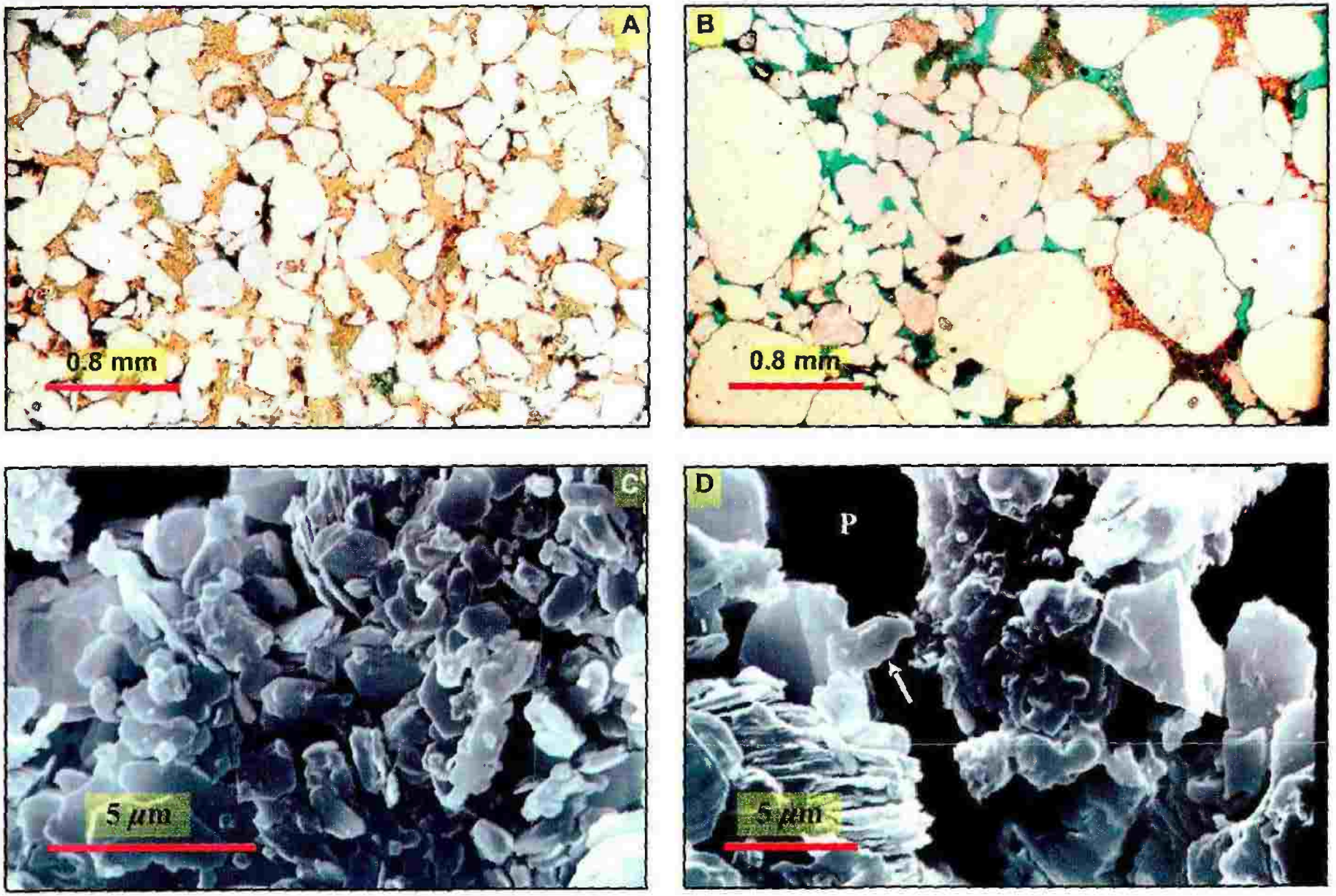

Plate 4.35

A-C) Photomicrographs showing pore-filling authigenic clays. Crossed polarizers, samples Ar-5, Na-28 and Na-85, respectively.

D) SEM micrograph showing a cluster of typical well-crystallized pseudohexagonal kaolinite platelets. Some crystals show well-developed pseudohexagonal basal scales in curved vermicular stacks (arrow), a characteristic structure for kaolinite. The kaolinite platelets have considerable intercrystalline porosity. Sample RB-B3 (12357 ft).

Plate 4.35

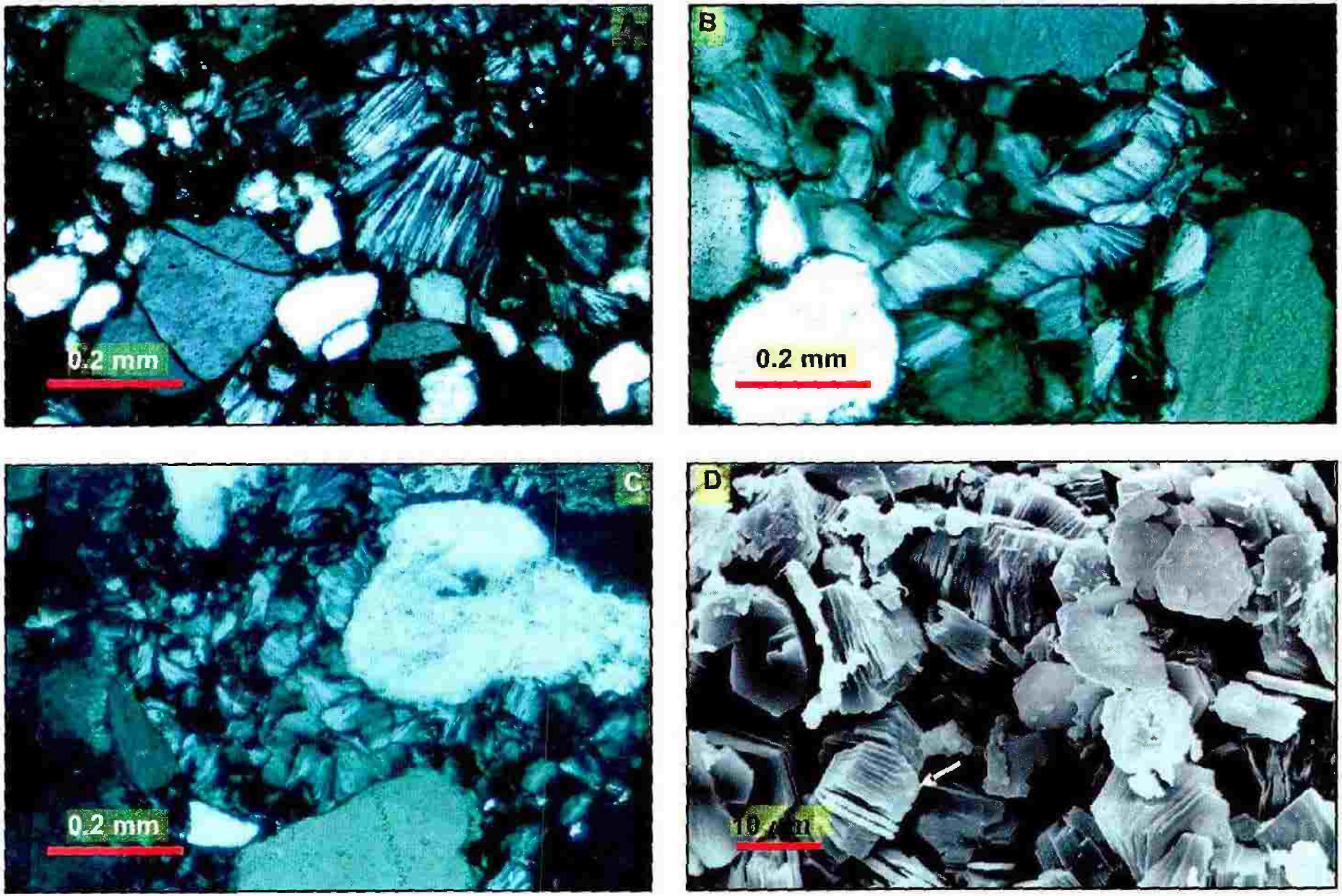

Plate 4.36

SEM micrographs showing clusters of well-crystallized pseudohexagonal kaolinite platelets. Some platelets (Ka) are engulfed in quartz overgrowths (q) probably reflecting co-precipitation of the two minerals. Note the micropores (P) between kaolinite platelets. Samples Na-51 (A, B) and RB-A1 (12341 ft), respectively.

Plate 4.36

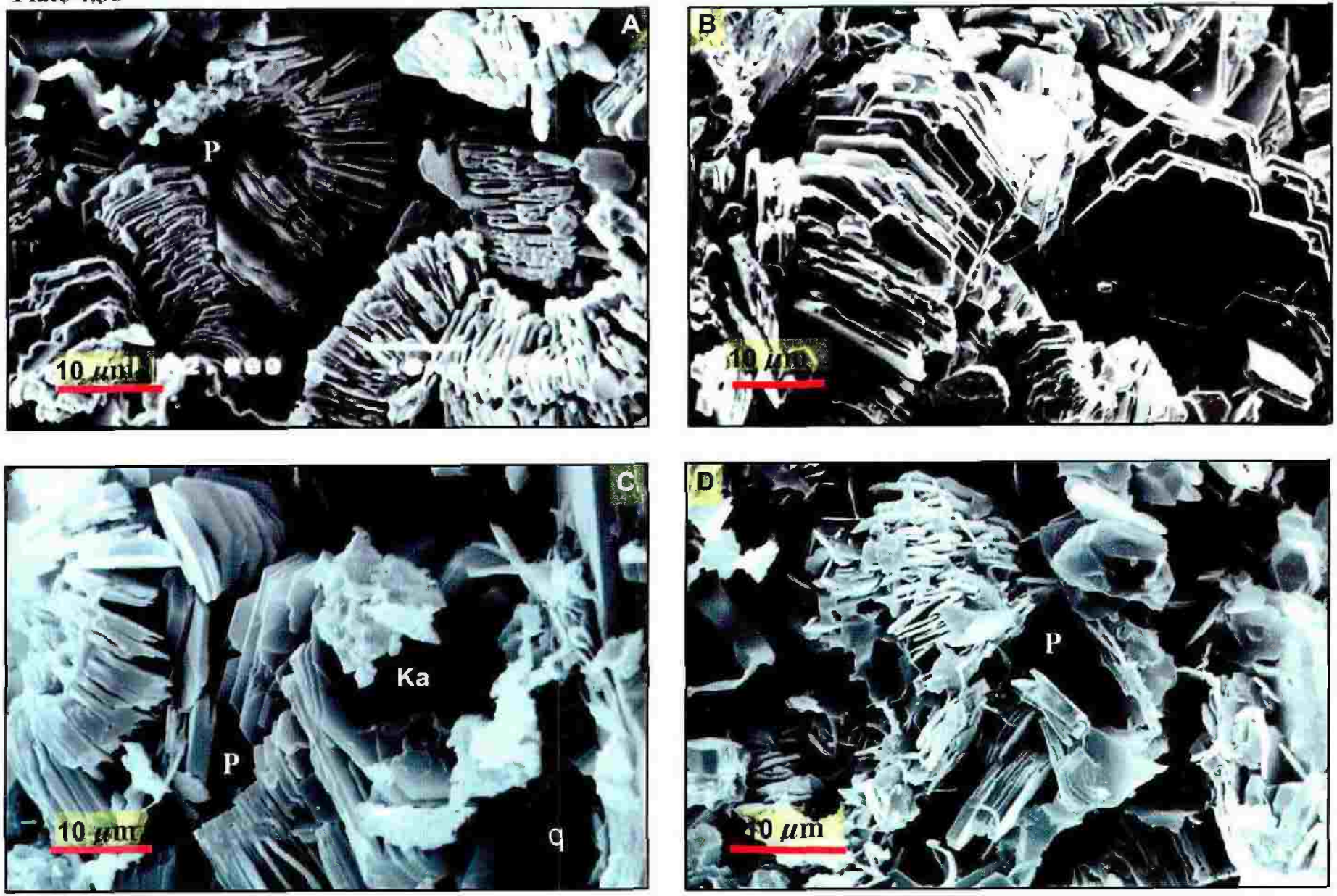

Plate 4.37

A, B) SEM micrographs showing typical tripartite vermicular kaolinite (VKa). Samples Ar-9 and RB-C2 (12368 ft), respectively.

C) SEM micrograph showing blocky masses of kaolinite crystals (arrow). Sample Ar-7.

D) SEM micrograph showing fan-shaped kaolinite (arrow) occuring as radiating, stacked sheets forming fan-like aggregate. Sample Na-26.

Plate 4.37

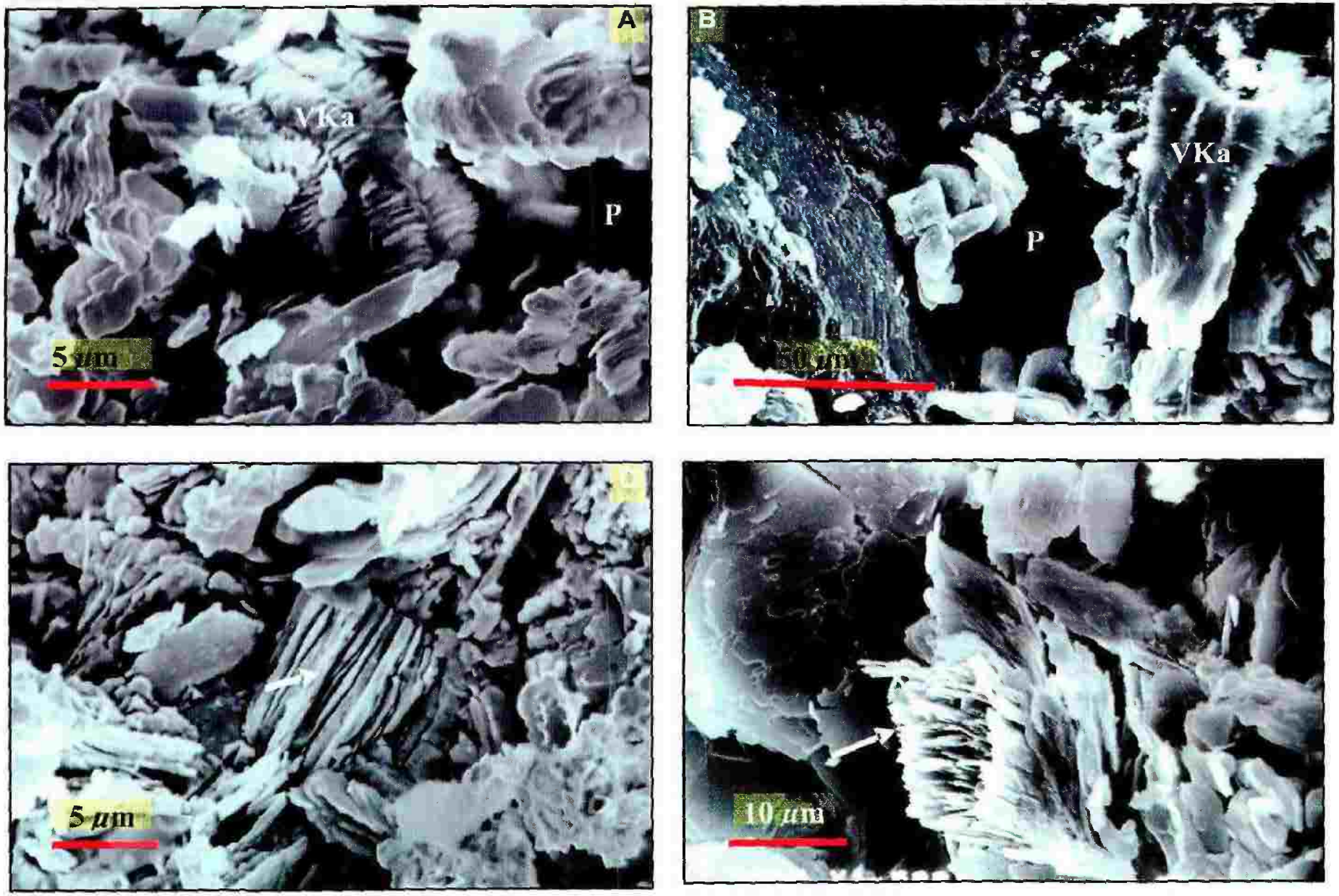

Plate 4.38

A) Photomicrograph showing alteration of K-feldspar. Plane light, sample Ar-9.

B) A in crossed polarizers.

C) Photomicrograph showing alteration of mica (M). Plane light, sample Ar-5.

D) SEM micrograph showing mica altered to kaolinite (arrow) which preserved the precursor grain habit. Sample Ar-9.

Plate 4.38

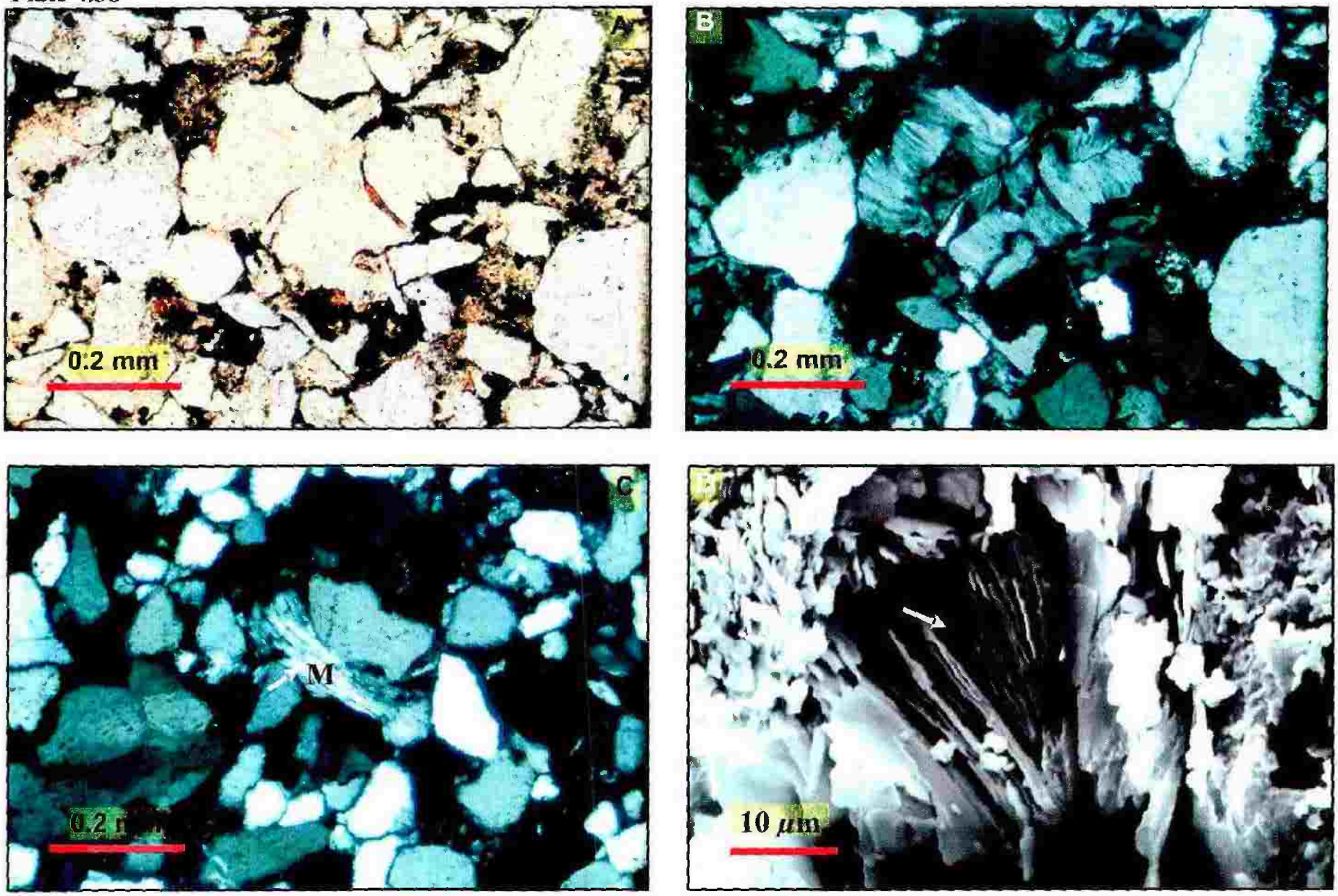

Plate 4.39

A) SEM micrograph showing delicate fibers of authigenic illite (arrows). Sample RB-B3 (12357 ft).

B, C) SEM micrographs showing a crinkly form of smectite (Sm). The highly crenulated, honeycombed, interlocking crystals are typical of smectite in SEM view. The well developed thick blocky kaolinite platelets (Ka) postdates smectite. Samples RB-A1 (12341 ft) and RB-B3 (12357 ft), respectively.

D) SEM micrograph showing authigenic chlorite (white arrow). Note thick kaolinite platelets at the bottom of the photo (ka). Sample RB-A1 (12341 ft).

Plate 4.39

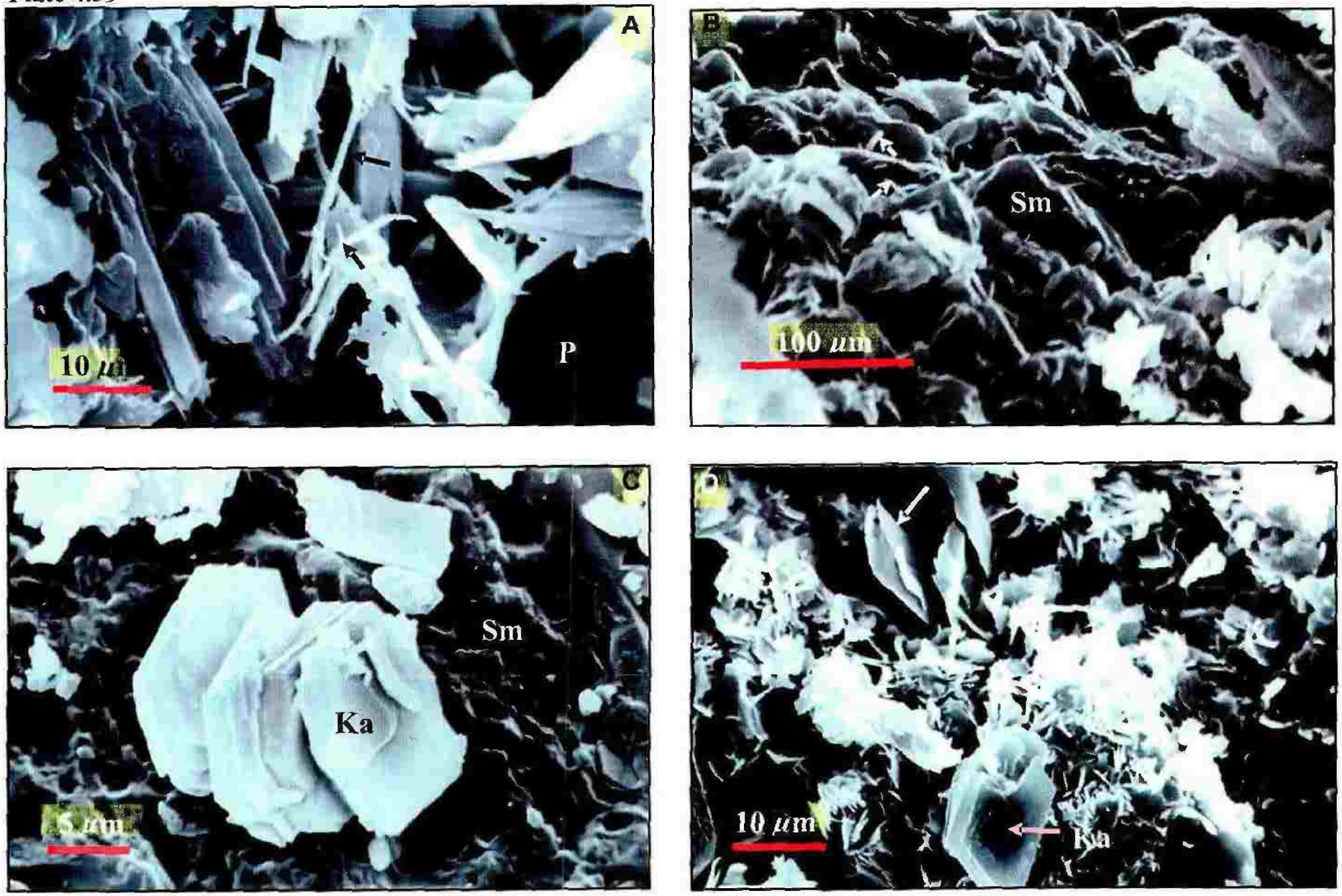

Plate 4.40

A) Photomicrograph showing precipitation of Fe-bearing minerals along stylolitic solution surface. The dark zone that passes through the center of the photo is the stylolitic interval in which other insoluble material, such as clays and/or organic matter, has been concentrated yielding the very dark appearance. Note truncation of quartz grains along stylolite. Plane light, sample RB-B4 (12479 ft).

B), C) Photomicrograph showing precipitation of Fe-bearing minerals along solution seams and sutured grain contacts. The solution zones or seams, also termed horsetail seams or microstylolites, have concentrations of other relatively insoluble material such as clays and/or organic matter yielding the very dark appearance. Compactional drape and pressure solution took place most effectively around such zones and contacts providing a source of silica for subsurface quartz cementation. Plane light, sample RB-B4 (12479 ft).

D) Photomicrograph showing authigenic hematite (Hm) existing as pore-filling cement. Note the high intergranular porosity (P) probably resulted from calcite dissolution. Embayed ouliness of some quartz grains (arrows) are evidence of the former presence of calcite that was later dissolved. Plane light, sample Ar-3.

Plate 4.40

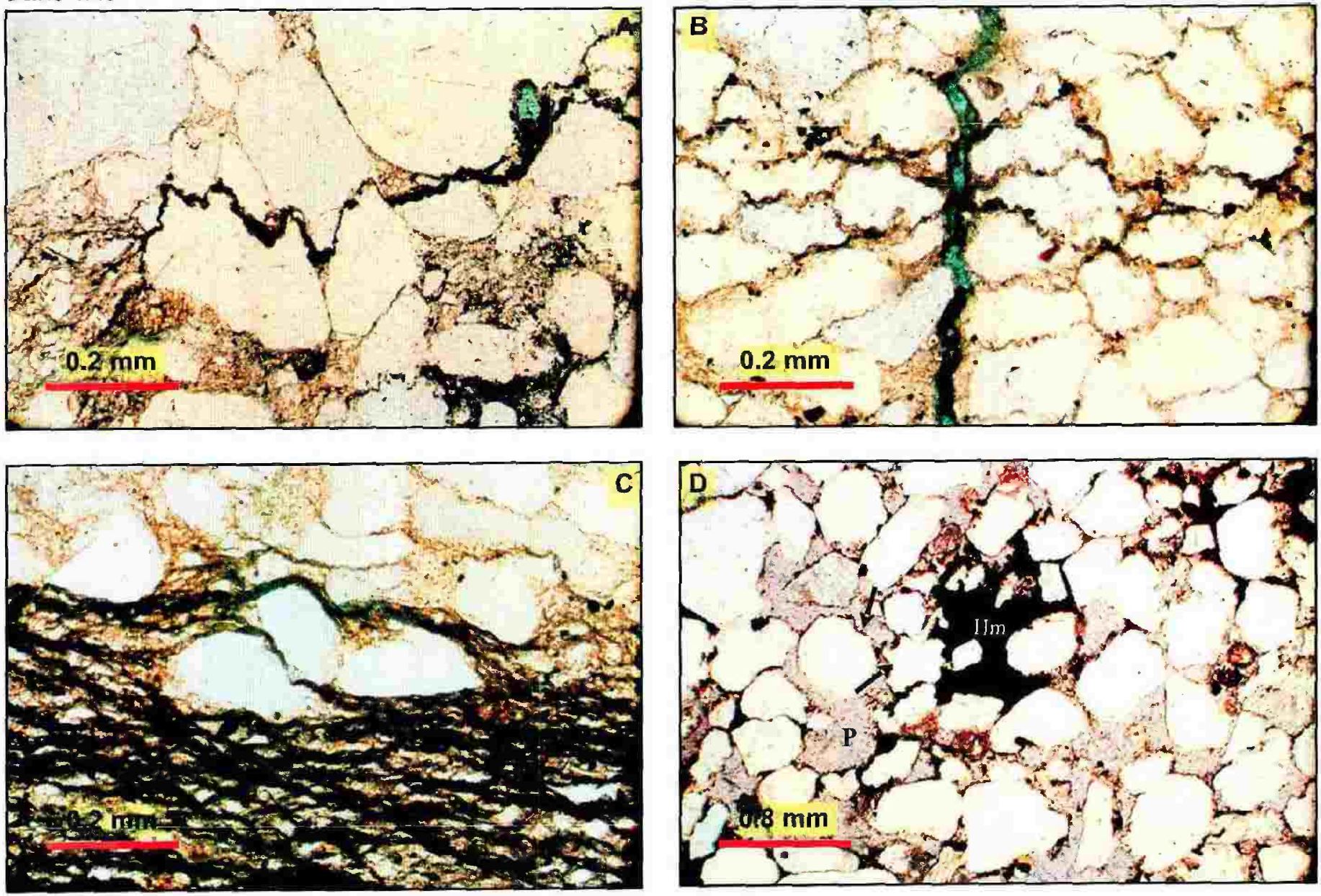

Plate 4.41

A) Photomicrograph showing pore-filling authigenic hematite (Hm). Plane light, sample RB-C2 (12341 ft).

B) Photomicrograph showing authigenic hematite (Hm) as pore-filling cement. Hematite postdates quartz overgrowth (arrow). Note clay cement (Cl) embedded in the hematite cement indicating earlier formation. Plane light, sample Ar-2.

C) Photomicrograph showing pore-filling authigenic hematite (Hm) in abundance to warrant the term ferricrete. Note hematite (Hm) filling the intercrystalline boundaries of a polycrystalline grain. Plane light, sample RB-C2 (12253 ft).

D) Close up view of C.

Plate 4.41

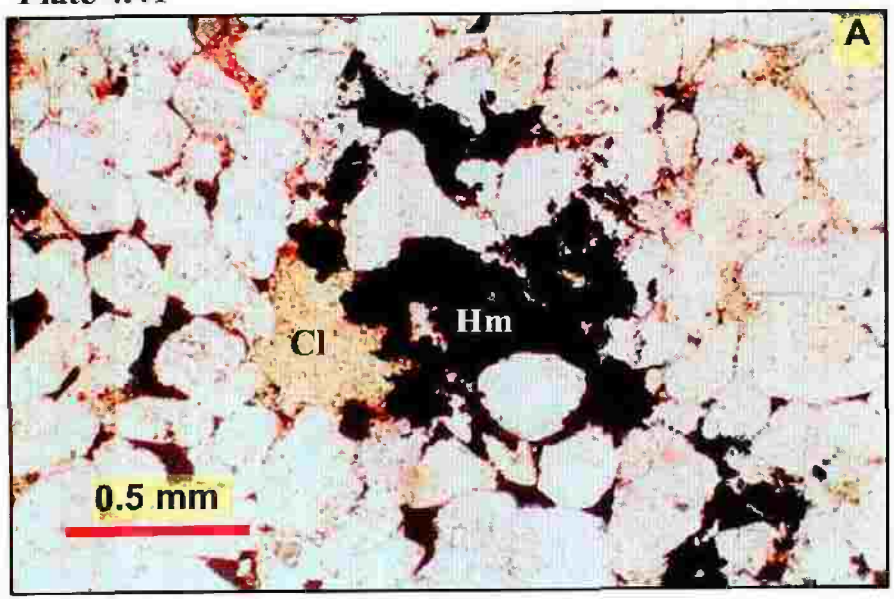

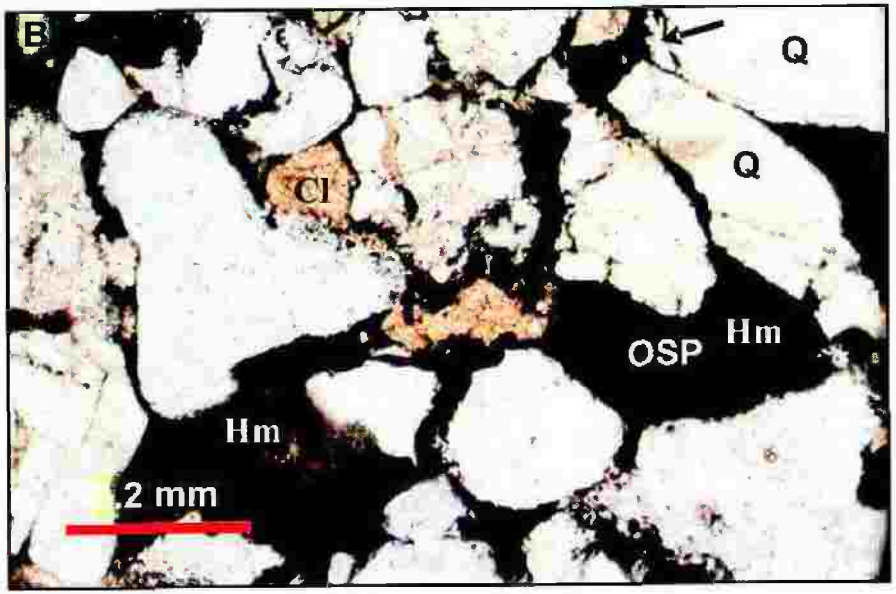

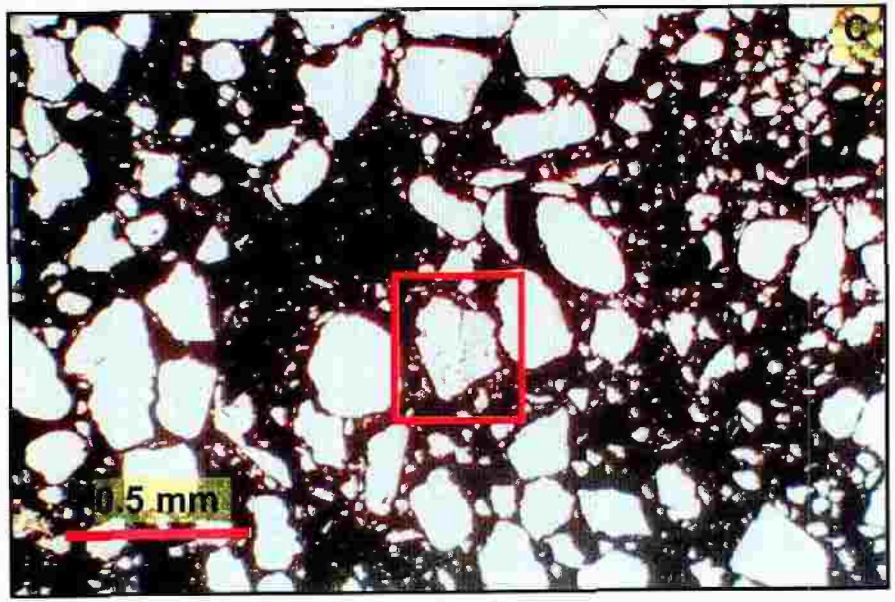

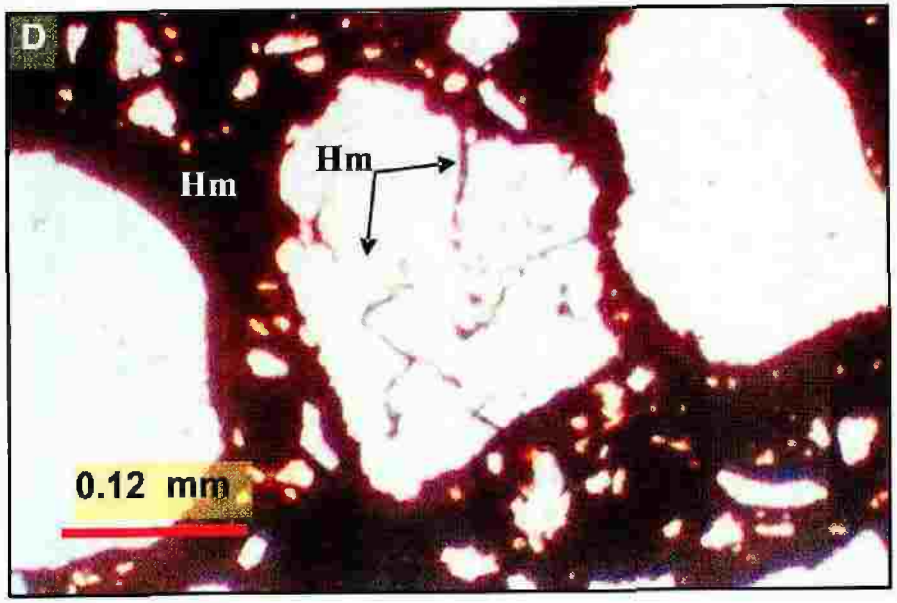

Plate 4.42

A) SEM micrograph showing authigenic hematite as grain coating. Sample Na-112.

B) Close up view of A showing the botryoidal texture of hematite (Hm).

C) SEM micrograph showing pore-filling authigenic botryoidal hematite (Hm). Sample RB-A1 (12341 ft).

D) SEM micrograph showing authigenic botryoidal hematite (Hm) postdating quartz overgrowth (q). Sample Na-112.

Plate 4.42

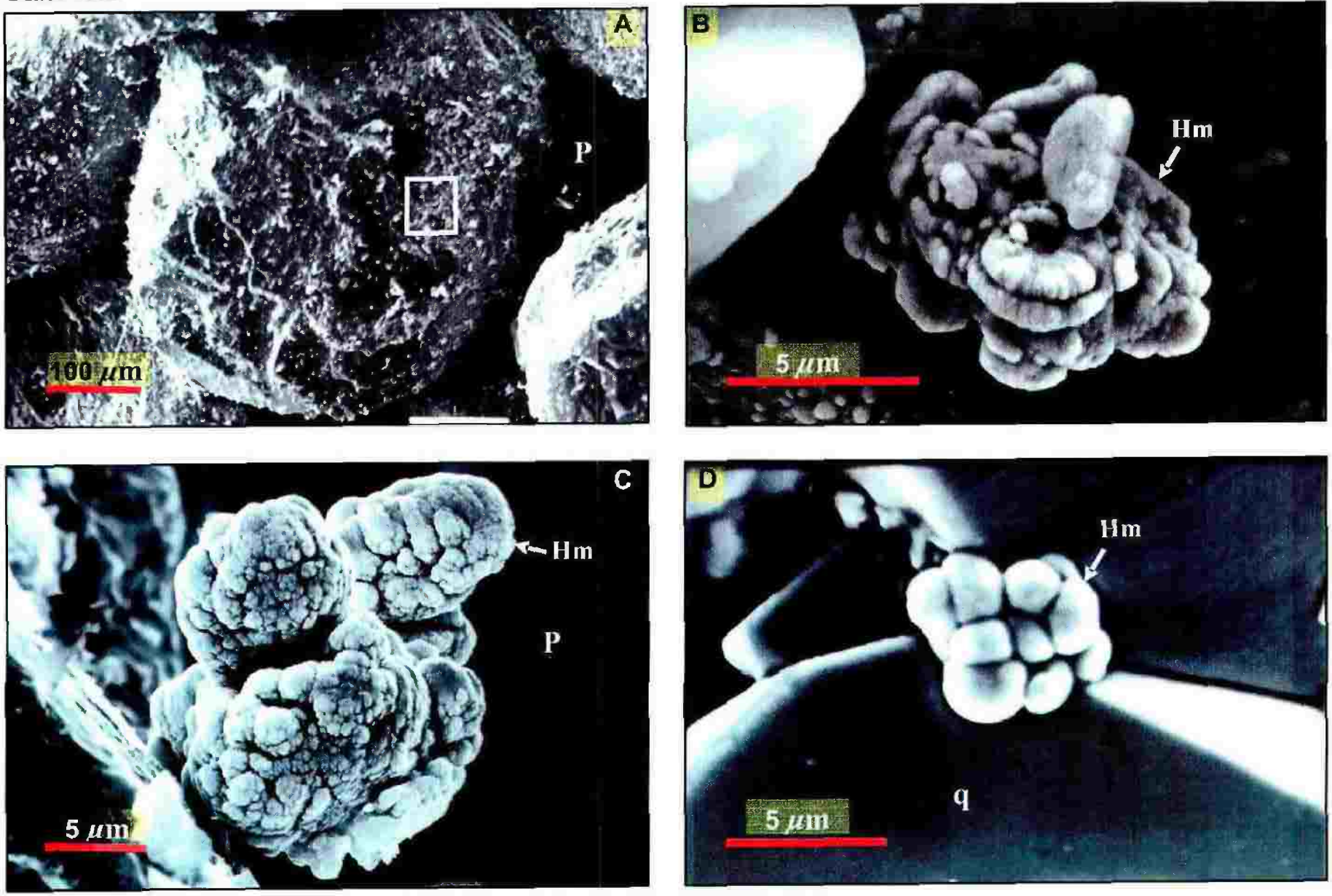

Plate 4.43

A) SEM micrograph showing typical authigenic botryoidal hematite (Hm) coating quartz overgrowth (q) and partially filling pore space. Sample Na-112.

B) SEM micrograph showing typical microrosettes of authigenic hematite as interstitial aggregates and drusy coatings. Sample RB-A5 (12825 ft).

C) Close up view of the microrosettes in B showing the elongated (rod-like) shape of the crystals.

D) SEM micrograph of platelets of hematite that is aggregated into rosette-like clusters. Sample RB-A1 (12341 ft).

Plate 4.43

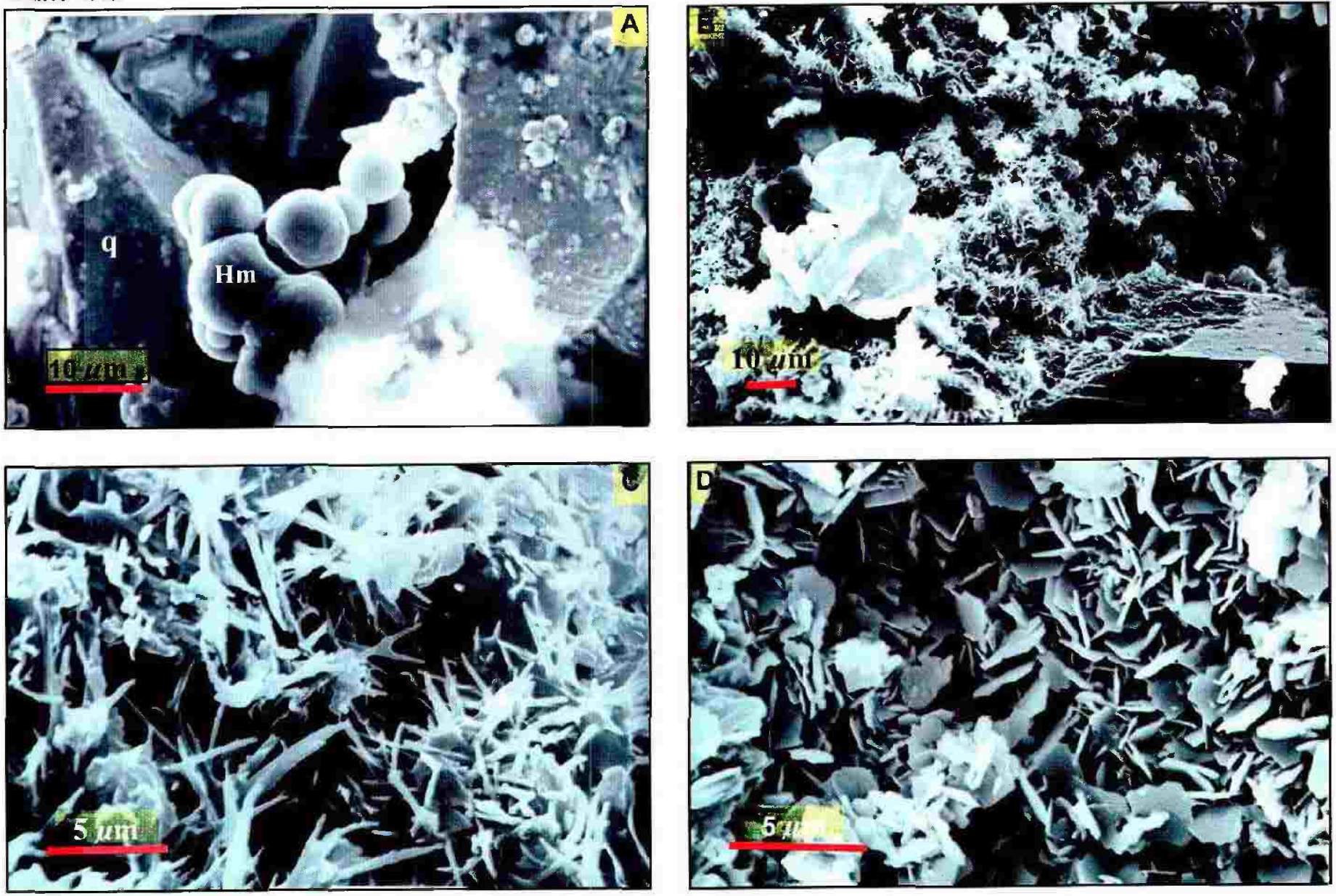

Plate 4.44

A, B) Photomicrographs showing poikilotopic calcite (Ca) occurring both as pore-filling (P) and oversized cement (OSP). Some quartz grains show conspicuous embayments as a result of corrosion and replacement by calcite. Note the two sets of cleavage (arrows) characteristic of calcite. Plane light, sample Ar-7c.

C) Photomicrograph showing micritic calcite occurring both as pore-filling (P) and oversized cements (OSP). Some quartz grains show conspicuous embayed outlines (arrows) indicating replacement by calcite. Crossed polarizers, sample Ar-7c.

D) SEM micrograph showing drusey calcite cement. Note hematite (Hm) postdating calcite. Sample Ar-7c.

Plate 4.44

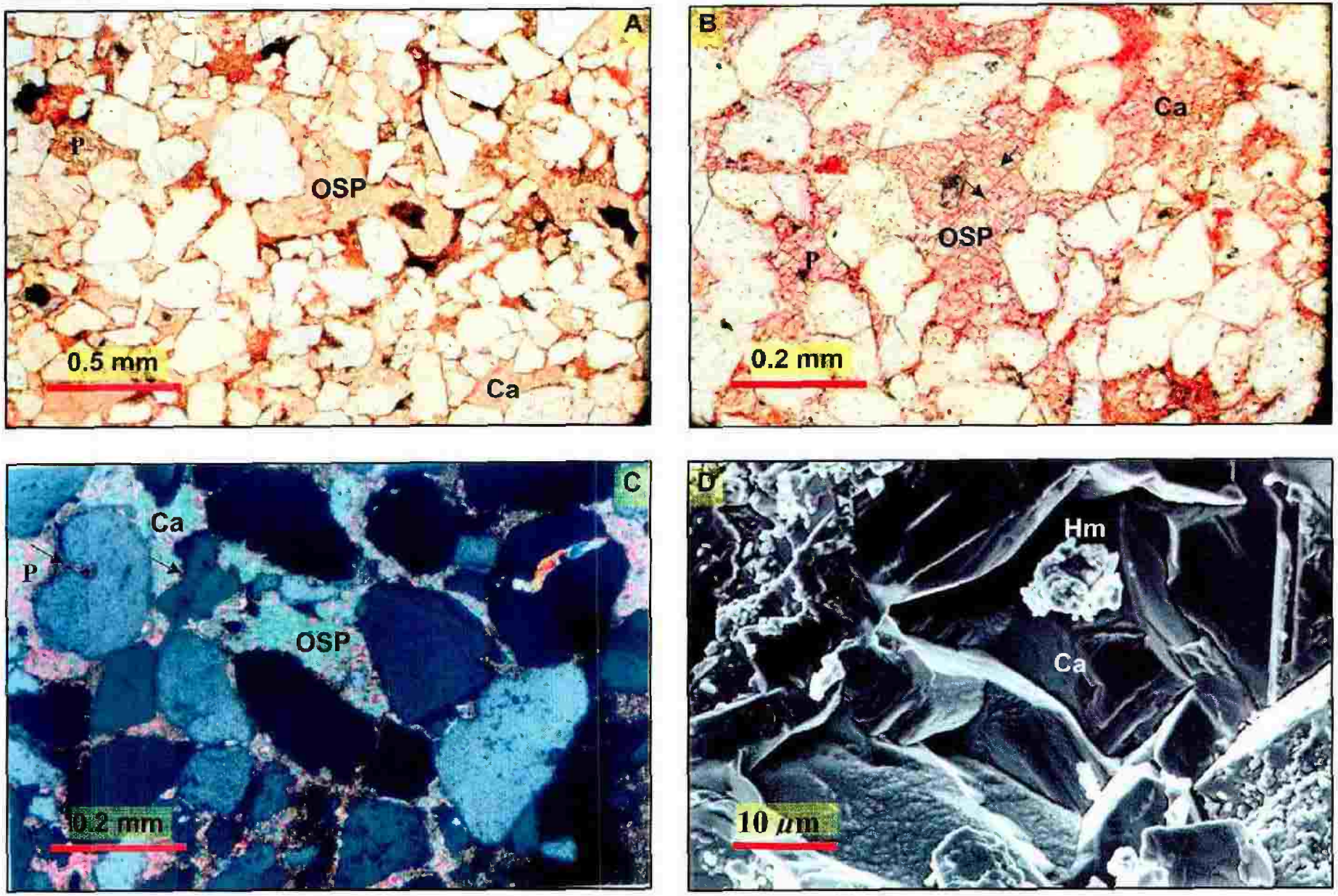

Plate 4.45

A) SEM micrograph showing successive blocky mosaics of pore-filling calcite cement. Sample Ar-4.

B, C) SEM micrographs showing euhedral calcite crystals (white arrows). Spikes (black arrows) in calcite is considered as one of common dissolution features. Samples Ar-4 and Ar-7c, respectively.

D) Photomicrograph showing calcite-cemented sandstone with small patches of poikilotopic calcite. The calcite cement (Ca) postdates quartz overgrowth (q) and probably compaction. The corrosion (arrows) on both detrital quartz grains and their overgrowths are due to dissolution. Plane light, sample RB-B3 (12401 ft).

Plate 4.45

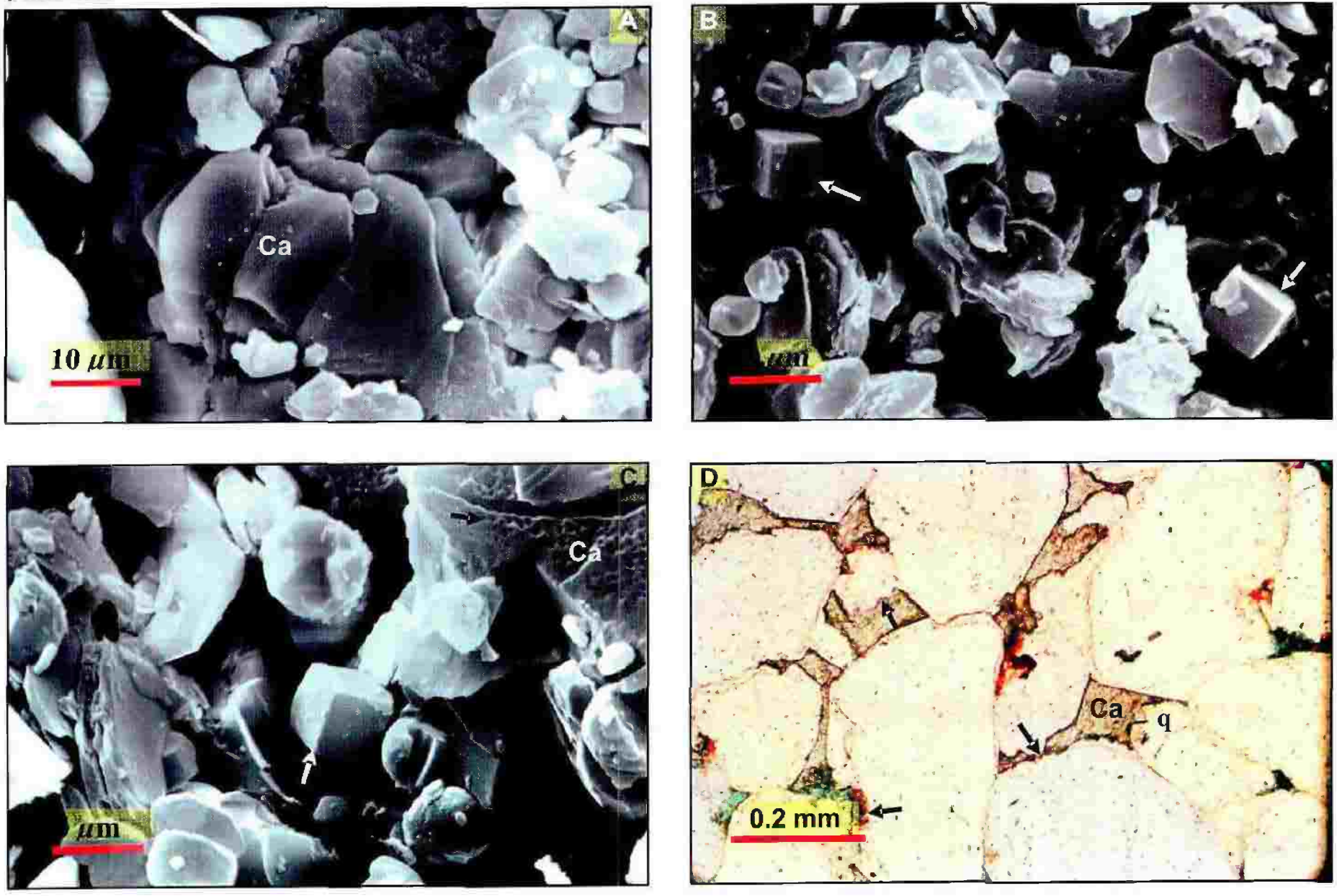

Plate 4.46

A) Photomicrograph showing calcite-cemented sandstone in which small patches of poikilotopic cement are present. The calcite cement (Ca) postdates quartz overgrowth (q) and compaction. The overgrowth (q) penetrated the adjacent quartz grain (Q) due to compaction effect. Plane light, sample RB-B3 (12401 ft).

B) Photomicrograph showing oversized pore (OSP) probably due to dissolution of pre-existing calcite cement. Note oversized pore filled with halite (Ha). Halite probably post-dates calcite dissolution. Plane light, sample RB-B4 (12414 ft).

C) Photomicrograph showing loose packing probably due to dissolution of calcite cement. Plane light, sample Na-15.

D) Photomicrograph showing corrosion (arrows) in both detrital quartz grain and authigenic quartz overgrowth probably caused by calcite. Plane light, sample RB-B4 (12404 ft).

Plate 4.46

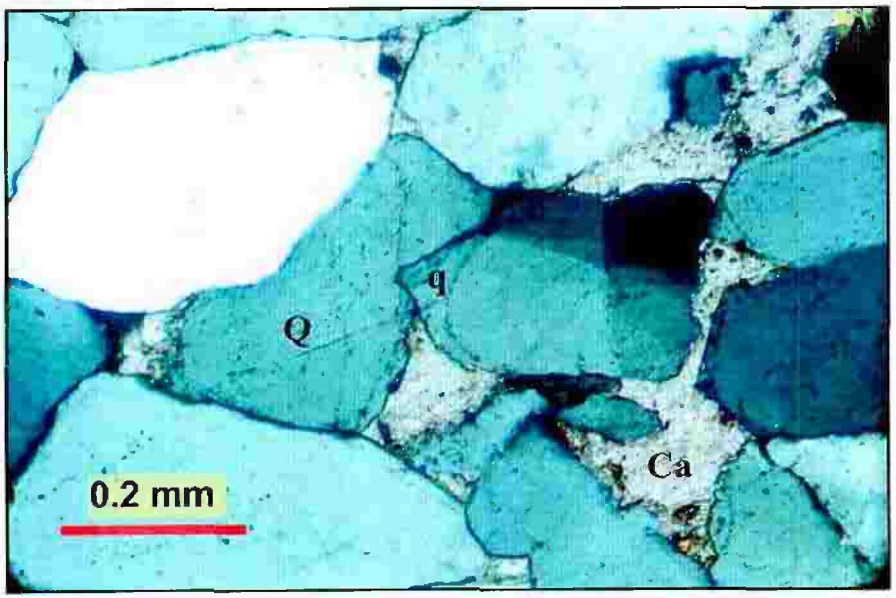

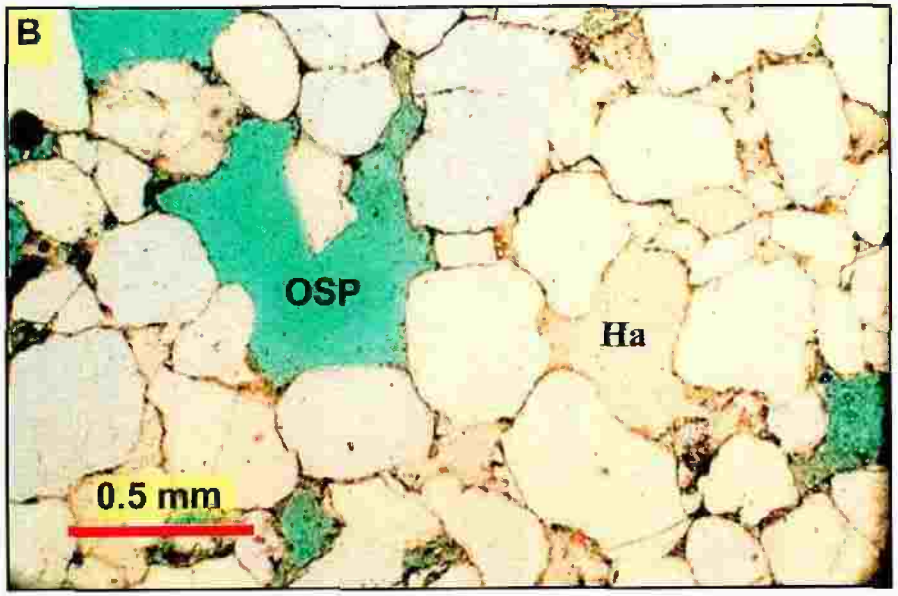

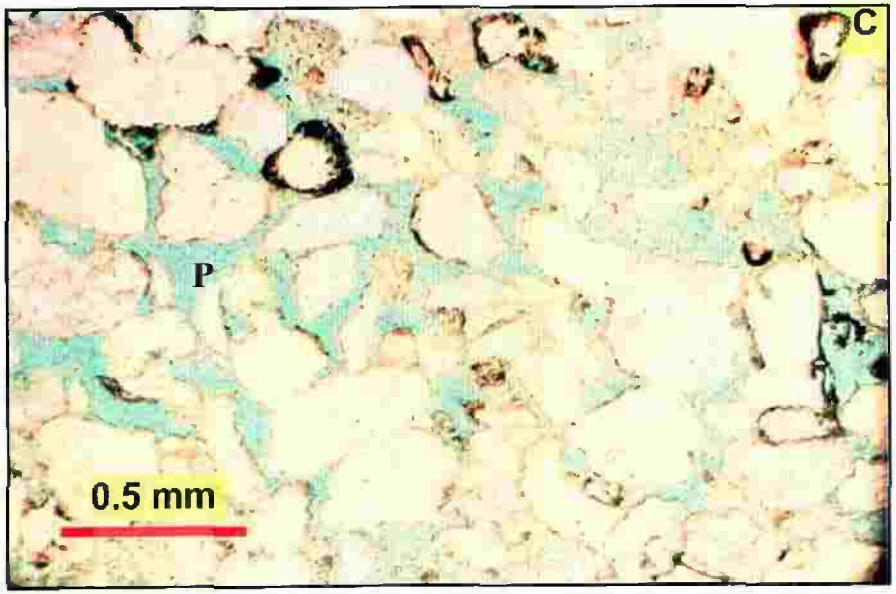

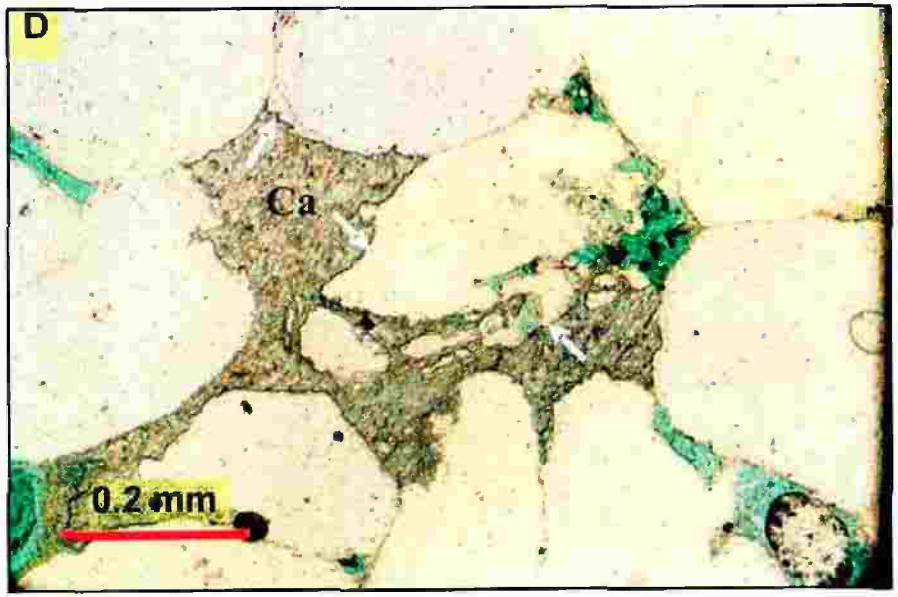

Plate 4.47

A-C) Photomicrographs showing halite (Ha) as a pore-filling and oversized cement. Note partial dissolution of halite forming a waxy pattern (B). Plane light, samples RB-C2 (12368 ft), Na-26 and RB-A5 (12268 ft), respectively.

D) Photomicrograph showing halite cement (black arrow) filling fractures in detrital quartz grain. Note oversized pore (OSP) due to dissolution of a pre-existing grain, clay rim (blue arrows) indicates original grain boundary. Plane light, sample RB-C2 (12368 ft).

Plate 4.47

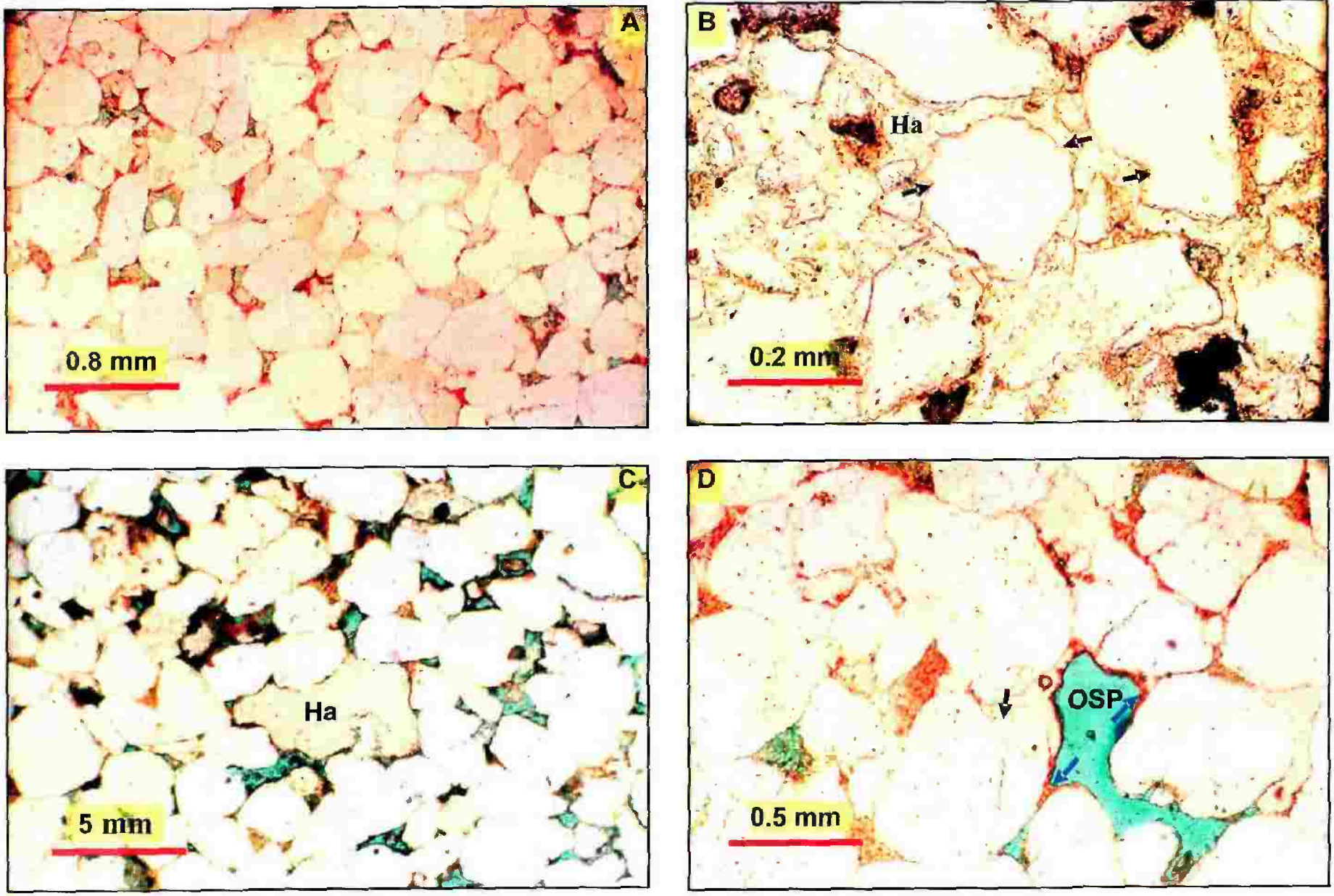

Plate 4.48

A, B) SEM micrographs showing small cubic halite crystals as pore-filling and grain coating. Note smooth, rounded edges due to dissolution. Sample Na-26.

C, D) SEM micrographs showing halite as a massive cement and forming also waxy coatings. Note dissolution (arrows) in the halite cement. Samples RB-C2 (12368 ft) and RB-A1 (12341 ft), respectively.

Plate 4.48

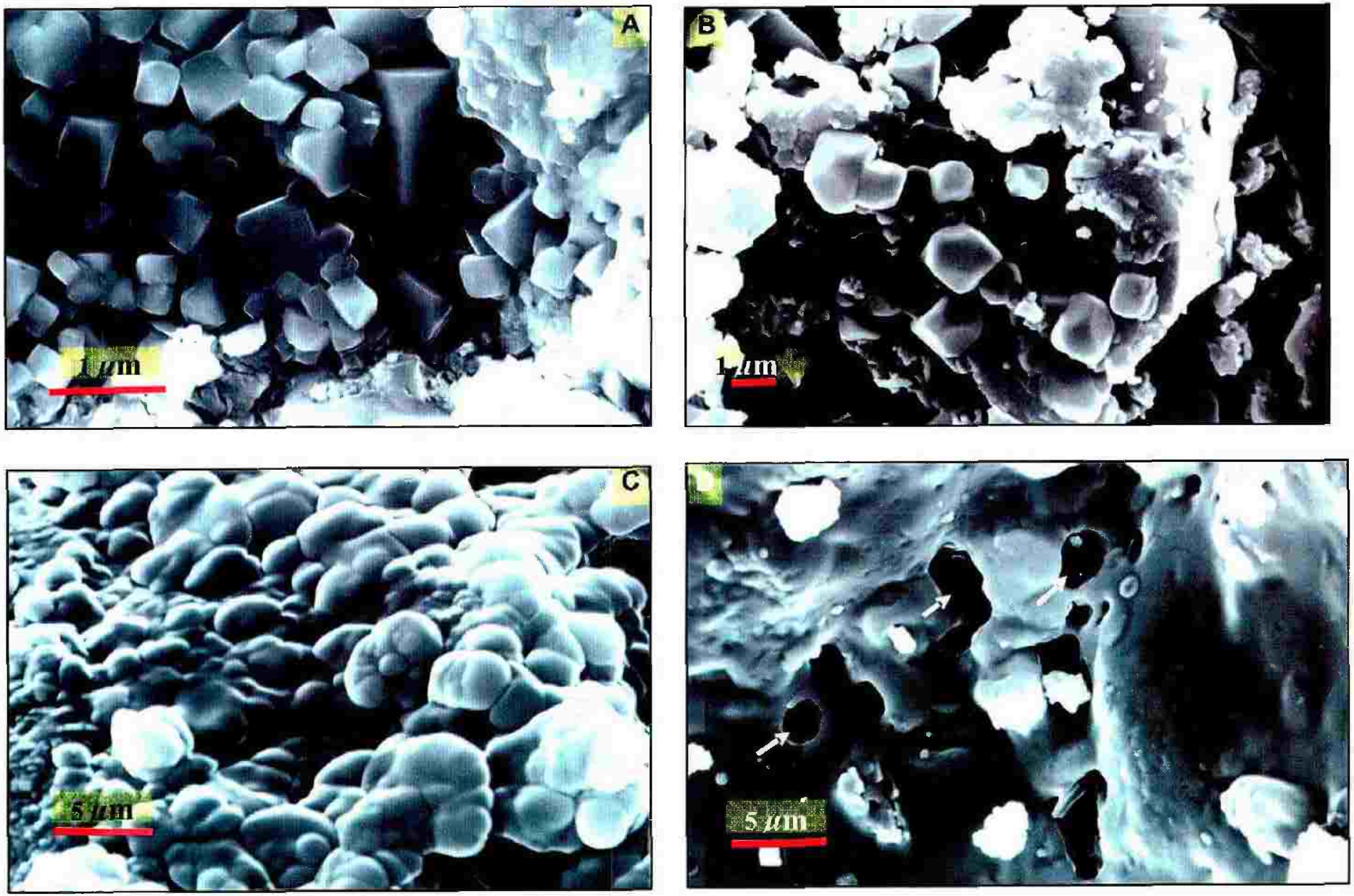

Plate 4.49

A), B) Photomicrographs showing preserved primary intergranular porosity (green stain). Plane light, samples RB-A1 (12460 ft) and Na-12, respectively.

C) Photomicrograph showing an example of secondary porosity development (OSP) due to complete dissolution of unstable detrital grains or carbonate cement. Plane light, sample RB-B7 (12253 ft).

D) Photomicrograph showing elongate secondary porosity (green stain) probably due to leaching of calcite cement under subsurface conditions. Subsurface leaching of carbonate minerals may result from meteoric flushing, biogenic CO_2 formation or maturation of organic matter in deeper subsurface environments. Plane light, sample RB-B4 (12470 ft).

Plate 4.49

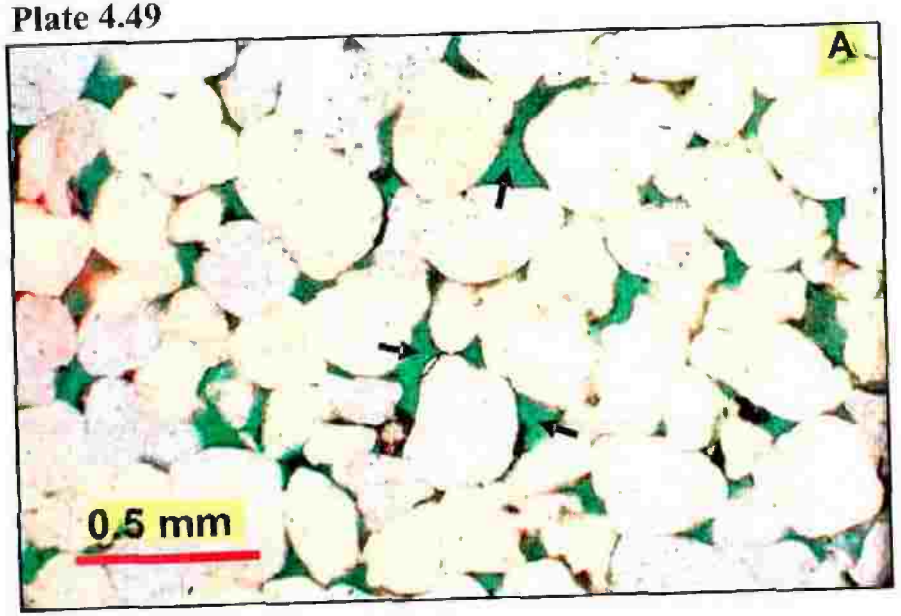

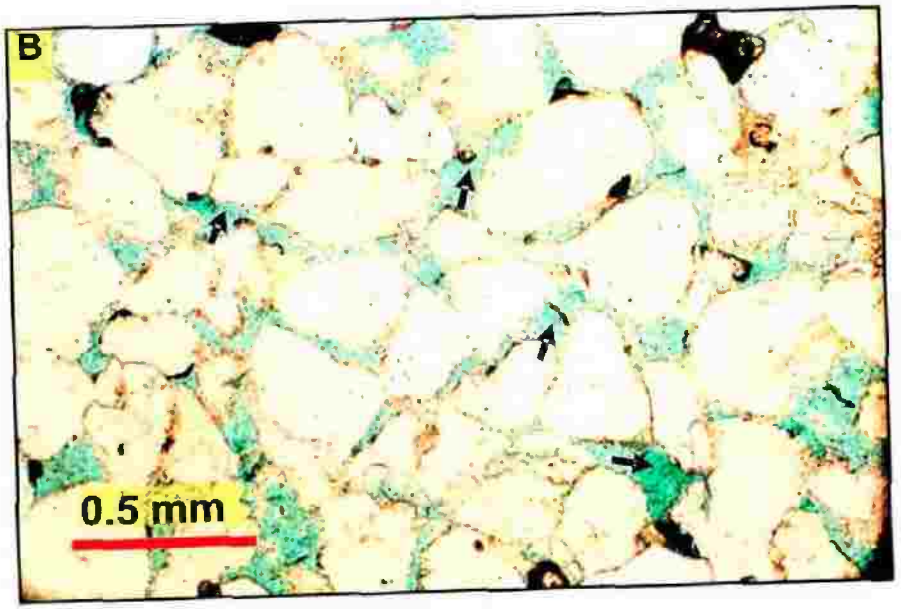

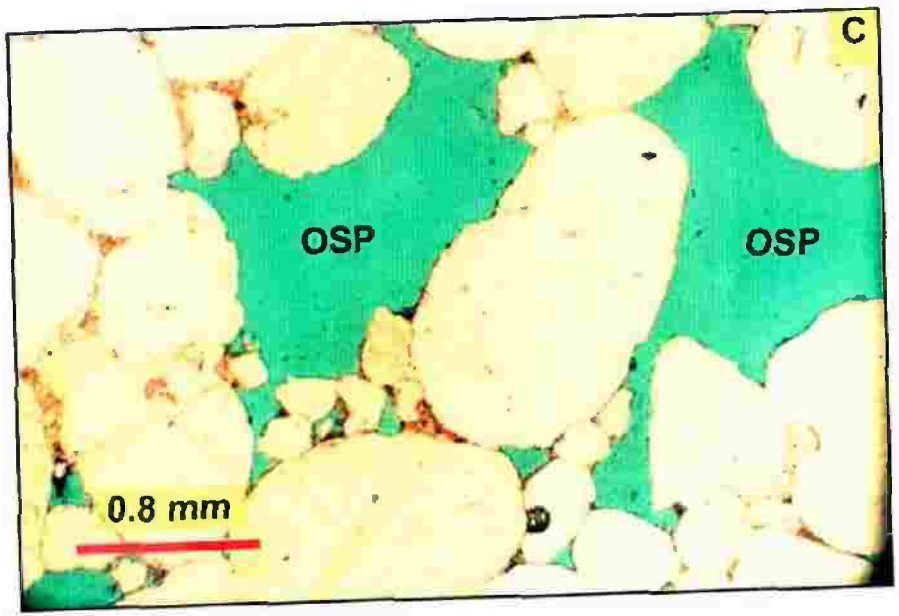

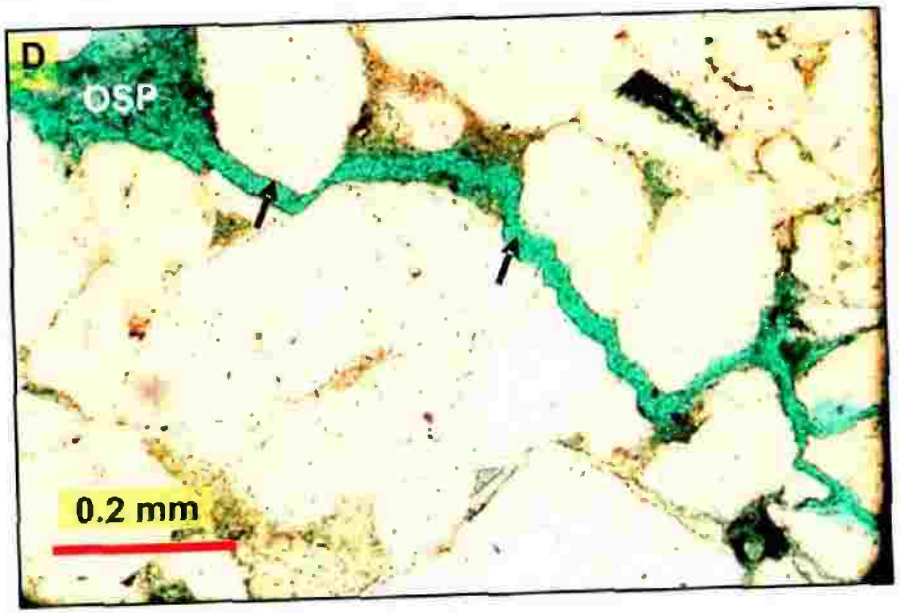

Plate 4.50

A) Photomicrograph showing intragranular porosity in a quartz grain due to selective dissolution along internal strain boundaries. Note oversize pore (OSP). Plane light, sample RB-B4 (12404 ft).

B) Photomicrograph showing microfracture porosity within individual quartz grain. The grain has been fractured after partial leaching of carbonate cement. Subsurface removal of cements commonly leads to fracturing of grains as the stabilizing and supporting material is removed and grain contacts begin to support a greater portion of the overburden stress. Note oversize pore (OSP). Plane light, sample RB-B4 (12404 ft).

C) Photomicrograph showing fracture porosity. The large, unfilled fracture (Fr shown in blue) which transects sample provides a significant percentage of the total porosity in this sample and may improve overall permeability as well. Plane light, sample Ar-1.

D) Photomicrograph showing filled secondary (fracture) porosity. The fracture (Fr) in this example has been completely healed by the growth of clay cement. Plane light, sample Ar-1.

Plate 4.50